THE GRADUATE UNIVERSITY FOR ADVANCED STUDIES, SOKENDAI

DOCTORAL THESIS

Spectral sum of hadronic correlation functions from lattice Quantum Chromodynamics

---

Author:
ISHIKAWA, Tsutomu

Supervisor:
Prof. HASHIMOTO, Shoji

A thesis submitted in fulfillment of the requirements
for the degree of Doctor of Philosophy

in the

Department of Particle and Nuclear Physics
School of High Energy Accelerator Science

Abstract

Spectral sum of hadronic correlation functions from lattice Quantum Chromodynamics

by ISHIKAWA, Tsutomu

Quantum Chromodynamics (QCD) describes the strong interaction among quarks and gluons. Quarks are the elementary particles that constitute hadrons. Therefore, QCD plays an important role even in various electroweak precision tests where hadrons appear.

An important property of QCD is the asymptotic freedom. The coupling of QCD is scale-dependent and becomes smaller at higher energy scales. This property is unique to QCD. Other interactions of the Standard Model do not have it. The scale dependence restricts the region where perturbative calculation can be safely applied. At low energies, quarks become strongly coupled to gluons, and the perturbative calculation breaks down. Therefore, it is difficult to investigate hadron physics directly from QCD without using the effective theory.

Lattice QCD has become a standard tool to study quarks and gluons. It provides a fully non-perturbative calculation that does not rely on perturbative expansions. Since Wilson proposed the lattice gauge theory to demonstrate quark confinement in 1974, lattice QCD has achieved a lot of success. Measuring two- and three-point correlation functions, one can determine physical quantities such as decay constants and form factors from hadronic matrix elements. These parameters are important inputs for phenomenological studies of the Standard Model.

Apart from lattice QCD, another approach to the nonperturbative physics of QCD has been evolved, based on the analyticity of the correlation functions and quark-hadron duality. This approach enables us to link quarks in the Euclidean domain to hadrons in the physical energy domain. The spectral sum of hadronic correlation functions, such as the vacuum polarization function $\Pi(q^2)$, of the form,

$$\int ds\, e^{-s/M^2}\, \mathrm{Im}\, \Pi(s), \tag{1}$$

has often been introduced since the seminal work of Shifman, Vainshtein, and Zakharov in the late 1970's. The spectral sum (1) is equivalent to the Borel transform of the function $\Pi(q^2)$. The integral over invariant mass squared s smears out contributions of individual resonances so that one can use perturbative treatment of QCD with quarks and gluons as fundamental degrees of freedom, as far as the Borel mass M, a parameter to control the typical energy scale, is sufficiently large. The integral is a quantity effectively defined in the space-like momentum region, and there would be no issue of the violation of the quark-hadron duality.

The integral suppresses the contributions from the energy region above M, and thus is more sensitive to low-lying hadronic states. If one can find a window where M^2 is large enough to use perturbative expansion of QCD with non-perturbative corrections included by operator product expansion (OPE) and at the same time sufficiently small to be sensitive to lowest-lying hadronic states, the spectral sum may be used to obtain constraints on the parameters of low-lying hadrons, such as their masses and decay constants. This method, called the QCD sum rule, has been widely applied to estimate masses, decay constants, and other properties of hadronic states in various channels. However, an important question of how well the perturbative QCD with some non-perturbative corrections included through OPE can represent the spectral sum is yet to be addressed, especially when the correlation function is not always fully available from the experimental data, e.g. due to a limitation of accessible kinematical region.

In this thesis, we propose a method to use lattice QCD to compute the Borel transform of the vacuum polarization function appearing in the QCD sum rule. We construct the spectral sum corresponding to the Borel transform from two-point functions computed on the Euclidean lattice. As a proof of principle, we compute the $s\bar{s}$ correlators at three lattice spacings and take the continuum limit. We confirm that the method yields results that are consistent with the operator product expansion in the large Borel mass region. The method provides a ground on which the OPE analyses can be directly compared with non-perturbative lattice computations.

We find a good agreement between the lattice data and OPE in the region of $M > 1.0$ GeV. The OPE is truncated at the order of $1/M^6$. Since the OPE involves unknown condensates, this comparison can be used to determine these parameters, provided that the lattice data are sufficiently precise. As the first example, we attempt to extract the gluon condensate, which appears in OPE at the order $1/M^4$. The size of the error is comparable to those of previous phenomenological estimates. With more precise lattice data in various channels, one would be able to determine the condensates of higher dimensions as well, which have not been determined well solely from phenomenological inputs.

Our work provides a technique to relate two major tools to study nonperturbative aspects of QCD, i.e. the QCD sum rule and the lattice QCD. There would be a number of applications, for which new insights into the QCD phenomenology are expected.

Acknowledgements

I am deeply grateful to my PhD supervisor, Shoji Hashimoto, for his great advice, invaluable discussions, and continuous support. Without his help, I could not write my PhD thesis.

I was helped and supported by many people during my PhD studies. I thank the members of the JLQCD collaboration for discussions and for providing the computational framework and lattice data. In particular, I am indebted to my collaborators, Takashi Kaneko, Gabriela Bailas, and Katsumasa Nakayama. I also thank the members of the Field Theory Research Team at the RIKEN Center for Computational Science (R-CCS) for their warm welcome as a research associate; in particular, I appreciate Yasumich Aoki and Issaku Kanamori for constructive comments on this work. Moreover, I thank the past and present members of the Theory Center at High Energy Accelerator Research Organization (KEK). I am grateful to Kei Suzuki, Masaaki Tomii, Hiromasa Takaura, Kohta Hatakeyama, Mitsuaki Hirasawa, Jun-Sik Yoo, and Akira Matsumoto for fruitful discussions. Special thanks go to a secretary of the lattice group in KEK Theory Center, Maki Oishi, for her administrative support.

This work was supported by RIKEN Junior Research Associate Program. Numerical calculations are performed on SX-Aurora TSUBASA at KEK under its Particle, Nuclear and Astro Physics Simulation Program, as well as on Oakforest-PACS supercomputer operated by Joint Center for Advanced High Performance Computing (JCAHPC). This work used computational resources of supercomputer Fugaku provided by R-CCS through the HPCI System Research Project (Project ID: hp210146).

Finally, I would like to thank my family for their continuous encouragements and unconditional support.

Contents

List of Figures

List of Tables

Chapter 1

Introduction

Quantum Chromodynamics (QCD) describes the strong interaction between quarks and gluons. Quarks are the elementary particles that constitute hadrons. Therefore, QCD plays an important role even in various electroweak precision tests where hadrons appear.

An important property of QCD is the asymptotic freedom. The coupling of QCD is scale-dependent and becomes smaller at higher energy scales. This property is unique to QCD. Other interactions of the standard model do not have it. The scale dependence restricts the region where perturbative calculation can be safely applied. At low energies, quarks become strongly coupled to gluons, and the perturbative calculation breaks down. Therefore, it is difficult to investigate hadron physics directly from QCD without using the effective theory.

Lattice QCD has become a standard tool to study quarks and gluons. It provides a fully nonperturbative calculation that does not rely on the perturbative expansion. Since Wilson proposed the lattice gauge theory to demonstrate quark confinement in 1974 [1], lattice QCD has achieved a lot of success. Following the Monte Carlo calculations of the pure SU(2) gauge theory by Creutz in 1979 [2], various computational methods and algorithms have been introduced. Recent lattice studies have become more realistic and reliable. Those yield better understandings of the nonperturbative nature of QCD.

To study low-energy hadrons, lattice fermions are necessary. Nevertheless, the fermion action on the lattice cannot be defined by naively replacing derivatives by differences. This naive fermion has undesired poles, which is called the doublers. Wilson introduced a term in the action to remove the doublers, which breaks the chiral symmetry. With this fermion, Wilson fermion, hadron masses were computed using lattice QCD in 1981 [3, 4].

Including dynamical quarks in the lattice calculation is computationally demanding since those require a determinant of the Dirac operator. The early studies used the quenched approximation, which ignores these sea quark effects. Several methods have been proposed to overcome this problem, *e.g.* Hybrid Monte Carlo [5] or R-algorithm [6]. The state-of-the-art lattice simulation realize the simulation involving the dynamical light quarks.

A success of lattice QCD is the prediction of the hadron mass spectra. Comparison with experimental values requires the continuum limit, sufficiently large lattice volume s, and an extrapolation to the physical quark masses. The lattice results using Wilson fermions in quenched QCD have been reported in the literature *e.g.* [7, 8], where these requirements are satisfied. In [8], the deviation of the mass spectra from experiments is at most 11%. This would imply the limitation of the quenched approximation. Finally, the reproduction of the mass spectra was accomplished by the BMW Collaboration [9], using the Wilson fermions for dynamical u, d, and s quarks. These spectra were predicted with errors of several percents except for the Δ baryon. Those agreed with the masses in the experiments well. This success indicates a key role of the lattice QCD towards the search for new physics.

Chiral symmetry is an essential property of QCD and preserving the symmetry on the lattice would be desirable. In 1981, Ginsparg and Wilson proposed a relation which defines the lattice version of chiral symmetry; it is called Ginsparg-Wilson relation [10]. Several formulations of the fermion action satisfying this relation were discovered in the 1990s, such as domain-wall fermions [11, 12] and overlap fermions [13–15]. Recently, these Ginsparg-Wilson fermions are extensively used in actual simulations where chiral symmetry plays a significant role.

For the precise verification of the Standard Model and the search for new physics, it is essential to improve the accuracy of lattice QCD. The development of lattice QCD has been accompanied by the evolution of computational science. The realistic simulations of QCD can be implemented on massively parallel computers. The appearance of high-performance computers , such as Fugaku, will promote the development.

Apart from lattice QCD, another approach to explore nonperturbative dynamics has been developed, which is based on the analyticity of the correlation functions and quark-hadron duality. This approach enables us to link quarks in the Euclidean domain to hadrons in the physical energy domain. In particular, the spectral sum of hadronic correlation functions, such as the vacuum polarization function $\Pi(q^2)$, of the form,

$$\int ds\, e^{-s/M^2} \mathrm{Im}\, \Pi(s) \tag{1.1}$$

has often been introduced since the seminal work of Shifman, Vainshtein, and Zakharov [16, 17]. The integral over invariant mass squared s smears out contributions of individual resonances so that one can use perturbative treatment of QCD with quarks and gluons as fundamental degrees of freedom, as far as the Borel mass M, a parameter to control the typical energy scale, is sufficiently large. The integral (1.1) is a quantity effectively defined in the spacelike momentum region, and there would be no issue of the violation of the quark-hadron duality [18].

The integral (1.1) suppresses the contributions from the energy region above M and thus, is more sensitive to low-lying hadronic states. If one can find a window

where M^2 is large enough to use perturbative expansion of QCD with nonperturbative corrections included by operator product expansion (OPE) and at the same time sufficiently small to be sensitive to lowest-lying hadronic states, the spectral sum (1.1) may be used to obtain constraints on the parameters of low-lying hadrons, such as their masses and decay constants. This method, called the QCD sum rule, has been widely applied to estimate masses, decay constants, and other properties of hadronic states in various channels [16, 17]. However, an important question of how well the perturbative QCD with some nonperturbative corrections included through OPE can represent the spectral sum is yet to be addressed, especially when the correlation function is not always fully available from the experimental data, *e.g.* due to a limitation of accessible kinematical region.

In principle, the test of perturbative expansion and OPE can be performed using nonperturbatively calculated correlation functions using lattice QCD. Comparison of the lattice correlators at short distances with perturbative QCD may be found, *e.g.*, in [19–22] for light-hadron current-current correlators and in [23, 24] for charmonium correlators. The energy scale where the comparison is made has to be sufficiently low to avoid discretization effects in the lattice calculations, while the OPE analysis is more reliable at high energy scales. It has been pointed out that the convergence of OPE is a crucial problem in the energy region for which lattice QCD can provide reliable calculations by now [22, 25].

In this work, we perform another test of perturbative QCD and OPE against nonperturbative lattice computation using the spectral sum of the form (1.1). It has an advantage that the OPE converges more rapidly compared to that applied for the correlator itself either in the coordinate space or in the momentum space. And, this is exactly the quantity that has been used in many QCD sum rule analyses, hence it serves as a test of those sum rule calculations as well.

On the lattice, computation of the spectral sum (1.1) is highly nontrivial because it requires the spectral function $\rho(q^2) \propto \mathrm{Im}\,\Pi(q^2)$ for all values of timelike q^2 above the threshold where a cut begins. Extraction of the spectral function from the lattice correlators is a notoriously difficult problem that requires solving an ill-posed inverse problem. Namely, one has to extract $\rho(q^2)$ by solving

$$C(t) \equiv \sum_{\boldsymbol{x}} \langle 0|J(t,\boldsymbol{x})J(0,\boldsymbol{0})|0\rangle = \int_0^\infty d\omega\, \omega^2 \rho(\omega^2) e^{-\omega t} \tag{1.2}$$

with a lattice correlator $C(t)$ of a current operator J calculated at a discrete set of time separations. There have been several methods developed to perform this inverse-Laplace transform, including the maximum entropy method (MEM) [26–28], Bayesian approach [29], Backus-Gilbert approach [30–33], the sparse modeling method [34], but none of them succeeded to achieve sufficiently precise extraction of $\rho(\omega^2)$ that can be used for the purpose of this work.

In this work, instead, we apply the method developed in [35]. It is based on

a representation of the weight function $e^{-\omega^2/M^2}$ in (1.1) as a polynomial of $e^{-a\omega}$, which is then related to the transfer matrix $e^{-a\hat{H}}$ defined on the lattice. (Here, a stands for the lattice spacing.) The method relates the spectral sum directly to the lattice correlators without explicitly solving the spectral function $\rho(\omega^2)$, so that the inverse-Laplace transformation can be avoided. The method has so far been applied to the B meson inclusive semileptonic decays [36] as well as the inelastic lepton-nucleon scatterings [37]. As we demonstrate in the next sections, the method allows us to construct the spectral sum with small and controlled systematic errors.

This thesis is organized as follows. First, we review the basics of lattice QCD in Chap. 2. In Chap. 3 we introduce the spectral sum for the Borel transform in the continuum theory. We also introduce our method to compute the spectral sum from lattice QCD in Chap. 4. We discuss lattice calculations and their errors in Chap. 5. We also show comparison with OPE and the ground state contribution in this chapter. Chap. 6 is devoted to our conclusion and outlook.

Chapter 2

Basics of lattice QCD

2.1 QCD in the continuum theory

Before we discuss lattice QCD, we review the continuum theory of QCD which is a part of the Standard Model in this section.

QCD is an SU(3) Yang-Mills theory with fermions in the fundamental representation. The fermions and gauge boson are called quarks and gluons, respectively. We denote the quark fields by $q(x)$ and the gluon fields by $A_\mu(x) \equiv A^a_\mu(x)\lambda_a/2$, where λ_a is the Gell-Mann matrices. The Lagrangian density of QCD is constructed as

$$\mathcal{L} = -\frac{1}{2}\,\mathrm{tr}\left[G^{\mu\nu}G_{\mu\nu}\right] + \sum_{q=u,d,s,\cdots} \bar{q}(i\not{D} - m_q)q, \tag{2.1}$$

The gauge field strength tensor is defined by

$$G_{\mu\nu} = G^a_{\mu\nu}\frac{\lambda_a}{2}, \tag{2.2}$$

$$G^a_{\mu\nu} = \partial_\mu A^a_\nu - \partial_\nu A^a_\mu - g f^{abc} A^b_\mu A^c_\nu, \tag{2.3}$$

where g is the coupling constant and f^{abc} is the structure constant of $SU(3)$. The covariant derivative is written as

$$D_\mu = \partial_\mu - igA^a_\mu\frac{\lambda_a}{2}. \tag{2.4}$$

Due to the last term of (2.3), there exist gluon self-interactions, unlike Quantum Electrodynamics (QED). This leads to the asymptotic freedom of QCD.

Six quarks have been discovered by experiments. Some properties of the quarks, such as masses, electric charges, and quantum numbers are shown in Table 2.1. The third component of the isospin I_z is associated with an $SU(2)$ symmetry for u and d quarks. The other quarks also carry flavor quantum numbers and S, C, B, T stand for strangeness, charm, bottomness, and topness, respectively. The electric charges in the table are expressed in units of $e > 0$. We show the masses of the light quarks, u, d, and s, in the $\overline{\mathrm{MS}}$ scheme at the scale $\mu = 2$ GeV. On the other hand, m_c and m_b

	mass [GeV]	charge	I_z	S	C	B	T
u	$2.16^{+0.49}_{-0.26} \times 10^{-3}$	$+2/3$	$+1/2$				
d	$4.67^{+0.48}_{-0.17} \times 10^{-3}$	$-1/3$	$-1/2$				
s	$93^{+11}_{-5} \times 10^{-3}$	$-1/3$		-1			
c	1.27 ± 0.02	$+2/3$			$+1$		
b	$4.18^{+0.03}_{-0.02}$	$-1/3$				-1	
t	172.76 ± 0.30	$+2/3$					$+1$

TABLE 2.1: Quarks in the Standard Model.

is shown at the scale $\mu = m_c$ and $\mu = m_b$, respectively. These mass are taken from the Particle Data Group (PDG) [38].

2.1.1 Strong coupling constant

An essential parameter in QCD is the strong coupling constant α_s. In fact, we expand a variety of physical quantities by the coupling constant α_s in perturbative QCD. This enable s us to predict the quantities theoretically. For the computations, the expression of the α_s at a scale μ is necessary. In the following, we use $a_s \equiv \alpha_s/\pi$ rather than α_s itself for brevity.

The renormalization group (RG) equation of the strong coupling constant is expressed as

$$\mu^2 \frac{\mathrm{d}a_s}{\mathrm{d}\mu^2} = \beta(a_s), \tag{2.5}$$

where $\beta(a_s)$ is the β function of the coupling constant. At one-loop level where $\beta(a_s) = -\beta_0 a_s^2$, we can exactly solve the equation as

$$a_s(\mu^2) = \frac{1}{\beta_0 \log \mu^2 - C}. \tag{2.6}$$

One can define the integration constant C at $\mu^2 = \Lambda^2_{\mathrm{QCD}}$, where the coupling constant diverge *i.e.*

$$C = \beta_0 \log \Lambda^2_{\mathrm{QCD}}. \tag{2.7}$$

Then the running coupling at one-loop level is expressed as

$$a_s(\mu^2) = \frac{1}{\beta_0 \log\left(\mu^2/\Lambda^2_{\mathrm{QCD}}\right)}. \tag{2.8}$$

Currently, the β function at five-loop level is available [39–43], namely,

$$\beta(a_s) = -\sum_{i=0}^{4} \beta_i a_s^{2+i}, \tag{2.9}$$

with the coefficients in the $\overline{\text{MS}}$ scheme,

$$4\beta_0 = 11 - \frac{2}{3}n_f, \quad 4^2\beta_1 = 102 - \frac{38}{3}n_f, \tag{2.10}$$

$$4^3\beta_2 = \frac{2857}{2} - \frac{5033}{18}n_f + \frac{325}{54}n_f^2, \tag{2.11}$$

$$\begin{aligned} 4^4\beta_3 = {} & \frac{149753}{6} + 3564\zeta_3 - \left(\frac{1078361}{162} + \frac{6508}{27}\zeta_3\right)n_f \\ & + \left(\frac{50065}{162} + \frac{6472}{81}\zeta_3\right)n_f^2 + \frac{1093}{729}n_f^3, \end{aligned} \tag{2.12}$$

$$\begin{aligned} 4^5\beta_4 = {} & \frac{8157455}{16} + \frac{621885}{2}\zeta_3 - \frac{88209}{2}\zeta_4 - 288090\zeta_5 \\ & + n_f\left(-\frac{336460813}{1944} - \frac{4811164}{81}\zeta_3 + \frac{33935}{6}\zeta_4 + \frac{1358995}{27}\zeta_5\right) \\ & + n_f^2\left(\frac{25960913}{1944} + \frac{698531}{81}\zeta_3 - \frac{10526}{9}\zeta_4 - \frac{381760}{81}\zeta_5\right) \\ & + n_f^3\left(-\frac{630559}{5832} - \frac{48722}{243}\zeta_3 + \frac{1618}{27}\zeta_4 + \frac{460}{9}\zeta_5\right) \\ & + n_f^4\left(\frac{1205}{2916} - \frac{152}{81}\zeta_3\right), \end{aligned} \tag{2.13}$$

where n_f is the number of the active flavors and ζ_n denote the values of the Riemann zeta function. The first two coefficients β_0 and β_1 are renormalization scheme independent.

The sign of the β function leads to a remarkable property of QCD. At leading order, $\beta(a_s)$ is negative for $n_f \leq 16$ [44, 45]. This indicates the asymptotic freedom of QCD; that is, the coupling constant α_s decreases as the scale μ increases. This behavior is confirmed beyond the leading order. The two- and three-loop corrections are also negative for $n_f \leq 8$ [46, 47] and $n_f \leq 5$ [48, 49], respectively. Furthermore, the four-loop correction is always negative [50, 51]. The five-loop correction is negative except for extremely large n_f. Based on the asymptotic freedom, physical quantities may be calculable in perturbative QCD at sufficiently short distances.

Solving the equation (2.9) iteratively, we can obtain an expression of a_s up to $\mathcal{O}(1/L^4)$, where $L \equiv \log\left(\mu^2/\Lambda_{\text{QCD}}^2\right)$. We derive the solution in Appendix A. We show the numerical expression of the coupling constant in $\overline{\text{MS}}$ scheme for $n_f = 3$ as

$$a_s^{(4)}(\mu^2) = \sum_{n=1}^{4}\sum_{m=0}^{n} a_{nm} L^{-n} \log^m L, \tag{2.14}$$

where the coefficients a_{nm} are listed in Table 2.2. We plot the scale dependence of $a_s(\mu^2)$ in Fig. 2.1, where we set the QCD scale parameter $\Lambda_{\text{QCD}} = 0.332\,\text{GeV}$ and use

n	a_{n0}	a_{n1}	a_{n2}	a_{n3}	a_{n4}
1	0.44444444				
2		−0.35116598			
3	0.11505699	−0.27746448	0.27746448		
4	0.29988763	−0.49195886	0.54807798	−0.21923119	
5	0.26396881	−1.3365013	1.2104657	−0.75061873	0.17321971

TABLE 2.2: The coefficients of the coupling constant a_s for $n_f = 3$.

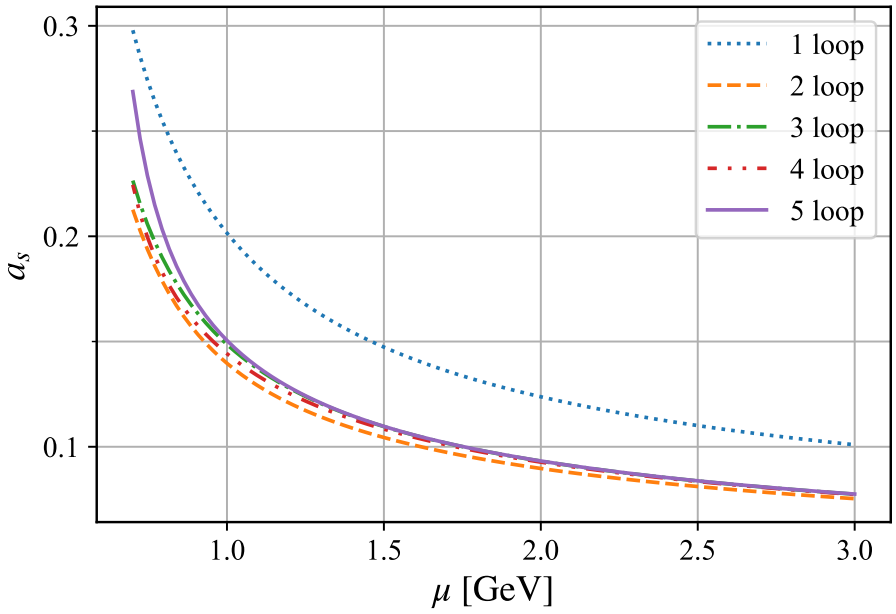

FIGURE 2.1: Running coupling constant a_s for given Λ_{QCD}. The dotted, dashed dash-dotted, and dash-dot-dotted lines correspond to a_s with $\beta(a_s)$ truncated at 1–4 loop level. The solid line corresponds to the coupling constant computed by the β function at five-loop level, which we will use in this work.

`RunDec` [52, 53] for the numerical calculation. The plot shows that the perturbative series converges well.

2.1.2 Quark mass

The quark mass appears at the next-to-leading order of OPE. For u and d quarks, the quark mass is negligibly small comparing to the scale where OPE is applicable. One would expect that the strange quark mass is also negligible. On the contrary, we will see that the mass correction significantly affects the Borel transform which is the main object of this thesis. In this subsection, we discuss the scale dependence of the quark mass. We will use the expression of the mass at a given scale in the following chapters.

The running of the quark mass is described by

$$\mu^2 \frac{\mathrm{d}m}{\mathrm{d}\mu^2} = m(\mu^2)\gamma_m(a_s), \tag{2.15}$$

where γ_m is the anomalous dimension. The anomalous dimension at five-loop level in the $\overline{\mathrm{MS}}$ scheme is expressed as follows [54–61]:

$$\gamma_m(a_s) = -\sum_{i=0}^{4} \gamma_{m,i} a_s^{i+1}, \tag{2.16}$$

where

$$\gamma_{m,0} = 1, \tag{2.17}$$

$$\gamma_{m,1} = \frac{101}{24} - \frac{5}{36} n_f, \tag{2.18}$$

$$\gamma_{m,2} = \frac{1249}{64} + n_f\left(-\frac{277}{216} - \frac{5}{6}\zeta_3\right) - \frac{35}{1296} n_f^2, \tag{2.19}$$

$$\begin{aligned}\gamma_{m,3} = {} & \frac{4603055}{41472} + \frac{530}{27}\zeta_3 - \frac{275}{8}\zeta_5 \\ & + n_f\left(-\frac{91723}{6912} - \frac{2137}{144}\zeta_3 + \frac{55}{16}\zeta_4 + \frac{575}{72}\zeta_5\right) \\ & + n_f^2\left(\frac{2621}{31104} + \frac{25}{72}\zeta_3 - \frac{5}{24}\zeta_4\right) + n_f^3\left(-\frac{83}{15552} + \frac{1}{108}\zeta_3\right),\end{aligned} \tag{2.20}$$

and

$$\begin{aligned}4^5\gamma_{m,4} = {} & \frac{99512327}{162} + \frac{46402466}{243}\zeta_3 + 96800\zeta_3^2 - \frac{698126}{9}\zeta_4 \\ & - \frac{231757160}{243}\zeta_5 + 242000\zeta_6 + 412720\zeta_7 \\ & + n_f\left(-\frac{150736283}{1458} - \frac{12538016}{81}\zeta_3 - \frac{75680}{9}\zeta_3^2 + \frac{2038742}{27}\zeta_4\right. \\ & \left. + \frac{49876180}{243}\zeta_5 - \frac{638000}{9}\zeta_6 - \frac{1820000}{27}\zeta_7\right) \\ & + n_f^2\left(\frac{1320742}{729} + \frac{2010824}{243}\zeta_3 + \frac{46400}{27}\zeta_3^2\right. \\ & \left. - \frac{166300}{27}\zeta_4 - \frac{264040}{81}\zeta_5 + \frac{92000}{27}\zeta_6\right) \\ & + n_f^3\left(\frac{91865}{1458} + \frac{12848}{81}\zeta_3 + \frac{448}{9}\zeta_4 - \frac{5120}{27}\zeta_5\right) \\ & + n_f^4\left(-\frac{260}{243} - \frac{320}{243}\zeta_3 + \frac{64}{27}\zeta_4\right).\end{aligned} \tag{2.21}$$

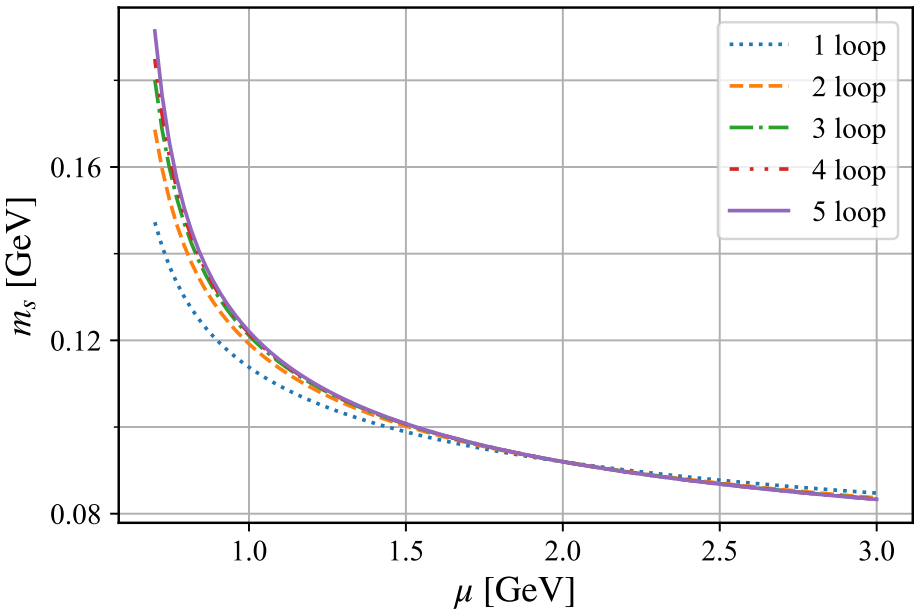

FIGURE 2.2: Running of the strange quark mass m_s. The dotted, dashed dash-dotted, and dash-dot-dotted lines correspond to $m_s(\mu)$ with $c(x)$ of (2.23) truncated at 1–4 loop level. The solid line corresponds to $m_s(\mu)$ computed by the β function and the anomalous dimension $\gamma_m(a_s)$ at five-loop level, which we will use in this work.

The solution of (2.15) has the following form:

$$\frac{m(\mu^2)}{m(\mu_0^2)} = \frac{c(a_s(\mu^2))}{c(a_s(\mu_0^2))}, \tag{2.22}$$

where the numerical expression of the function $c(x)$ at $n_f = 3$ is

$$\begin{aligned} c(x) = x^{\frac{4}{9}}(1 &+ 0.28490700x + 0.13895521x^2 \\ &+ 0.062944781x^3 + 0.096610252x^4). \end{aligned} \tag{2.23}$$

The derivation of this expression is given in Appendix B. The reference point μ is often taken at $\mu_0 = 2$ GeV for the light (u, d, and s) quarks. In contrast, for heavy quarks, $\mu_0 = m_c$ and $\mu_0 = m_b$ is often used. The numerical calculation of the running mass $m(\mu^2)$ can be performed by `RunDec` [52, 53] as well as the coupling constant $\alpha_s(\mu^2)$. We show running of the strange quark mass at the scale μ in Fig. 2.2. To plot this figure, we truncate (2.23) at the l-th order of x while the strong coupling constant $a_s(\mu^2)$ is computed at 5-loop level. We use $\Lambda_{QCD} = 0.332$ GeV and $m_s(2\,\text{GeV}) = 0.092$ GeV as inputs. The figure indicates that the truncation error is quite small.

2.2 The Euclidean action

The measurement in Lattice QCD is implemented by the Euclidean path integral. Introducing the Euclidean time, we identify the phase factor e^{iS} in the path integral as the Boltzmann weight. This allows us to use techniques of the statistical mechanics for lattice QCD in the Euclidean spacetime.

First, we discuss the gauge action in the Euclidean spacetime. We rescale the gauge field in (2.1) hereafter for brevity,

$$gA_\mu(x) \to A_\mu(x). \tag{2.24}$$

After the Wick rotation,

$$x_0 \to -ix_4,\ A_0 \to iA_4, \tag{2.25}$$

the components of the field strength tenser are redefined by

$$G^a_{\mu\nu} \equiv \partial_\mu A^a_\nu - \partial_\nu A^a_\mu - f^{abc} A^b_\mu A^c_\nu, \tag{2.26}$$

and the Euclidean action is given by

$$S_G = \frac{1}{4g^2} \int d^4x G^a_{\mu\nu} G^a_{\mu\nu}, \tag{2.27}$$

where μ and ν run from 1 to 4.

We turn to the Euclidean action for quark fields. The γ matriices in the Euclidean space fulfill the following anti-commutation relations,

$$\{\gamma_\mu, \gamma_\nu\} = 2\delta_{\mu\nu}. \tag{2.28}$$

The fermion action is given as

$$S_F = \sum_{q=u,d,s,\cdots} \int d^4x \bar{q}(\not{D} + m_q)q, \tag{2.29}$$

where the covariant derivative is redefined by

$$D_\mu = \partial_\mu - iA^a_\mu \frac{\lambda_a}{2}. \tag{2.30}$$

The use of the Euclidean action gives clear connection between the path integral in quantum field theory and statistical mechanics. In the Euclidean space, the phase in the path integral is replaced by the Boltzmann weight,

$$\exp(iS_{\rm QCD}) \to \exp(-S_{\rm QCD}), \tag{2.31}$$

where $S_{QCD} = S_G + S_F$ is the QCD action in the Euclidean space. The vacuum expectation value of a physical quantity O is given by

$$\langle O \rangle = \frac{1}{Z} \int \mathcal{D}\bar{\psi}\mathcal{D}\psi\mathcal{D}A\, e^{-S_{\rm QCD}} O, \tag{2.32}$$

where Z is the partition function defined as

$$Z \equiv \int \mathcal{D}\bar{\psi}\mathcal{D}\psi\mathcal{D}A\, e^{-S_{\rm QCD}}. \tag{2.33}$$

This path integral brings about analogy with the statistical mechanics. Hence, we can use several numerical techniques, such as Monte Carlo methods. In the subsequent sections, we review computations of lattice QCD using the Euclidean path integral.

2.3 Gluons in lattice QCD

We discuss the lattice action of gluons. First, we introduce link variables,

$$U_\mu(x) \equiv e^{iaA_\mu(x)}, \tag{2.34}$$

where a is the lattice spacing and g is the coupling constant. Let us consider a closed loop of these link valuables, the so-called plaquette,

$$U_{\mu\nu}(x) \equiv U_\mu(x) U_\nu(x+\hat{\mu}) U_\mu(x+\hat{\nu})^\dagger U_\nu(x)^\dagger, \tag{2.35}$$

where $\hat{\mu}$ is an unit vector in the μ-direction. We illustrate the link variable and the plaquette schematically in Fig. 2.3. This plaquette leads to the field strength $G_{\mu\nu}(x)$ towards the continuum limit $a \to 0$,

$$U_{\mu\nu}(x) \to \exp\bigl(ia^2 G_{\mu\nu}(x) + \mathcal{O}(a^3)\bigr). \tag{2.36}$$

Thus, we can construct the gauge action in terms of the plaquettes through

$$S_G = \frac{\beta}{3} \sum_x \sum_{\mu<\nu} \mathrm{Re}\,\mathrm{tr}\bigl[\mathbb{1} - U_{\mu\nu}(x)\bigr], \tag{2.37}$$

where the inverse coupling $\beta = 6/g^2$ is conventionally used instead of the coupling constant itself. The action (2.37) is called the Wilson action. In fact, this action reproduce the correct continuum limit up to the discretization effect,

$$S_G \simeq \frac{1}{4g^2} \int d^4x G^a_{\mu\nu} G^a_{\mu\nu}. \tag{2.38}$$

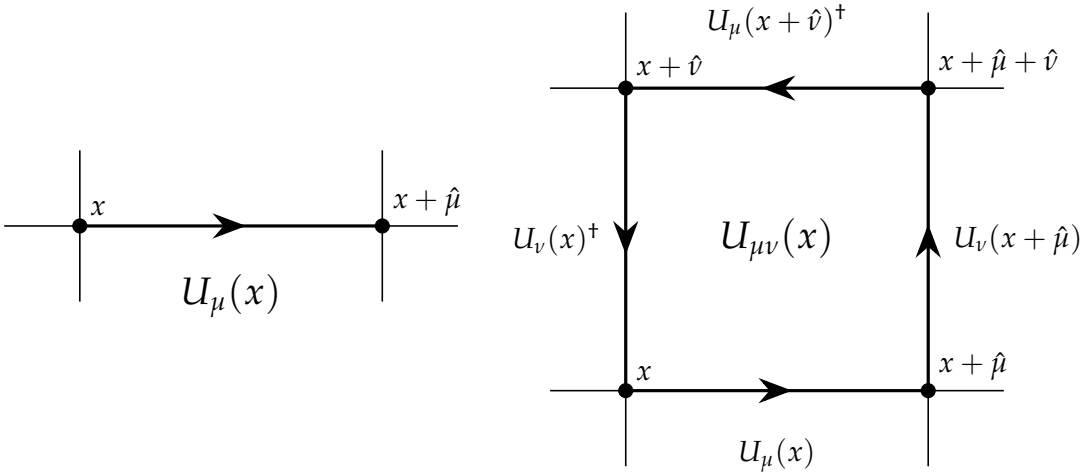

FIGURE 2.3: The link valuable and the plaquette.

The discretization error can be reduced by adding other loops, such as rectangles and parallelograms, to (2.37) [62]. In the small a expansion, the discretization effect is restricted due to the symmetry on the lattice and the dimension-five operators do not appear. Consequently, the dimension-six operators give rise to the leading $\mathcal{O}(a^2)$ corrections. In the present work, we use the tree-level Symanzik improved gauge action. This action contains the rectangular terms and the leading corrections become $\mathcal{O}(\alpha_s a^2)$.

2.4 Fermions in lattice QCD

We discuss lattice fermions in this section. We limit ourselves to the single-flavor case for notational convenience. The extension to multi flavor is straightforward.

Let us consider the discretization of the Dirac operator in the QCD action. On the lattice, we may replace the partial derivative by a finite-difference,

$$\partial_\mu \psi(x) \to \frac{\psi(x+\hat{\mu}) - \psi(x-\hat{\mu})}{2a}. \tag{2.39}$$

We realize that the term $\bar{\psi}(x)\gamma_\mu\psi(x+\hat{\mu})$ appearing in the fermion action breaks the gauge invariance. To make the lattice action gauge-invariant, we introduce the link variables $U_\mu(x)$ and construct the so-called naive fermion action as

$$\begin{aligned} S_F = a^4 \sum_x \Bigg[& \frac{1}{2a}\bar{\psi}(x)\gamma_\mu \Big(U_\mu(x)\psi(x+\hat{\mu}) - U_\mu(x-\hat{\mu})^\dagger \psi(x-\hat{\mu}) \Big) \\ & + m\bar{\psi}(x)\psi(x) \Bigg]. \end{aligned} \tag{2.40}$$

This action is consistent with (2.29) at the leading order of the small-a expansion. One might imagine that there would be no issue of the continuum limit. On the contrary, the naive fermion gives rise to the incorrect limit.

We demonstrate a well-known problem of the naive fermion action. As the simplest example, we consider the free fermion. The Fourier transform of the Dirac operator is given by

$$\tilde{D}(p) = m\mathbb{1} + \frac{i}{a}\sum_{\mu}\gamma_\mu \sin(p_\mu a), \tag{2.41}$$

and its inverse, *i.e.* the quark propagator, has the following form:

$$\tilde{D}(p)^{-1} = \frac{m\mathbb{1} - ia^{-1}\sum_\mu \gamma_\mu \sin(p_\mu a)}{m^2 + a^{-2}\sum_\mu \sin^2(p_\mu a)}. \tag{2.42}$$

In the massless limit, the denominator vanishes at $p_\mu = 0$ or π/a. This causes unphysical poles except for the pole at $p_\mu = (0,0,0,0)$. These 15 poles are called doublers. We have to remove the doublers to predict physical quantities from lattice QCD.

One can introduce the Wilson term in the Dirac operator to make the doublers irrelevant in the continuum limit,

$$\tilde{D}(p) = m\mathbb{1} + \frac{i}{a}\sum_{\mu}\gamma_\mu \sin(p_\mu a) + \mathbb{1}\frac{1}{a}\sum_{\mu}\big(1 - \cos(p_\mu a)\big). \tag{2.43}$$

The extra term is the higher-order correction for small a,

$$\frac{1}{a}\sum_{\mu}\big(1 - \cos(p_\mu a)\big) = \frac{a}{2}\sum_{\mu} p_\mu^2 + \mathcal{O}(a^3), \tag{2.44}$$

which corresponds to the discretization of the quadratic derivative $\partial_\mu\partial_\mu$. The Wilson term vanishes at $p_\mu = (0,0,0,0)$. In contrast, it leads to the additional mass for the doubler,

$$m + \frac{2\ell}{a}, \tag{2.45}$$

where ℓ is the number of the momentum components $p_\mu = \pi/a$. In the continuum limit $a \to 0$, the masses of the doublers become substantially large. Consequently, the doublers decouple from the continuum theory.

We return to the Dirac operator with the gauge interaction in the position space. One can derive the Wilson term as

$$-\frac{1}{2a}\sum_{\mu}\Big(U_\mu(x)\delta_{x+\hat{\mu},y} - 2\delta_{x,y} + U_\mu(x-\hat{\mu})^\dagger\delta_{x-\hat{\mu},y}\Big). \tag{2.46}$$

The fermion action of the Wilson fermion is given by

$$S_F = a^4\sum_{x,y}\bar{\psi}(x)D_W(x|y)\psi(y), \tag{2.47}$$

with the Wilson-Dirac operator,

$$D_W(x|y) = \left(m + \frac{4}{a}\right)\delta_{x,y} - \frac{1}{2a}\sum_\mu (\mathbb{1} - \gamma_\mu) U_\mu(x)\delta_{x+\hat{\mu},y} - \frac{1}{2a}\sum_\mu (\mathbb{1} + \gamma_\mu) U_\mu(x-\hat{\mu})^\dagger \delta_{x-\hat{\mu},y}. \tag{2.48}$$

The Wilson fermion action is explicitly breaks chiral symmetry even in the massless limit $m \to 0$. In the continuum limit, chiral symmetry of the fermion action can be expressed as

$$D\gamma_5 + \gamma_5 D = 0. \tag{2.49}$$

In fact, the operator $D = \gamma_\mu(\partial_\mu + iA_\mu)$ fulfills this equation. In contrast, the Wilson term (2.46) does not anti-commute with γ_5 since the term is proportional to $\mathbb{1}$.

The breaking of chiral symmetry is inseparable from the fermion doubling problem. According to the Nielsen–Ninomiya theorem [63, 64], one cannot preserve chiral symmetry in the lattice theory where the doublers do not appear. This would give rise to the limitation of lattice QCD, especially for the physics strongly related to chiral symmetry.

One expects that the relation (2.49) is modified by $\mathcal{O}(a)$ on the lattice. Based on a renormalization group transformation, Ginsparg and Wilson proposed the relation in [10], which is given by

$$D\gamma_5 + \gamma_5 D = aD\gamma_5 D. \tag{2.50}$$

The Dirac operator in the relation does not anti-commute with γ_5; therefore, it does not satisfy the assumption of the Nielsen–Ninomiya theorem. The extra term in r.h.s. vanishes in the continuum limit and the symmetry is recovered. The Ginsparg–Wilson relation (2.50) defines the lattice version of chiral symmetry.

There are several formulations of the fermion action that satisfy the Ginsparg–Wilson relation. In this work, we use the domain-wall fermion [11, 12] that obeys the relation in a certain limit. The action of the fermion is quite similar to the Wilson fermion action. Therefore, one can apply the same numerical techniques to the domain-Wall fermion as well as the Wilson fermion. More discussion of the Domain-Wall fermion is in Sec. 2.6.

2.5 Measurements of meson correlators

In this section, we discuss the computation of meson correlators. For later convenience, we separate the path integral into the fermionic part and the gluonic part.

The fermionic part is defined by

$$\langle O \rangle_F \equiv \frac{1}{Z_F} \int \mathcal{D}\bar{\psi}\mathcal{D}\psi \, e^{-S_F} O. \tag{2.51}$$

The denominator Z_F is the fermion determinant,

$$Z_F = \int \mathcal{D}\bar{\psi}\mathcal{D}\psi \, e^{-S_F} = \det D, \tag{2.52}$$

where D is a Dirac operator on the lattice. The fermion path integral can be performed by the Wick contraction as discussed in Sec. 2.5.3 later. The total path integral is written as

$$\langle O \rangle \equiv \frac{1}{Z} \int \mathcal{D}U \, e^{-S_G} \det D \, \langle O \rangle_F \,, \tag{2.53}$$

with the partition function

$$Z = \int \mathcal{D}U \, e^{-S_G} \det D. \tag{2.54}$$

This path integral can be computed numerically.

The determinant in (2.53) corresponds to the effect of sea quarks, that is, quark-antiquark pair creation and annihilation in the vacuum. Including the determinant in the simulation is, however, numerically hard since the Dirac matrix D has $(12 \times \text{lattice size})^2$ elements and the dimension $12 \times$ lattice size is typically $\gtrsim 10^6$. Hence, the quenched approximation was often used in early studies of lattice QCD, where dynamical sea quark loops are neglected by a replacement $\det D \to 1$. Currently, massively parallel computers provide accurate simulations with dynamical quarks using various numerical techniques.

The fermion determinant can be considered as a part of the Boltzmann weight. Using

$$\log \det D = \operatorname{tr} \log D, \tag{2.55}$$

we define an effective action

$$S_{\text{eff}} = S_G - \operatorname{tr} \log D. \tag{2.56}$$

Hence, the path integral can be rewritten as

$$\langle O \rangle = \frac{1}{Z} \int \mathcal{D}U \, e^{-S_{\text{eff}}} \langle O \rangle_F \,. \tag{2.57}$$

In Monte Carlo simulations, the path integral is approximated by an average of the values on gauge configurations distributed with the probability $\propto e^{-S_{\text{eff}}}$. We let $\langle O \rangle_F^{(i)}$ be the fermionic part of the path integral on the i-th gauge configuration. The

total path integral can be obtained through

$$\langle O \rangle \simeq \frac{1}{N_{\rm conf}} \sum_{i}^{N_{\rm conf}} \langle O \rangle_F^{(i)}, \tag{2.58}$$

where $N_{\rm conf}$ is the number of the configurations. In this work, we use the gauge configurations with $n_f = 2 + 1$ dynamical quarks, which are generated by the hybrid Monte Carlo algorithm [5].

2.5.1 Point-to-all propagator

For lattice fermions, completely solving the inverse of the Dirac operator is a quite difficult problem due to the limitations of computer memory and numerical costs. In practice, we do not compute the full inverse matrix of D. Instead, we consider the propagator G and the source S as vectors with a fixed source position of propagator $(t_0, \mathbf{x_0}, c_0, s_0)$, where c_0 is the color index and s_0 is the Dirac index. Using a local source vector,

$$S^{(\alpha_0, c_0)}(t, \mathbf{x})_{\substack{\alpha \\ c}} = \delta_{t,t_0}\delta_{\mathbf{x},\mathbf{x_0}}\delta_{\alpha,\alpha_0}\delta_{c,c_0}, \tag{2.59}$$

we write the solution of the Dirac equation as

$$\begin{aligned} G_{\rm local}^{(\alpha_0, c_0)}(t, \mathbf{x})_{\substack{\alpha \\ c}} &= \sum_{t', \mathbf{x}'} \sum_{\beta, d} D^{-1}(t, \mathbf{x} | t', \mathbf{x}')_{\substack{\alpha\beta \\ cd}} S^{(\alpha_0, c_0)}(t', \mathbf{x}')_{\substack{\beta \\ d}} \\ &= D^{-1}(t, \mathbf{x} | t_0, \mathbf{x_0})_{\substack{\alpha\alpha_0 \\ cc_0}}. \end{aligned} \tag{2.60}$$

The solution $G_{\rm local}^{(\alpha_0, c_0)}(t, \mathbf{x})_{\substack{\alpha \\ c}}$ is a quark propagator from the fixed source point $(t_0, \mathbf{x_0}, c_0, s_0)$ to the all sink point $(t, \mathbf{x}, c, s)$, namely point-to-all propagator.

In the following, we limit ourselves to a computation of connecting diagrams with degenerate quark masses. As we will see, it turns out that only 12 solutions, for all c_0 and s_0, are necessary.

2.5.2 γ_5-hermiticity

Most of lattice fermions are γ_5-hermitian, *i.e.* the Dirac operator satisfy the relation

$$\gamma_5 D \gamma_5 = D^\dagger. \tag{2.61}$$

In addition, the inverse of the operator D^{-1} is also γ_5-hermitian. This property can be used to compute meson correlators.

Let us consider the case of the Wilson fermions. We demonstrate that the the γ_5-hermiticity holds. The Dirac operator with the quark mass m in lattice unit is

given by

$$\begin{aligned} D_W(x|y)_{\alpha\beta} =& (m+4)\mathbb{1}_{\alpha\beta}\delta_{x,y} \\ & - \frac{1}{2}\sum_{\mu=1}^{4}(\mathbb{1}-\gamma_\mu)_{\alpha\beta}U_\mu(x)\delta_{x+\hat{\mu},y} \\ & - \frac{1}{2}\sum_{\mu=1}^{4}(\mathbb{1}+\gamma_\mu)_{\alpha\beta}U_\mu(x-\hat{\mu})^\dagger\delta_{x-\hat{\mu},y}, \end{aligned} \tag{2.62}$$

where $\hat{\mu}$ is an unit vector along the μ-direction. We omit the color indices for simplicity since the link variables U_μ commute with γ_5. Then,

$$\begin{aligned} (\gamma_5 D_W \gamma_5)_{\alpha\beta} =& (m+4)\mathbb{1}_{\alpha\beta}\delta_{x,y} \\ & - \frac{1}{2}\sum_{\mu=1}^{4}(\mathbb{1}+\gamma_\mu^\dagger)_{\alpha\beta}U_\mu(y-\hat{\mu})\delta_{x,y-\hat{\mu}} \\ & - \frac{1}{2}\sum_{\mu=1}^{4}(\mathbb{1}-\gamma_\mu^\dagger)_{\alpha\beta}U_\mu(y)^\dagger\delta_{x,y+\hat{\mu}} \\ =& D_W(x|y)^\dagger_{\alpha\beta}. \end{aligned} \tag{2.63}$$

Here, we use $\gamma_\mu^\dagger = \gamma_\mu$ and $\delta_{x\pm\hat{\mu},y} = \delta_{x,y\mp\hat{\mu}}$. We have derived the relation (2.61). This property is inherited by the domain-wall fermions since they consist of the Wilson fermions.

2.5.3 Correlation functions in coordinate space

The meson spectroscopy and amplitudes can be calculated from the correlation functions of operators with the corresponding quantum numbers. To extract QCD or low-energy parameters, we can use various quantities from the correlation functions, *e.g.*, time separated correlator $C(t)$, hadron vacuum polarization $\Pi(q^2)$, and temporal moment M_n. In particular, the two-point correlators in coordinate space have a clearer physical interpretation.

In this section, we only focus on the long-distance behavior of correlators. However we remark that the short-distance correlator also plays a role; renormalization [19] and determination of the strong coupling constant α_s [22, 24]. We will return to renormalization through the short-distance correlator in Sec. 2.7.

Let us consider the operator $J_P = i\bar{u}\gamma_5 d$, which corresponds to π^-. The two-point function in the coordinate space (X-space) is related to the quark propagators

by using the Wick theorem:

$$\begin{aligned}\langle 0|J_P(t,\mathbf{x})J_P^\dagger(0,\mathbf{0})|0\rangle_F &= \langle i\bar{u}\gamma_5 d(t,\mathbf{x})\, i\bar{d}\gamma_5 u(0,\mathbf{0})\rangle \\ &= \mathrm{tr}\left[\langle u(0,\mathbf{0})\bar{u}(t,\mathbf{x})\rangle_F \gamma_5 \langle d(t,\mathbf{x})\bar{d}(0,\mathbf{0})\rangle_F \gamma_5\right] \\ &= \mathrm{tr}\left[D_u^{-1}(0,\mathbf{0}|t,\mathbf{x})\gamma_5 D_d^{-1}(t,\mathbf{x}|0,\mathbf{0})\gamma_5\right], \end{aligned} \tag{2.64}$$

where tr denotes the trace of color and Dirac matrices. We ignore the isospin braking: $m_u = m_d = m$ and $D_u^{-1}(t,\mathbf{x}|0,\mathbf{0}) = D_d^{-1}(t,\mathbf{x}|0,\mathbf{0}) = D^{-1}(t,\mathbf{x}|0,\mathbf{0})$. Using the γ_5-hermiticity (2.61), the two-point correlator is written in terms of the propagator vector with the local sources (2.60):

$$\begin{aligned}\langle 0|J_P(t,\mathbf{x})J_P^\dagger(0,\mathbf{0})|0\rangle_F &= \mathrm{tr}\left[D^{-1}(0,\mathbf{0}|t,\mathbf{x})^\dagger D^{-1}(t,\mathbf{x}|0,\mathbf{0})\right] \\ &= \sum_{\alpha,\beta}\sum_{c,d}\left|D^{-1}(t,\mathbf{x}|0,\mathbf{0})_{\substack{\beta\alpha\\ dc}}\right|^2 \\ &= \sum_{\alpha,\beta}\sum_{c,d}\left|G^{(\alpha,c)}_{\mathrm{local}}(t,\mathbf{x})_{\substack{\beta\\ d}}\right|^2. \end{aligned} \tag{2.65}$$

The equation (2.65) implies that measurements of $\langle 0|J_P(t,\mathbf{x})J_P^\dagger(0,\mathbf{0})|0\rangle$ require the propagator from $(0,\mathbf{0})$ to $(t,\mathbf{x})$ with 12 local sources.

We extend (2.65) to other color singlet operators $J_\Gamma = \bar{u}\Gamma d$. Here, we assume $\Gamma = \mathbb{1}, \gamma_5, \gamma_\mu, \gamma_\mu\gamma_5, \sigma_{\mu\nu}$. We can easily check that the hermitian conjugate of these operators are equal to the operators swapped u and d up to the signature: $J_\Gamma^\dagger = d^\dagger\Gamma^\dagger\gamma_4 u = \pm\bar{d}\Gamma u$. The signature depends on Γ which we choose. Letting $\bar{J}_\Gamma \equiv \bar{d}\Gamma u$, we obtain the expression of the two-point correlation function as

$$\begin{aligned}\langle 0|J_\Gamma(t,\mathbf{x})\bar{J}_\Gamma(0,\mathbf{0})|0\rangle_F &= -\,\mathrm{tr}\left[D^{-1}(0,\mathbf{0}|t,\mathbf{x})^\dagger\gamma_5\Gamma D^{-1}(t,\mathbf{x}|0,\mathbf{0})\Gamma\gamma_5\right] \\ &= -\sum_{\substack{\alpha,\beta\\ \rho,\sigma}}\sum_{c,d} D^{-1}(t,\mathbf{x}|0,\mathbf{0})^*_{\substack{\rho\sigma\\ dc}}(\gamma_5\Gamma)_{\rho\beta} D^{-1}(t,\mathbf{x}|0,\mathbf{0})_{\substack{\beta\alpha\\ dc}}(\Gamma\gamma_5)_{\alpha\sigma} \\ &= -\sum_{\substack{\alpha,\beta\\ \rho,\sigma}}\sum_{c,d} G^{(\sigma,c)}_{\mathrm{local}}(t,\mathbf{x})^*_{\substack{\rho\\ d}}(\gamma_5\Gamma)_{\rho\beta} G^{(\alpha,c)}_{\mathrm{local}}(t,\mathbf{x})_{\substack{\beta\\ d}}(\Gamma\gamma_5)_{\alpha\sigma}. \end{aligned} \tag{2.66}$$

The two operators of the correlation function may have the different matrix Γ. We show the correlation function for $J_{\Gamma_1} = \bar{u}\Gamma_1 d$ and $\bar{J}_{\Gamma_2} = \bar{d}\Gamma_2 u$

$$\begin{aligned}\langle 0|J_{\Gamma_1}(t,\mathbf{x})\bar{J}_{\Gamma_2}(0,\mathbf{0})|0\rangle_F &= -\,\mathrm{tr}\left[D^{-1}(0,\mathbf{0}|t,\mathbf{x})^\dagger\gamma_5\Gamma_1 D^{-1}(t,\mathbf{x}|0,\mathbf{0})\Gamma_2\gamma_5\right] \\ &= -\sum_{\substack{\alpha,\beta\\ \rho,\sigma}}\sum_{c,d} G^{(\sigma,c)}(t,\mathbf{x})^*_{\substack{\rho\\ d}}(\gamma_5\Gamma_1)_{\rho\beta} G^{(\alpha,c)}(t,\mathbf{x})_{\substack{\beta\\ d}}(\Gamma_2\gamma_5)_{\alpha\sigma}. \end{aligned} \tag{2.67}$$

However, not all combinations are worth to measure, since the possible intermediate states are restricted by the quantum numbers of operators. A nonzero and important combination of operators is, for example, $J_{\Gamma_1} = \bar{u}\gamma_5 d$ and $J_{\Gamma_2} = \bar{d}\gamma_4\gamma_5 d$, which will

be appear in the discussion of the PCAC relation in Sec. 2.8.

2.5.4 Correlation functions with zero momentum

Let us consider the sum of the two-point correlator over all spatial point, that is, the projection to zero momentum. Accordingly we can measure the spectra of the mesons in the rest frame from the sum. For large time separation t, the correlation function (with zero momentum) is dominated by the lowest-lying state. We can express the correlator as an exponential function:

$$C(t) \equiv \sum_{\mathbf{x}} \langle 0|J(t,\mathbf{x})J^{\dagger}(0,\mathbf{0})|0\rangle \tag{2.68}$$

$$\simeq \frac{|\langle 0|J|h\rangle|^2}{2m_h} e^{-m_h t}, \tag{2.69}$$

where h is the ground-state hadron and m_h is its mass.

We may estimate the mass by taking the logarithm since the correlator decrease exponentially. We define

$$m_{\text{eff}} \equiv \log \frac{C(t)}{C(t+1)}, \tag{2.70}$$

which is called the effective mass. Under periodic boundary conditions, the correlator is modified as

$$C(t) \simeq \frac{|\langle 0|J|h\rangle|^2}{2m_h}\left(e^{-m_h t} + e^{-m_h(T-t)}\right), \tag{2.71}$$

where T is the temporal extent of the lattice. Since a ratio of correlators is approximately proportional to a cosh function ,

$$\frac{C(t+1)+C(t-1)}{C(t)} \simeq e^{-m_h} + e^{+m_h}, \tag{2.72}$$

we can redefine the effective mass as

$$m_{\text{eff}} \equiv \cosh^{-1}\left(\frac{C(t+1)+C(t-1)}{2C(t)}\right) \tag{2.73}$$

to take the periodicity into account. In practice, the effective mass is used as a criterion of the fit range. To determine the mass or the hadronic matrix element, we fit the function (2.69) or (2.71) in the range where the the effective mass shows a plateau. The effective mass quantitatively indicates whether the grand state sufficiently saturates the correlator, or not.

The excited states are also of interest in the study of (lattice) QCD. However, the measurements of these state are more difficult than that of the ground state. Letting an energy of a state E, the state exponentially decay as $e^{-(E-m_h)t}$ and is buried in

the ground state. Moreover, the contribution of the excited state would be called "contamination" if one were interested in the low-energy reaction. By contrast, this contribution is important in this work, since we investigate the intermediate regime where the short-distance effect competes with the long-distance one. Our analysis of the spectral sum may shed light on the role of the higher energy spectra.

2.5.5 Noise source

We introduce a noise source for estimating the sum over the spatial position of the source points $\mathbf{x_0}$. As we discussed in Sec. 2.5.1, the local source fixes the source position to a single point. If the calculation of the correlation function were performed only once for each gauge configuration, a lot of information would be wasted. In addition, the number of the configuration has to be limited. Solving the Dirac equation with a translated source position, we increase not only the statistics, but also the numerical cost. Nevertheless, the noise source enables us to estimate the propagator from all spatial point $\mathbf{x_0}$ with the same cost.

We discuss the correlation function $C(t)$ with the noise source and the relation between the noisy and local sources. Let us consider a noise vector η assigned a random number at each spatial point, which satisfy

$$\left\langle\!\left\langle \eta(\mathbf{x})\eta(\mathbf{y})^\dagger \right\rangle\!\right\rangle = \delta_{\mathbf{x},\mathbf{y}}. \tag{2.74}$$

Here, $\langle\!\langle\cdot\rangle\!\rangle$ denotes an expectation value for the random numbers. The equation implies that the random numbers are independent. The type of the random numbers are optional. In this work, we use the Z_2 random number, that is, $\eta(\mathbf{x}) = \pm 1$. [1] We define a Z_2 noise source distributed at a time slice t_0 as

$$S_{Z_2}^{(\alpha_0,c_0)}(t,\mathbf{x})_{\substack{\alpha\\c}} = \delta_{t,t_0}\delta_{\alpha,\alpha_0},\delta_{c,c_0}\eta(\mathbf{x}). \tag{2.75}$$

The solution of the Dirac equation with the source $S_{Z_2}^{(\alpha_0,c_0)}$ is expressed as

$$G_{Z_2}^{(\alpha_0,c_0)}(t,\mathbf{x})_{\substack{\alpha\\c}} = \sum_{\mathbf{x_0}} D^{-1}(t,\mathbf{x}|t_0,\mathbf{x_0})_{\substack{\alpha\alpha_0\\cc_0}}\eta(\mathbf{x_0}). \tag{2.76}$$

[1] We can extend the Z_2 noise to a complex one as $\eta(\mathbf{x}) = (\pm 1 \pm i)/\sqrt{2}$, which obviously satisfy (2.74). It is often called a $Z_2 \otimes Z_2$ source.

Replacing $G^{(\alpha,c)}_{\rm local}(t,\mathbf{x})$ with $G^{(\alpha_0,c_0)}_{Z_2}(t,\mathbf{x})$ in (2.66), we obtain a zero momentum projected correlator $C(t)$:

$$
\begin{aligned}
&-\left\langle\!\!\left\langle \sum_{\substack{\alpha,\beta\\ \rho,\sigma}}\sum_{c,d} G^{(\sigma,c)}_{Z_2}(t,\mathbf{x})^*_{\rho\,d}(\gamma_5\Gamma)_{\rho\beta}G^{(\alpha,c)}_{Z_2}(t,\mathbf{x})_{\beta\,d}(\Gamma\gamma_5)_{\alpha\sigma}\right\rangle\!\!\right\rangle \\
&= -\sum_{\mathbf{x},\mathbf{x_0}\mathbf{y_0}}\left\langle\!\!\left\langle \mathrm{tr}\left[\eta(\mathbf{y_0})^\dagger D^{-1}(t_0,\mathbf{y_0}|t,\mathbf{x})^\dagger\gamma_5\Gamma D^{-1}(t,\mathbf{x}|t_0,\mathbf{x_0})\eta(\mathbf{x_0})\Gamma\gamma_5\right]\right\rangle\!\!\right\rangle \\
&\simeq -\sum_{\mathbf{x},\mathbf{x_0}}\mathrm{tr}\left[D^{-1}(t_0,\mathbf{x_0}|t,\mathbf{x})^\dagger\gamma_5\Gamma D^{-1}(t,\mathbf{x}|t_0,\mathbf{x_0}))\Gamma\gamma_5\right] \\
&= \sum_{\mathbf{x},\mathbf{x_0}}\langle 0|J_\Gamma(t,\mathbf{x})\bar{J}_\Gamma(t_0,\mathbf{x_0})|0\rangle_F\,.
\end{aligned}
\tag{2.77}
$$

In the third step, we have used (2.74). From the result (2.77), we have demonstrated that the noise source indeed estimates the sum of the local correlator over the source position $\mathbf{x_0}$.

Considering the coordinates $\mathbf{x}$ and $\mathbf{x_0}$ simply as indices of the propagator matrix, the noise vector stochastically estimate the trace. We may estimate the color or spin trace by distributing the noise vector over the corresponding internal degrees of freedom. For example, the linked source distributed over the color space [65, 66],

$$
S^{(\alpha_0)}_{\rm linked}(t,\mathbf{x})^\alpha_{\ c} = \delta_{t,t_0}\delta_{\alpha,\alpha_0}\eta(\mathbf{x})_c, \tag{2.78}
$$

$$
\left\langle\!\!\left\langle \eta(\mathbf{x})_c\eta(\mathbf{y})^\dagger_d\right\rangle\!\!\right\rangle = \delta_{\mathbf{x},\mathbf{y}}\delta_{c,d}, \tag{2.79}
$$

and the source distributed over the color and spinor space [67],

$$
\tilde{S}_{Z_2}(t,\mathbf{x})^\alpha_{\ c} = \delta_{t,t_0}\tilde{\eta}(\mathbf{x})^\alpha_{\ c}, \tag{2.80}
$$

$$
\left\langle\!\!\left\langle \tilde{\eta}(\mathbf{x})^\alpha_{\ c}\tilde{\eta}(\mathbf{y})^\dagger_{\beta\ d}\right\rangle\!\!\right\rangle = \delta_{\mathbf{x},\mathbf{y}}\delta_{c,d}\delta_{\alpha,\beta}, \tag{2.81}
$$

are used in the literature. These sources save the computational costs, however, the results are more affected by the stochastic noise. Moreover, if $\gamma_5\Gamma$ is not diagonal, we can not simply measure the correlators by the source $\tilde{S}_{Z_2}$. In this case, we need the following solution vectors for each Γ:

$$
\tilde{G}^\Gamma_{Z_2}(t,\mathbf{x}) = \sum_{\mathbf{x_0}} D^{-1}(t,\mathbf{x}|t_0,\mathbf{x_0})(\Gamma\gamma_5)^\dagger\tilde{\eta}(\mathbf{x_0}), \tag{2.82}
$$

besides the solution for the source $\tilde{S}_{Z_2}$,

$$
\tilde{G}_{Z_2}(t,\mathbf{x}) = \sum_{\mathbf{x_0}} D^{-1}(t,\mathbf{x}|t_0,\mathbf{x_0})\tilde{\eta}(\mathbf{x_0}). \tag{2.83}
$$

Similarly, the source distributed over the color space can not simply measure the two-point correlation function of the color octets. We have to choose the appropriate

source for the correlator to measure. More detailed discussion can be found in [68].

2.6 Möbius Domain-Wall fermions

In this work, we use the Möbius Domain-Wall (MDW) fermions [69]. MDW fermions are defined on a 5D lattice, which consists of 4D spacetime and one extra dimension. This lattice fermions have a good chiral property. The chiral symmetry is broken by the finite extent of the extra dimension, L_s. In our ensembles, the symmetry breaking effect is negligibly small. Therefore some chiral relations in the continuum limit hold even at finite lattice spacing. For instance, the short-distance correlators for the vector (scalar) and axial vector (pseudo scalar) are consistent up to finite mass and nonperturbative corrections. It helps us to compare lattice results with the counterparts in the continuum limit.

The domain-wall fermion action for 5D fermion fields $\psi(x,s)$ is defined by

$$S_{\mathrm{DW}} = \sum_{x,y} \sum_{s,r=0}^{L_s-1} \bar{\psi}(x,s) D_{\mathrm{GDW}}(x,s|y,r) \psi(y,r), \tag{2.84}$$

where x, y are the coordinates in the 4D spacetime and s, r are the indices of the extra dimension. The operator D_{GDW} is a generalized domain-wall Dirac operator, including the Shamir-type [70] and Boriçi-type [71, 72]. This operator D_{GDW} can be written as a band matrix for s and r, except for the mass term:

$$D_{\mathrm{GDW}} = \begin{pmatrix} \tilde{D} & -P_- & & & & mP_+ \\ -P_+ & \tilde{D} & -P_- & & & \\ & -P_+ & \tilde{D} & -P_- & & \\ & & \ddots & \ddots & \ddots & \\ & & & -P_+ & \tilde{D} & -P_- \\ mP_- & & & & -P_+ & \tilde{D} \end{pmatrix}. \tag{2.85}$$

Here, m is the bare mass of the fermions and $P_\pm = (1 \pm \gamma_5)/2$ are chirality projection operators. The operator $\tilde{D}$ is defined by the 4D Wilson-Dirac operator $D_W(-M)$ with a negative mass M [2]:

$$\tilde{D} = D_-^{-1} D_+ \tag{2.86}$$

$$D_- = 1 - c D_W(-M) \tag{2.87}$$

$$D_+ = 1 + b D_W(-M). \tag{2.88}$$

[2] M corresponds to the domain-wall height.

Setting $(b,c) = (3/2, 1/2)$, we define the MDW fermions D_{MDW}.[3] By the definition (2.85), we have to solve the inverse of D_- for all diagonal components. Thus we multiply the definition (2.85) by D_- and redefine the operator,

$$\hat{D}_{\mathrm{MDW}} \equiv D_- D_{\mathrm{MDW}} \tag{2.89}$$

$$= \begin{pmatrix} D_+ & -D_-P_- & & & & & mD_-P_+ \\ -D_-P_+ & D_+ & -D_-P_- & & & & \\ & -D_-P_+ & D_+ & -D_-P_- & & & \\ & & \ddots & \ddots & \ddots & & \\ & & & -D_-P_+ & D_+ & -D_-P_- & \\ mD_-P_- & & & & -D_-P_+ & D_+ & \end{pmatrix}. \tag{2.90}$$

In practice, we solve equations for $\hat{D}_{\mathrm{MDW}}$ rather than D_{MDW} to obtain the 4D quark propagator.

Letting S and G be the source and the propagator for the Dirac operator D_{MDW}, those are related as

$$\hat{D}_{\mathrm{MDW}}(x,s|y,r)G(y,r|x_0,s_0) = S(x,s|x_0,s_0), \tag{2.91}$$

where x, y, x_0 are the coordinate in the 4D spacetime and s, r, s_0 are the indices of the extra dimension. The color and spinor indices are omitted. We can compute hadron correlators from the solution

$$G(x,s|x_0,s_0) = \hat{D}^{-1}_{\mathrm{MDW}}(x,s|y,r)S(y,r|x_0,s_0) \tag{2.92}$$

following Wick contraction as discussed in Section 2.5.

To obtain physical quantities composed by 4D quark s, we have to properly project 5D fermion fields $\psi(x,s)$ onto 4D spacetime. We construct the 4D quark fields as

$$q(x) = P_-\psi(x,0) + P_+\psi(x,L_s-1), \tag{2.93}$$

$$\bar{q}(x) = \bar{\psi}(x,0)P_+ + \bar{\psi}(x,L_s-1)P_- \tag{2.94}$$

[3] The sets of the coefficients $(b,c) = (1,0)$ and $(b,c) = (1,1)$ correspond to the Shamir- and Borici-type domain wall fermions, respectively.

since the left-handed and right-handed mode live near $s = 0$ and $s = L_s - 1$, respectively . Thus the 4D quark propagator D_{4D}^{-1} can be related to $\hat{D}_{\rm MDW}^{-1}$:

$$\begin{aligned} D_{\rm 4D}^{-1}(x|y) &\equiv \langle q(x)\bar{q}(y)\rangle_F \\ &= P_- D_{\rm MDW}^{-1}(x,0;y,0)P_+ + P_- D_{\rm MDW}^{-1}(x,0;y,L_s-1)P_- \\ &\quad + P_+ D_{\rm MDW}^{-1}(x,L_s-1;y,0)P_+ + P_+ D_{\rm MDW}^{-1}(x,L_s-1;y,L_s-1)P_- \\ &= (\delta_{s,0}P_- + \delta_{s,L_s-1}P_+) D_{\rm MDW}^{-1}(x,s|y,r)(\delta_{r,0}P_+ + \delta_{r,L_s-1}P_-) \\ &= (\delta_{s,0}P_- + \delta_{s,L_s-1}P_+) \hat{D}_{\rm MDW}^{-1}(x,s;y,r) D_-(\delta_{r,0}P_+ + \delta_{r,L_s-1}P_-). \end{aligned} \tag{2.95}$$

We can obtain the 4D propagator by multiplying the source S and the solution $G(x,s|x_0,s_0)$ in the equation (2.92) by $D_-(\delta_{r,0}P_+ + \delta_{r,L_s-1}P_-)$ and $(\delta_{s,0}P_- + \delta_{s,L_s-1}P_+)$, respectively. Using the solution (2.92) with the relation (2.95), we can measure hadron correlation functions as discussed in the previous sections.

2.7 Renormalization of lattice operators

Lattice QCD has been used to study hadronic decays and transition processes nonperturbatively. Measuring two- and three-point correlation functions, one extracts parameters such as decay constants and form factors from hadronic matrix elements. These parameters are important inputs for the phenomenological study of the Standard Model.

Renormalization is necessary in the calculation of hadronic matrix elements. These matrix elements from lattice QCD do not correspond to the values in the renormalization scheme of the continuum theory (usually $\overline{\rm MS}$). Even if an operator involved in these matrix elements has no anomalous dimensions, such as locally constructed vector currents $\bar{q}\gamma_\mu q$, the renormalization has to be done since the current does not conserve due to lattice artifacts. These physical quantities computed on the lattice can be used in the continuum theory after the renormalization.

We can perform renormalization through matching. The basic strategy is as follows. We measure some physical quantity containing the operator in lattice QCD. We calculate the same quantity in the $\overline{\rm MS}$ scheme perturbatively. Then we determine the renormalization constant by requiring them to be equal. Notice that it is also possible to match via an intermediate scheme such as the RI/MOM scheme [73]. However, we focus on the direct renormalization method in this work. The quantity used for the matching should be easy to control the discretization error in lattice QCD. At the same time, the typical energy scale of the quantity has to be sufficiently large to use the perturbative expansion and operator product expansion (OPE). If we find the quantity which satisfies these requirements, the renormalization constant will be less affected by the systematic error.

We review the X-space method, which gives the renormalization constant [19] we will use in Chap. 5. The X-space method use a correlation function with a finite separation $|x|$:

$$\Pi^{\rm lat}(x^2, a^2) = \langle 0|J_\Gamma(x)\bar{J}_\Gamma(0)|0\rangle \tag{2.96}$$

We can directly measure the correlator (see Sec. 2.5.3). Using a renormalization constant $Z_\Gamma^{\overline{\rm MS}/{\rm lat}}$ for J_Γ, we may relate the correlator up to the nonperturbative and discretization effect ,

$$\Pi^{\overline{\rm MS}}(\mu^2; x^2) = \left(Z_\Gamma^{\overline{\rm MS}/{\rm lat}}(\mu^2, a^2)\right)^2 \Pi^{\rm lat}(a^2; x). \tag{2.97}$$

Here, $\Pi^{\overline{\rm MS}}$ is the corresponding perturbative series in the $\overline{\rm MS}$ scheme. We consider this equation as the renormalization condition. Solving it for $Z_\Gamma^{\overline{\rm MS}/{\rm lat}}$, we can express the solution in the following form:

$$\tilde{Z}_\Gamma^{\overline{\rm MS}/{\rm lat}}(\mu^2, a^2; x) \equiv \sqrt{\frac{\Pi^{\overline{\rm MS}}(\mu^2; x^2)}{\Pi^{\rm lat}(a^2; x)}} \tag{2.98}$$

$$= Z_\Gamma^{\overline{\rm MS}/{\rm lat}}(\mu^2, a^2) + C_{-2}(a/x)^2 + C_4 x^4 + C_6 x^6. \tag{2.99}$$

The discretization error is incorporated into this function as C_{-2}. The coefficient C_4 and C_6 correspond to the nonperturbative correction of the mass-dimension four and six operators, respectively. Accordingly, we can determine the renormalization constant $Z_\Gamma^{\overline{\rm MS}/{\rm lat}}(\mu^2, a^2)$ by a fit of $\tilde{Z}_\Gamma^{\overline{\rm MS}/{\rm lat}}(\mu^2, a^2; x)$.

The renormalization constants for the MDW fermion has the chiral symmetry. In other words, the renormalization constant of the vector courent $\bar{q}\gamma_\mu q$ is equivalent to that of the axial current $\bar{q}\gamma_\mu\gamma_5 q$:

$$Z_V^{\overline{\rm MS}/{\rm lat}}(a^2) = Z_A^{\overline{\rm MS}/{\rm lat}}(a^2). \tag{2.100}$$

Here, we omit the dependence on the scale μ since the (axial) vector has zero anomalous dimension. Similarly, For the (pseudo) scalar density

$$Z_S^{\overline{\rm MS}/{\rm lat}}(\mu^2, a^2) = Z_P^{\overline{\rm MS}/{\rm lat}}(\mu^2, a^2) \tag{2.101}$$

holds. Taking advantage of these chiral property, [19] determines the renormalization constant by combining $\tilde{Z}_\Gamma^{\overline{\rm MS}/{\rm lat}}(\mu^2, a^2; x)$ to cancel some of the nonperturbative effects that appear in the fit. Respecting the symmetry not only makes the renormalization procedure simpler, but also helps us to determine the constant Z_Γ.

2.8 PCAC relation of the Domain-wall fermion

In this section we summarize the partially conserved axial vector current (PCAC) relations associated with chiral symmetry. We discuss how it holds on the lattice and see how it affects the correlation function. We refer to [74, 75] in this section.

First, we review the PCAC relation in the continuum theory. We define isovector axial currents and pseudoscalar density operators

$$A_\mu^a \equiv \frac{1}{2}\bar{\psi}\gamma_\mu\gamma_5\tau^a\psi, \tag{2.102}$$

$$P^a \equiv \frac{1}{2}\bar{\psi}\gamma_5\tau^a\psi, \tag{2.103}$$

where, $\psi = (u, d)^T$ and τ^a is the Pauli matrix. We consider an infinitesimal chiral rotation

$$\delta\psi(x) = \frac{1}{2}\omega^a(x)\gamma_5\tau^a\psi(x), \tag{2.104}$$

$$\delta\bar{\psi}(x) = \frac{1}{2}\omega^a(x)\bar{\psi}(x)\gamma_5\tau^a. \tag{2.105}$$

According to the Ward-Takahashi identity, we can relate the change of the action S and an operator $\mathcal{O}$ under this transformation as

$$\langle 0|\delta S O|0\rangle = \langle 0|\delta\mathcal{O}|0\rangle\,. \tag{2.106}$$

The expression of the change of the action is

$$\delta S = \int d^4x\,\omega^a\Big(-\partial_\mu A_\mu^a + 2mP^a\Big), \tag{2.107}$$

where we ignore the isospin breaking, namely $m = m_u = m_d$. Specifying $\omega^b(x) = \omega\delta_{ab}\delta(x-y)$ and $\mathcal{O} = P^a(y)$, one can derive

$$\delta\mathcal{O} = 2\omega\delta(x-y)\bar{\psi}\psi(y). \tag{2.108}$$

Therefore, we obtain an identity

$$\langle 0|\partial_\mu A_\mu^a(x)P^a(y)|0\rangle - 2m\langle 0|P^a(x)P^a(y)|0\rangle = 2\delta(x-y)\langle 0|\bar{\psi}\psi(y)|0\rangle\,. \tag{2.109}$$

Focusing on the low energy, we derive the PCAC relation from (2.109). We consider correlators with a time separation t by summing over the spatial coordinate $\mathbf{x}$. For simplicity, we assume $y = (0, \mathbf{0})$. The first term in the l.h.s. of (2.109) yields a non-zero value only if $\mu = 4$ since the operator $\partial_\mu A_\mu^a(x)$ is projected to zero momentum. For large t, the contribution of π mesons is dominant. By the definition of the pion

decay constant, the matrix element of the axial current is written as

$$\partial_t \langle 0|A_4^a(x)|\pi^a(\mathbf{p}=\mathbf{0})\rangle = m_\pi^2 f_\pi e^{-m_\pi t}. \tag{2.110}$$

Therefore, we can express an asymptotic form of the correlator

$$\begin{aligned}&\sum_{\mathbf{x}} \langle 0|\partial_t A_4^a(t,\mathbf{x}) P^a(0,\mathbf{0})|0\rangle \\ \simeq &\frac{m_\pi f_\pi}{2} e^{-m_\pi t} \langle \pi^a(\mathbf{0})|P^a|0\rangle .\end{aligned} \tag{2.111}$$

At the same time, the correlator of the pseudoscalar can be expressed as

$$\begin{aligned}&\sum_{\mathbf{x}} \langle 0|P^a(t,\mathbf{x}) P^a(0,\mathbf{0})|0\rangle \\ \simeq &\frac{e^{-m_\pi t}}{2m_\pi} \langle 0|P^a\,|\pi^a(\mathbf{0})\rangle\langle \pi^a(\mathbf{0})|\,P^a|0\rangle .\end{aligned} \tag{2.112}$$

Now the r.h.s. of (2.109) can be ignored since we consider $t \gg 0$. From the terms proportional to $e^{-m_\pi t}$, we obtain

$$m_\pi^2 f_\pi = 2m \langle 0|P^a|\pi^a(\mathbf{0})\rangle . \tag{2.113}$$

This equation relate the quark mass , which explicitly breaks the chiral symmetry, and the pion mass. The equation implies that the axial current is conserved in the chiral limit $m \to 0$. Therefore, (2.113) is called the PCAC relation.

On the lattice, we may expect a relation similar to (2.113) with some modifications. As we see 2.7, the local current $A_\mu^a(x)$ needs renormalization. In addition, the correction for the chiral symmetry is necessary due to the lattice regularization. The MDW fermions used in this work is defined in a finite L_s, which slightly breaks the chiral symmetry. Thus, the quark mass is modified from the bare mass m_{bare} as

$$m = m_{\text{bare}} + m_{\text{res}}, \tag{2.114}$$

where m_{res} is a residual quark mass parametrizing the symmetry breaking. We express the PCAC relation in our setup as

$$m_\pi^2 f_\pi = Z_A \langle 0|\partial_\mu A_\mu^a|\pi^a(\mathbf{0})\rangle = 2(m_{\text{bare}} + m_{\text{res}}) \langle 0|P^a|\pi^a(\mathbf{0})\rangle . \tag{2.115}$$

In this work, we use JLQCD ensembles with the MDW fermion where the residual mass $m_{\text{res}} \lesssim 1$ MeV [76]. The residual mass is estimated by the braking of the Ginsparg-Wilson relation. This indicates the good chiral property of our lattices. As we mentioned in Sec. 2.7, for the renormalization constants $Z_V = Z_A$ and $Z_S = Z_P$ hold from the chiral symmetry up to $\mathcal{O}(m_{\text{res}}^2)$ [77]. In the $s\bar{s}$ channel we focus on other chapters, the residual mass is negligible compared to the strange quark mass

$m_s \sim 100$ MeV. Thus, by using MDW fermions, the computations can be performed in the same way as in the continuum theory.

Chapter 3

Two-point correlation function and QCD sum rule

3.1 Dispersion relation and spectral functions

In this section, we discuss a dispersion relation bridging the gap between (perturbative) QCD and the nature of hadrons. The basis of that is the analyticity of correlators. We will see that a spectral function appears in the derivation of the relation. The dispersion relation is one of the key concepts in QCD sum rules.

We define the hadronic vacuum polarization (HVP) function as a Fourier transform of the current-current correlator,

$$(q_\mu q_\nu - q^2 g_{\mu\nu})\Pi(q^2) = i \int d^4x\, e^{iqx} \langle J_\mu(x) J_\nu(0) \rangle, \tag{3.1}$$

where $J_\mu = \bar{q}\gamma_\mu q$ is the quark vector current. The Lorentz tensor $q_\mu q_\nu - q^2 g_{\mu\nu}$ in the l.h.s. results from the current conservation. The HVP function is analytic except for the real axis $q^2 > 0$ where poles and a branch cut[1] may exist. Using the Cauchy's integral theorem, the function may be rewritten by an integral,

$$\Pi(q^2) = \frac{1}{2\pi i} \oint ds \frac{\Pi(s)}{s - q^2}. \tag{3.2}$$

The integration contour encircling the pole at $s = q^2$ is shown Fig. 3.1. The integrals around the positive real axis take the following form,

$$\int_{0+i\epsilon}^{\infty+i\epsilon} ds \frac{\Pi(s)}{s - q^2} + \int_{\infty-i\epsilon}^{0-i\epsilon} ds \frac{\Pi(s)}{s - q^2} = \int ds \frac{\Pi(s + i\epsilon) - \Pi(s - i\epsilon)}{s - q^2}, \tag{3.3}$$

where $\epsilon \to 0^+$. The discontinuity reduces to the imaginary part by the Schwarz reflection principle,

$$\Pi(s + i\epsilon) - \Pi(s - i\epsilon) = 2i \,\mathrm{Im}\, \Pi(s + i\epsilon). \tag{3.4}$$

[1] The branch point corresponds to the threshold energy of hadrons.

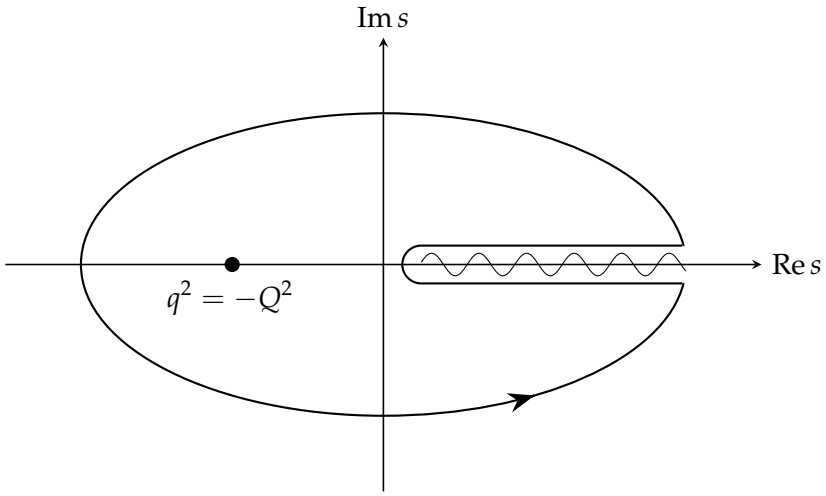

FIGURE 3.1: The integration contour in the complex s-plane.

If the function behaves as $\Pi(s) \sim 0$ at $|s| \sim \infty$, it would be written in terms of a spectral function $\rho(s)$:

$$\Pi(q^2) = \int_0^\infty ds \frac{\rho(s)}{s - q^2}, \tag{3.5}$$

$$\rho(s) = \frac{1}{\pi} \operatorname{Im} \Pi(s + i\epsilon). \tag{3.6}$$

The equation (3.5) is called the dispersion relation. The integral in the dispersion relation, however, diverges since the spectral function does not vanish in the limit $s \to \infty$. This is attributed to the ultraviolet (UV) divergence of the correlator (3.1). We can avoid this problem by subtracting once, for instance, $\Pi(0)$ at a point $q^2 = 0$ since the divergence is logarithmic. Finally, we obtain a once-subtracted dispersion relation,

$$\Pi(q^2) - \Pi(0) = q^2 \int_0^\infty ds \frac{\rho(s)}{s(s - q^2)}. \tag{3.7}$$

The dispersion relation links two kinematic regions, namely, $q^2 < 0$ and $q^2 > 0$. In the deep Euclidean region $Q^2 \equiv -q^2 \gg 0$, the perturbative expansion and OPE are applicable. In contrast, the spectral function $\rho(s)$ is understood as the density of hadronic states of a given energy. The relation (3.7) enables us to investigate the hadronic processes from QCD.

We demonstrate the role of the spectral function in a physical process. Let us consider electromagnetic currents with the electric charge of the quark, which appears in the process of the electron-positron annihilation into hadrons. Summing these currents over flavors,

$$J_\mu^{\mathrm{EM}} = \frac{2}{3} \bar{u} \gamma_\mu u - \frac{1}{3} \bar{d} \gamma_\mu d - \frac{1}{3} \bar{s} \gamma_\mu s + \cdots, \tag{3.8}$$

we define the HVP function $\Pi^{\rm EM}(q^2)$ and $\rho^{\rm EM}(s)$ as (3.1) and (3.6), respectively. According to the optical theorem, the function $\Pi^{\rm EM}(q^2)$ in the time-like region $q^2 > 0$ is intimately related with the total cross section $\sigma(e^+e^- \to \text{hadrons}; s)$,

$$\sigma(e^+e^- \to \text{hadrons}; s) = \frac{16\pi^2\alpha^2}{s} \,\text{Im}\,\Pi^{\rm EM}(s + i\epsilon). \tag{3.9}$$

Here, α is the fine structure constant and higher QED corrections are neglected. On the other hand, the total cross section $\sigma(e^+e^- \to \mu^-\mu^+; s)$ to the leading order in the massless limit $m_\mu^2 \ll s$ is expressed as

$$\sigma(e^+e^- \to \mu^-\mu^+; s) = \frac{4\pi\alpha^2}{3s}. \tag{3.10}$$

Thus, the spectral function is proportional to the ratio of these experimental observables,[2]

$$\rho^{\rm EM}(s) = \frac{1}{12\pi^2} \frac{\sigma(e^+e^- \to \text{hadrons}; s)}{\sigma(e^+e^- \to \mu^-\mu^+; s)}. \tag{3.11}$$

The spectral function appears in the physical process and is measurable experimentally. [3]

3.2 Quark-hadron duality

The other key concept in QCD sum rules is the quark-hadron duality. This duality gives the asymptotic behavior of the dispersion relation (3.7) in some limits of kinematic variables. It allows us to model the hadronization effects by QCD.

First, we consider the deep Euclidean domain $Q^2 \gg \Lambda^2_{\rm QCD}$. In this case, we can evaluate the HVP function $\Pi(-Q^2)$ by the OPE. In the limit of $Q^2 \to \infty$, all power corrections vanish since the dimension-D corrections are $\sim \Lambda^D_{\rm QCD}$. Defining the HVP in perturbative QCD as $\Pi^{\rm pert}(q^2)$, we obtain the asymptotic form of the spectral sum (integral) in (3.7),

$$\frac{Q^2}{\pi}\int_0^\infty ds \frac{\text{Im}\,\Pi(s+i\epsilon)}{s(s+Q^2)} \simeq \frac{Q^2}{\pi}\int_0^\infty ds \frac{\text{Im}\,\Pi^{\rm pert}(s+i\epsilon)}{s(s+Q^2)}, \tag{3.12}$$

where $Q^2 \to \infty$. Despite the l.h.s. is the spectral sum of the hadronic correlator, the r.h.s. is purely perturbative and calculable in terms of the quarks and gluons. This is an example of the quark-hadron duality.

Another example is in the timelike region $q^2 = s > 0$, where the spectral function is given a physical energy. Because of the asymptotic freedom of QCD, the integrand

[2] This ratio is called the R-ratio.

[3] The spectral function of the weak isospin triplet current can be obtained by hadronic τ decays.

of the dispersion relation is likely to become perturbative, *i.e.*,

$$\rho(s) \simeq \frac{1}{\pi} \operatorname{Im} \Pi^{\text{pert}}(s + i\epsilon), \tag{3.13}$$

where $s \to \infty$. As we have seen in the previous section, the spectral function (3.6) appears in the ratio of the cross section up to a constant. In fact, the duality (3.13) mostly holds in the e^+e^- annihilation when $\sqrt{s} \gtrsim 3$ GeV except for resonance peaks.

The duality assumption will be violated if the OPE does not describe nonperturbative effects well. In fact, the spectral function in the low energy regime ($\sqrt{s} \lesssim 2$ GeV) oscillates and disagree with perturbative QCD. This cannot be explained by the truncation uncertainties of the perturbative series and the power corrections. The duality violation has been explored in, *e.g.*, the Regge theory at large N_c. The duality violating term may be oscillating as trigonometric functions which do not appear in the OPE, such as, $\rho^{\text{DV}}(s) \sim e^{-\alpha s} \sin(\beta s)$ where α and β are constants. In the deep Euclidean region, this term becomes an exponentially decaying function and the violation of the quark-hadron duality would be negligible. The validity of this duality assumption has to be assessed, which is an important and open issue. This is, however, beyond the scope of this work. We refer the reader to [18] for more detailed discussion with some examples.

3.3 Two-point correlation functions in the massless limit

We consider the two-point correlation functions in the massless limit. The expression for the vector current will be used in the discussion of the QCD sum rule. The correlator is defined as

$$\Pi^{\Gamma}(q^2) \equiv i \int d^4x e^{iqx} \langle 0 | j_{\Gamma}(x) j_{\Gamma}(0) | 0 \rangle \,, \tag{3.14}$$

where $j_{\Gamma}(x)$ is a quark bilinear operator such as $\bar{q}\gamma_\mu q$, $\bar{q}q$, and $\bar{q}\sigma_{\mu\nu}q$. These operators correspond to $\Gamma = V$, S, and T, respectively. In the case of the vector current, we can write (3.14) as

$$(q_\mu q_\nu - q^2 g_{\mu\nu})\Pi(q^2) \equiv i \int d^4x e^{iqx} \langle 0 | j_\mu(x) j_\nu(0) | 0 \rangle \,. \tag{3.15}$$

The function $\Pi(q^2)$ is the so-called hadronic vacuum polarization (HVP) function. The scalar correlator in the momentum space, $\Pi^S(q^2)$, is proportional to Q^2. In contrast, the correlator of the tensor current has the following tensor structure,

$$\Pi^T(q^2) = \Pi_1^T T^{(1)}_{\mu\nu\rho\sigma} + \Pi_2^T T^{(2)}_{\mu\nu\rho\sigma}, \tag{3.16}$$

$$T^{(1)}_{\mu\nu\rho\sigma} = q^2 \left(g_{\mu\rho} g_{\nu\sigma} - g_{\mu\sigma} g_{\nu\rho} \right), \tag{3.17}$$

$$T^{(2)}_{\mu\nu\rho\sigma} = q_\mu q_\rho g_{\nu\sigma} - q_\mu q_\sigma g_{\nu\rho} - q_\nu q_\rho g_{\mu\sigma} + q_\nu q_\sigma g_{\mu\rho}. \tag{3.18}$$

The correlator in (3.14) has the UV divergence expected by a dimensional analysis and the subtractive renormalization is necessary. In addition, the operator $j_\Gamma(x)$ may also need the renormalization. Accordingly, the correlator is renormalization-scale dependent. Since we only consider the Euclidean region $Q^2 \equiv -q^2 > 0$, we redefine the correlator in (3.14) as $\Pi^\Gamma(\mu^2; Q^2)$.

The RG evolution of the Euclidean correlator is described by an inhomogeneous equation,

$$\mu^2 \frac{\mathrm{d}}{\mathrm{d}\mu^2} \Pi^\Gamma(\mu^2; Q^2) = 2\gamma^\Gamma(a_s)\Pi^\Gamma(\mu^2; Q^2) + \gamma^{\Gamma\Gamma}(a_s) T_\Gamma, \tag{3.19}$$

where T_Γ is a tensor that depends on the Euclidean momentum Q_μ, *e.g.* $T_S = Q^2$ and $T_V = (-Q^2\delta_{\mu\nu} + Q_\mu Q_\nu)$. For the tensor current, the RG equation can be decomposed into two parts corresponding to the Lorentz structures $T^{(1)}_{\mu\nu\rho\sigma}$ and $T^{(2)}_{\mu\nu\rho\sigma}$, respectively. The function $\gamma^\Gamma(a_s)$ is the anomalous dimension of the multiplicative renormalization factor for $j_\Gamma(x)$, while $\gamma^{\Gamma\Gamma}(a_s)$ is that of a subtractive counterterm. For the vector current which we use in this work, the anomalous dimension vanishes: $\gamma^V(a_s) = 0$. Nevertheless, we leave it in the following expressions to cover other operators. The solution to describe the evolution between two different scales μ_0 and μ_1 is

$$\Pi^\Gamma(\mu^2; Q^2) = \exp\left(\int_{a_s(\mu_0)}^{a_s(\mu)} da \frac{2\gamma^\Gamma(a)}{\beta(a)} \right) \left(\Pi^\Gamma(\mu_0^2; Q^2) + \Delta_\Gamma(\mu_1, \mu_0) T_\Gamma \right), \tag{3.20}$$

$$\Delta_\Gamma(\mu_1, \mu_0) = \int_{a_s(\mu_0)}^{a_s(\mu)} da \frac{\gamma^{\Gamma\Gamma}(a)}{\beta(a)} \exp\left(- \int_{a_s(\mu_0)}^{a} da' \frac{2\gamma^\Gamma(a')}{\beta(a')} \right). \tag{3.21}$$

An expression of the solution which explicitly depends on $\log(\mu^2/Q^2)$ is more useful to compute the Borel transformation[4]. Hence, we decompose the derivative as

$$\mu^2 \frac{\mathrm{d}}{\mathrm{d}\mu^2} = \mu^2 \frac{\partial}{\partial \mu^2} + \beta(a_s) \frac{\partial}{\partial a_s}, \tag{3.22}$$

and solve the following equation

$$\mu^2 \frac{\partial}{\partial \mu^2} \Pi^\Gamma(\mu^2; Q^2) = \left(2\gamma^\Gamma(a_s) - \beta(a_s) \frac{\partial}{\partial a_s} \right) \Pi^\Gamma(\mu^2; Q^2) + \gamma^{\Gamma\Gamma} T_\Gamma. \tag{3.23}$$

The partial derivative $\frac{\partial}{\partial \mu^2}$ acts only on the terms that explicitly depend on μ^2. The solution of this equation can be constructed recursively through

$$\Pi^{\Gamma(\ell)}(\mu^2; Q^2) = \int dL \left(2\gamma^\Gamma(a_s) - \beta(a_s) \frac{\partial}{\partial a_s} \right) \Pi^{\Gamma(\ell-1)}(\mu^2; Q^2) + \gamma^{\Gamma\Gamma} T_\Gamma L, \tag{3.24}$$

where $\Pi^{\Gamma(\ell)}(\mu^2; Q^2)$ stands for the solution up to $\mathcal{O}(a_s^\ell)$ and $L = \log(\mu^2/Q^2)$.

[4]The expression is also used for correlator in the coordinate space, which is derived by the Fourier transformation.

n	$\Pi_0^{n,0}$	$\Pi_0^{n,1}$	$\Pi_0^{n,2}$	$\Pi_0^{n,3}$	$\Pi_0^{n,4}$
0	0.042217160	0.025330296			
1	−0.0056966386	0.025330296			
2	0.021586071	0.041537156	0.028496583		
3	0.14154678	0.16137968	0.14411919	0.042744874	
4	unknown	1.2431020	0.83821512	0.40025907	0.072131975

TABLE 3.1: Perturbative coefficients of the HVP in the massless limit $\Pi_0(\mu^2; Q^2)$ [79, 80].

Let us now discuss the vector correlator. The perturbative series of HVP at $\mu^2 = Q^2$ is known to $\mathcal{O}(\alpha_s^3)$ [78, 79]. The anomalous dimension of the vector current is $\gamma^V(a_s) = 0$. This is due to the current conservation. The anomalous dimension $\gamma^{VV}(a_s)$ has been calculated at $\mathcal{O}(\alpha_s^4)$ [78, 79]. We derive the explicit form of the solution in Appendix C. Table 3.1 shows the numerical coefficients of the massless HVP function in the $\overline{\text{MS}}$ scheme,

$$\Pi_0(\mu^2; Q^2) = \sum_{n=0}^{4} \sum_{m=0}^{n} \Pi_0^{n,m} a_s^n(\mu^2) L^m, \tag{3.25}$$

where $L = \log(\mu^2/Q^2)$ and $n_f = 3$. Note that we can obtain the L-dependent terms up to $\mathcal{O}(a_s^4)$ although $\Pi_0^{4,0}$ is currently unknown. The L-independent terms are, however, irrelevant for the Borel transform.

3.4 Dimension-two corrections of the correlator

In this section, we discuss the dimension-two correction of the vector current correlator, which is at the next-to-leading order of OPE. Since the correlator is gauge invariant, dimension-two condensates do not exist. Therefore, the correction is proportional to the quark mass squared m^2. We expand the HVP function by $1/Q^2$ as

$$\Pi(\mu^2; Q^2) = \Pi_0(\mu^2; Q^2) + \frac{m^2}{Q^2}\Pi_2(\mu^2; Q^2) + \mathcal{O}(1/Q^4). \tag{3.26}$$

The function $\Pi_0(\mu^2; Q^2)$ has been discussed in the previous section. The perturbative coefficients $\Pi_2(\mu; Q^2)$ at $\mu^2 = Q^2$ has been calculated up to $\mathcal{O}(\alpha_s^3)$ [81, 82].

The L-dependence of the coefficient $\Pi_2(\mu; Q^2)$ is governed by the following equation:

$$\mu^2 \frac{\partial}{\partial \mu^2}\Pi_2(\mu^2; Q^2) = -\left(2\gamma_m(a_s) + \beta(a_s)\frac{\partial}{\partial a_s}\right)\Pi_2(\mu^2; Q^2) \tag{3.27}$$

n	$\Pi_2^{n,0}$	$\Pi_2^{n,1}$	$\Pi_2^{n,2}$	$\Pi_2^{n,3}$
0	−0.15198178			
1	−0.40528473	−0.30396355		
2	−3.6690614	−2.8749886	−0.64592255	
3	−38.067010	−32.318737	−11.104168	−1.3994988

TABLE 3.2: Perturbative coefficients of the dimension-two correction $\Pi_2(\mu^2; Q^2)$ [79].

This equation is derived by taking the derivative of HVP in (3.26),

$$\mu^2 \frac{\mathrm{d}}{\mathrm{d}\mu^2}\Pi(\mu^2; Q^2) = 0, \tag{3.28}$$

$$\mu^2 \frac{\mathrm{d}}{\mathrm{d}\mu^2} = \mu^2 \frac{\partial}{\partial \mu^2} + \beta(a_s)\frac{\partial}{\partial a_s} + 2\gamma_m m^2 \frac{\partial}{\partial m^2}, \tag{3.29}$$

and extracting the terms proportional to m^2. The solution can be constructed in the same way as the previous section but $\gamma^\Gamma = -\gamma_m$ and $\gamma^{\Gamma\Gamma} = 0$. We show the numerical expression of the perturbative coefficients in the $\overline{\mathrm{MS}}$ scheme,

$$\Pi_2^n(\mu^2; Q^2) = \sum_{n=0}^{3}\sum_{m=0}^{n} \Pi_2^{n,m} a_s^n(\mu^2) L^m, \tag{3.30}$$

in Table 3.2, where we set $n_f = 3$. The derivation of these coefficients is discussed in Appendix D. Comparing to the perturbative series of $\Pi_0(\mu^2; Q^2)$, we find that the dimension-two correction is less convergent. We will discuss the size of the truncation error after Borel transformation in the following section.

3.5 Borel transform of the vacuum polarization function

We briefly review the use of the spectral sum of QCD current correlators. More detailed reviews and discussions are found in the literature, *e.g.* [83, 84].

As a first step, we consider the dispersion relation (3.5) which links QCD to the hadronic physics. As discussed in Sec. 3.1, the integral in the dispersion relation is divergent. One can remove the divergence by differentiation,

$$\frac{\partial}{\partial Q^2}\Pi(-Q^2) = \int_0^\infty \frac{ds}{(s+Q^2)^2}\rho(s). \tag{3.31}$$

In general, the n-th derivative of $\Pi(-Q^2)$ with respect to Q^2 satisfies a modified form of the dispersion relation. This may lead to a series of sum rules.

For quarkonium systems, moments of the spectra have been studied for decades [85]. We define the moments as

$$M_n \equiv \int_0^\infty \frac{ds}{s^{n+1}}\rho(s). \tag{3.32}$$

From dimensional analysis, the moments do not contain the UV divergence for $n \geq 1$. Using the dispersion relation, we can write those in terms of the derivatives of HVP at $Q^2 = 0$,

$$M_n = \frac{1}{n!}\left(-\frac{\partial}{\partial Q^2}\right)^n \Pi(-Q^2)\bigg|_{Q^2=0}. \tag{3.33}$$

That appears in the heavy quark mass expansion of HVP,

$$\Pi(-Q^2) = \sum_{n=1} C_n^V \left(\frac{Q^2}{4m_q^2}\right)^n, \tag{3.34}$$

where the subtraction term is ignored. Typical length scale is given by an inverse of the quark mass m_q^{-1}, which is short enough to describe perturbatively for charm and bottom quarks. Thus, we can write the coefficient C_n^V as a function of $\alpha_s(\mu)$ and $L_m \equiv \log(m_q(\mu)/\mu)$.[5] This perturbative series of the moments are known to $\mathcal{O}(\alpha_s^3)$ in the $\overline{\text{MS}}$ scheme for $n = 1$–3 [87–90]. Using (3.32), the moment is evaluated by the e^+e^- cross section from experiments,

$$R_{e^+e^-\to q\bar{q}+X}(s) \equiv \frac{\sigma_{e^+e^-\to q\bar{q}+X}(s)}{\sigma_{e^+e^-\to\mu^+\mu^-}(s)} \propto \rho^{(\text{exp})}(s), \tag{3.35}$$

$$M_n^{\text{exp}} = \int_0^\infty \frac{ds}{s^{n+1}} \rho^{\text{exp}}(s). \tag{3.36}$$

One can determine the quark mass m_q by solving

$$m_q(\mu) = \frac{1}{2}\left(\frac{C_n^V(\alpha_s(\mu), L_m)}{M_n^{\text{exp}}}\right)^{\frac{1}{2n}}, \tag{3.37}$$

where α_s is used as an input parameter. This method is called the moment sum rule. The studies of moment sum rules can be found in, *e.g.*, [91–93].

Let us return to the light quark system. We define a spectral sum as

$$D^{(n)}(Q^2) \equiv \int_0^\infty ds\, W^{(n)}(Q^2; s)\rho(s), \tag{3.38}$$

$$W^{(n)}(Q^2; s) \equiv \frac{Q^{2n+2}}{n!}\left(-\frac{\partial}{\partial Q^2}\right)^n \frac{1}{s+Q^2} = \frac{Q^{2n+2}}{(s+Q^2)^{n+1}}, \tag{3.39}$$

which is equivalent to the derivative of $\Pi(-Q^2)$. The weight function is normalized at $s = 0$: $W^{(n)}(Q^2; 0) = 1$. As a first step, we consider the spectral sum at $n = 1$. To compute $D^{(1)}(Q^2)$ perturbatively, the scale Q^2 has to be large enough. Figure 3.2

[5] The perturbative series might be improved by OPE to include a part of nonperturbative effects. The leading power correction of the moment is the gluon condensate $\langle 0|\frac{\alpha_s}{\pi}G^2|0\rangle$ and its Wilson coefficient is known to $\mathcal{O}(\alpha_s)$ [86].

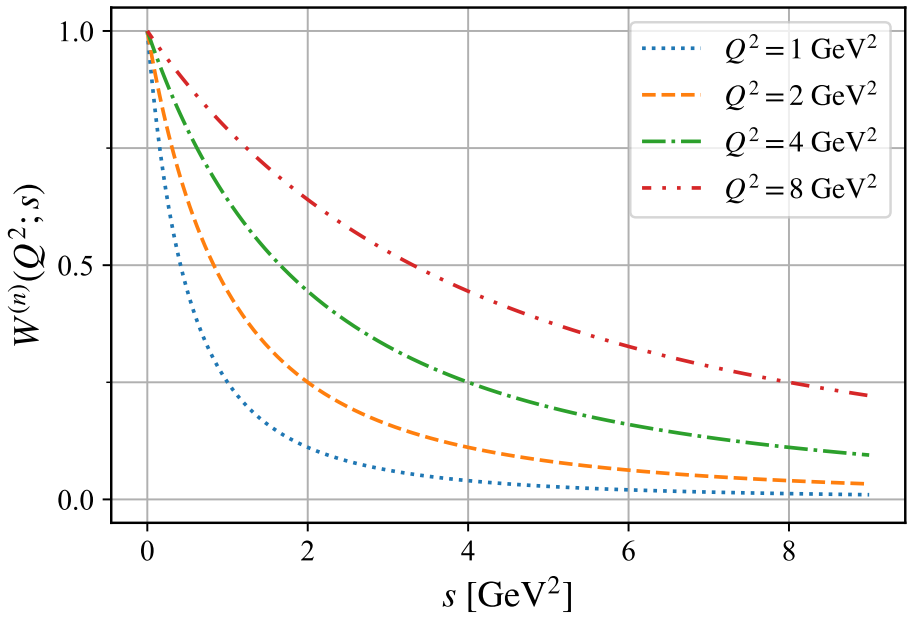

FIGURE 3.2: The weight function $W^{(n)}(Q^2;s)$ at $n=1$.

shows the weight function at certain values of Q^2. We naturally expect that this spectral sum at large Q^2 is not sensitive to the low-lying spectra. Therefore, that is not suitable to estimate the hadronic parameters. To enhance low-energy contributions, one may increase n as shown in Fig. 3.3. This leads to, however, a less convergent OPE since power corrections take the following form under the transformation (for large n),

$$\begin{aligned}&\frac{Q^{2n+2}}{n!}\left(-\frac{\partial}{\partial Q^2}\right)^n\left(\frac{1}{Q^2}\right)^m\\&=\frac{(n+1)(n+2)\cdots(n+m-1)}{1\cdot 2\cdots(m-1)}\left(\frac{1}{Q^2}\right)^{m-1}\sim\left(\frac{1}{Q^2/n}\right)^{m-1}.\end{aligned}\tag{3.40}$$

We have to take account of the tradeoff between the sensitivity to the low-lying spectra and the convergence of OPE. If we take the both limits $Q^2\to\infty$ and $n\to\infty$, where Q^2/n is fixed at M^2 (see Fig. 3.4), a spectral sum can reach, more or less, a balance of these requirements. In this limit, the weight function becomes the following form:

$$W^{(n)}(Q^2;s)=\left(1+\frac{s}{Q^2}\right)^{-n-1}\to e^{-s/M^2}.\tag{3.41}$$

This weight has been introduced by Shifman-Vainshtein-Zakharov (SVZ). In the remainder of this chapter, we discuss this form of the spectral sum in detail.

In the QCD sum rule analyses, one introduces the Borel transform of HVP to enhance the contributions from low-lying hadronic states. The Borel transformation

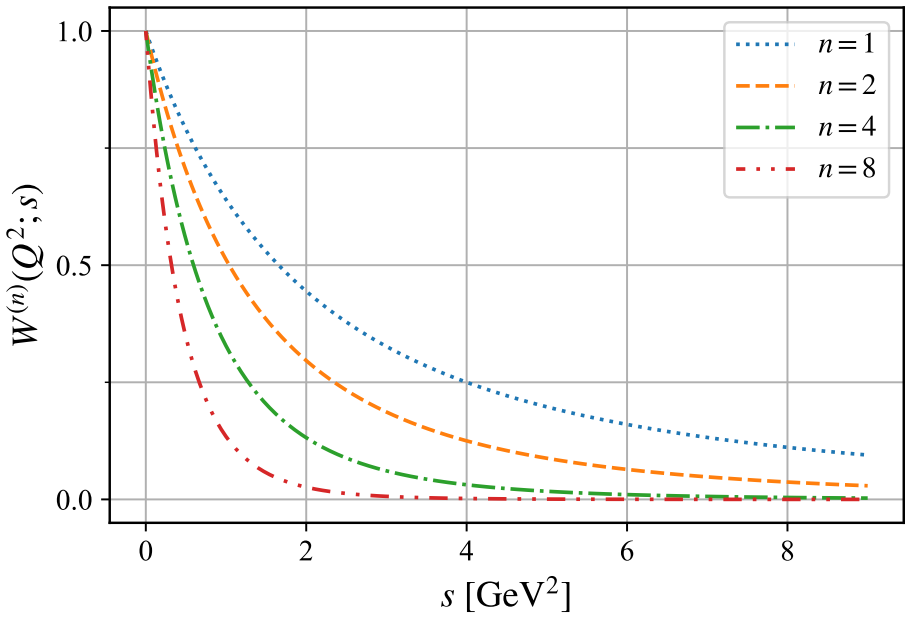

FIGURE 3.3: The weight function $W^{(n)}(Q^2;s)$ at $Q^2 = 4$ GeV^2.

is defined as

$$\mathcal{B}_M = \lim_{\substack{n,Q^2\to\infty \\ Q^2/n=M^2}} \frac{(Q^2)^n}{(n-1)!}\left(-\frac{\partial}{\partial Q^2}\right)^n, \tag{3.42}$$

where M is the Borel mass that specifies a typical energy scale. The Borel transform of HVP may then be written as

$$\tilde{\Pi}(M^2) \equiv \mathcal{B}_M\left[\Pi(-Q^2)\right] = \frac{1}{M^2}\int_0^\infty ds\,\rho(s)e^{-s/M^2}. \tag{3.43}$$

The exponential factor e^{-s/M^2} suppresses the contributions from high-energy states above M.

One can use OPE to evaluate $\tilde{\Pi}(M^2)$ including nonperturbative power corrections. We start from an expression of $\Pi(-Q^2)$ as an expansion in $1/Q^2$

$$\begin{aligned}\Pi^{\mathrm{OPE}}(-Q^2) = {}& \frac{1}{4\pi^2}\left(1+\frac{\alpha_s(\mu^2)}{\pi}\right)\log\left(\frac{\mu^2}{Q^2}\right) - \frac{3}{2\pi^2}\frac{m^2}{Q^2} \\ & + \frac{1}{12}\frac{\langle 0|\frac{\alpha_s}{\pi}G^2|0\rangle}{Q^4} + \frac{2m\langle 0|\bar{q}q|0\rangle}{Q^4} - \frac{224\pi\alpha_s(\mu^2)}{81}\frac{\kappa_0\langle 0|\bar{q}q|0\rangle^2}{Q^6} + \cdots,\end{aligned} \tag{3.44}$$

where $\alpha_s(\mu^2)$ is the strong coupling constant defined at a renormalization scale μ, m is the quark mass, and $\langle 0|\frac{\alpha_s}{\pi}G^2|0\rangle$ and $\langle 0|\bar{q}q|0\rangle$ are the gluon and chiral condensates,

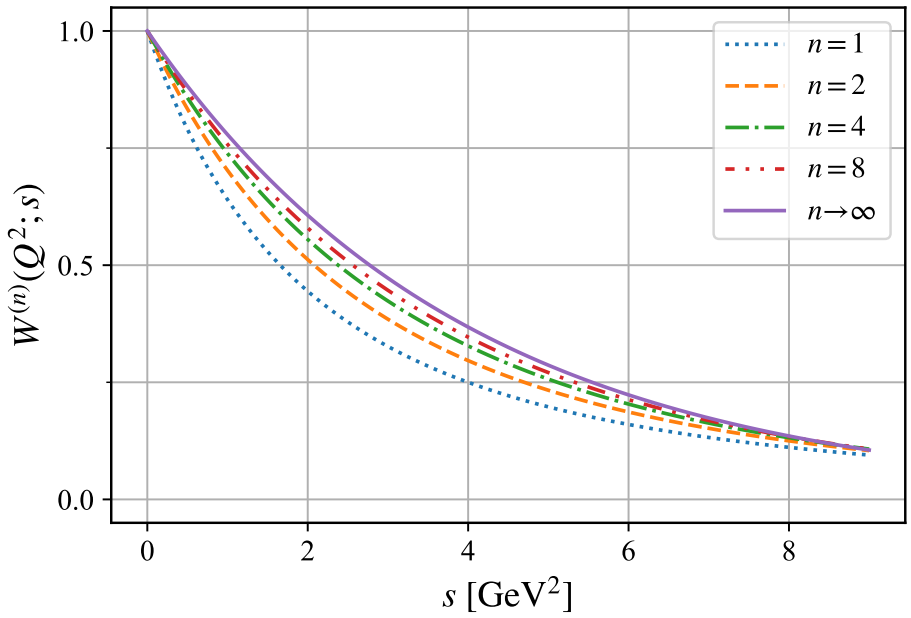

FIGURE 3.4: The weight function $W^{(n)}(Q^2;s)$ at $Q^2/n = 4$ GeV^2.

respectively. Here, the four-quark condensate is represented by a vacuum saturation approximation (VSA) with an overall factor κ_0, which represents the violation of VSA when $\kappa_0 \neq 1$. By the Borel transformation, the logarithmic function and negative powers of Q^2 are transformed as

$$\mathcal{B}_M\left[\log(Q^2)\right] = -1, \tag{3.45}$$

$$\mathcal{B}_M\left[\frac{1}{Q^{2n}}\right] = \frac{1}{(n-1)!}\frac{1}{M^{2n}}, \tag{3.46}$$

where n is a positive integer. Therefore, the Borel transform of HVP can be expressed as follows:

$$\begin{aligned}\tilde{\Pi}^{\mathrm{OPE}}(M^2) = {}& \frac{1}{4\pi^2}\left(1+\frac{\alpha_s(\mu^2)}{\pi}\right) - \frac{3}{2\pi^2}\frac{m^2}{M^2} \\ & + \frac{1}{12}\frac{\langle 0|\frac{\alpha_s}{\pi}G^2|0\rangle}{M^4} + \frac{2m\langle 0|\bar{q}q|0\rangle}{M^4} - \frac{112\pi\alpha_s(\mu^2)}{81}\frac{\kappa_0\langle 0|\bar{q}q|0\rangle^2}{M^6} + \cdots .\end{aligned} \tag{3.47}$$

The perturbative coefficients of the leading order term, $\mathcal{O}(1/M^0)$, in the massless limit are known up to $\mathcal{O}(\alpha_s^4)$ [80], where the disconnected diagrams are neglected. (See also Sec. 3.3.) The other corrections taken into account in this work are summarized in Sec. 5.2. Because of the factor $1/(n-1)!$ in (3.46), the Borel transform is less affected by higher dimensional condensates, and the OPE is made more convergent than that for HVP itself (3.44).

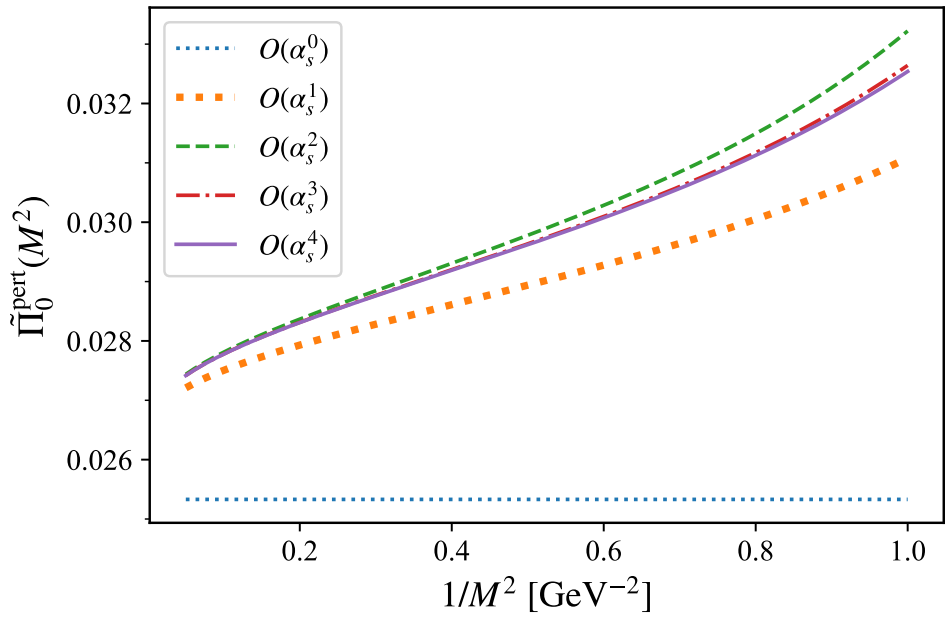

FIGURE 3.5: Perturbative expansion of $\tilde{\Pi}(M^2)$ at the leading order of OPE. The renormalization scale is set at $\mu^2 = M^2 e^{-\gamma_E}$.

Perturbative expansion of $\tilde{\Pi}^{\rm OPE}(M^2)$ in the massless limit shows a good convergence. We set the renormalization scale μ^2 to $M^2 e^{-\gamma_E}$ since the Borel transformation of the logarithmic function $\mathcal{B}_M[\log^n(\mu^2/Q^2)]$ appears as a polynomial of $\log(\mu^2/M^2 e^{-\gamma_E})$. (See Appendix E.) We show $\tilde{\Pi}_0^{\rm pert}(M^2)$, which is the leading order of the $1/M^2$ expansion, as a function of $1/M^2$ in Fig. 3.5. We set $\Lambda_{\overline{\rm MS}}^{(n_f=3)} = 332$ MeV for the coupling constant $\alpha_s(\mu^2)$. The running of $\alpha_s(\mu^2)$ is incorporated at five-loop level using `RunDec` [52, 53]. Figure 3.5 indicates that the truncation error of the perturbative expansion $\tilde{\Pi}_0^{\rm pert}(M^2)$ is not substantial for $M > 1$ GeV. Indeed, the $\mathcal{O}(\alpha_s^4)$ correction is at the level of 0.3% or smaller.

For the next-to-leading order terms of OPE, *i.e.*, the terms of m^2/Q^2, the perturbative coefficients are known to α_s^3 [82] as discussed Sec. 3.4,

$$\Pi_{m^2}^{\rm pert}(Q^2) = -\frac{3}{2\pi^2}\frac{m^2(Q^2)}{Q^2}\left(1 + 2.66667\frac{\alpha_s(Q^2)}{\pi} + 24.1415\frac{\alpha_s^2(Q^2)}{\pi^2} + 250.471\frac{\alpha_s^3(Q^2)}{\pi^3} + \cdots\right), \tag{3.48}$$

where the renormalization scale μ is set at $\mu^2 = Q^2$ and $n_f = 3$. The numerical expressions for different n_f's are found, *e.g.*, in [79]. We define the Borel transform of the correction $\tilde{\Pi}_{m^2}^{\rm pert}(M^2) \equiv \mathcal{B}_M[\Pi_{m^2}^{\rm pert}(Q^2)]$. Applying the formula in (E.2) and

setting $\mu^2 = M^2 e^{-\gamma_E}$, we found the expression,

$$\tilde{\Pi}^{\rm pert}_{m^2}(M^2) = -\frac{3}{2\pi^2}\frac{m^2(\mu^2)}{M^2}\left(1 + 2.66667\frac{\alpha_s(\mu^2)}{\pi} + 17.1505\frac{\alpha_s^2(\mu^2)}{\pi^2} + 152.426\frac{\alpha_s^3(\mu^2)}{\pi^3} + \cdots\right). \tag{3.49}$$

We plot $\tilde{\Pi}^{\rm pert}_{m^2}(M^2)$ in Fig. 3.6 (top). Unlike $\tilde{\Pi}^{\rm pert}_{0}(M^2)$, we observe significant dependence on the order of the perturbative expansion. To improve the convergence, we set the renormalization scale at $\mu^2 = 4M^2e^{-\gamma_E}$ as shown in Fig. 3.6 (middle). The dependence on the scale μ is demonstrated in Fig. 3.6 (bottom), where the perturbative expansion truncated at $\mathcal{O}(\alpha_s^3)$ is shown for $\mu^2 = 2M^2e^{-\gamma_E}$, $4M^2e^{-\gamma_E}$, $8M^2e^{-\gamma_E}$. Since $\tilde{\Pi}^{\rm pert}_{m^2}(M^2)$ should be independent of the renormalization scale up to truncation errors, we treat the variation due to the unphysical scale setting as the truncation error in the later sections.

In phenomenological studies, an ansatz for the spectral function of the form,

$$\rho_{\rm ph}(s) = f_V^2\delta(s - m_V^2) + \theta(s - s_{\rm th})\rho_{\rm cont}(s), \tag{3.50}$$

is often used. Here, m_V and f_V are a mass and a decay constant of the ground-state hadron, respectively. Excited states of hadrons are modeled by the continuum (or scattering) states calculated in perturbative QCD, and the spectral function of the continuum states $\rho_{\rm cont}(s)$ is introduced above the threshold $s_{\rm th}$. This replacement amounts to assume the quark-hadron duality. The Borel transformation reduces the dependence on this assumption. The integral in (3.43) with $\rho_{\rm ph}(s)$ corresponds to the OPE expression in (3.47). Namely,

$$\tilde{\Pi}^{\rm OPE}(M^2) = \frac{1}{M^2}\int_0^\infty ds\,\rho_{\rm ph}(s)e^{-s/M^2} \tag{3.51}$$

is used in the QCD sum rule analysis. Solving this equation for m_V and f_V, one can predict the mass and decay constant of this particular channel from the fundamental parameters of QCD, such as $\alpha_s(\mu^2)$, m as well as the condensates.

The QCD sum rule for the ϕ meson, which we mainly study in this work, is discussed in the literature, *e.g.*, [17, 94].

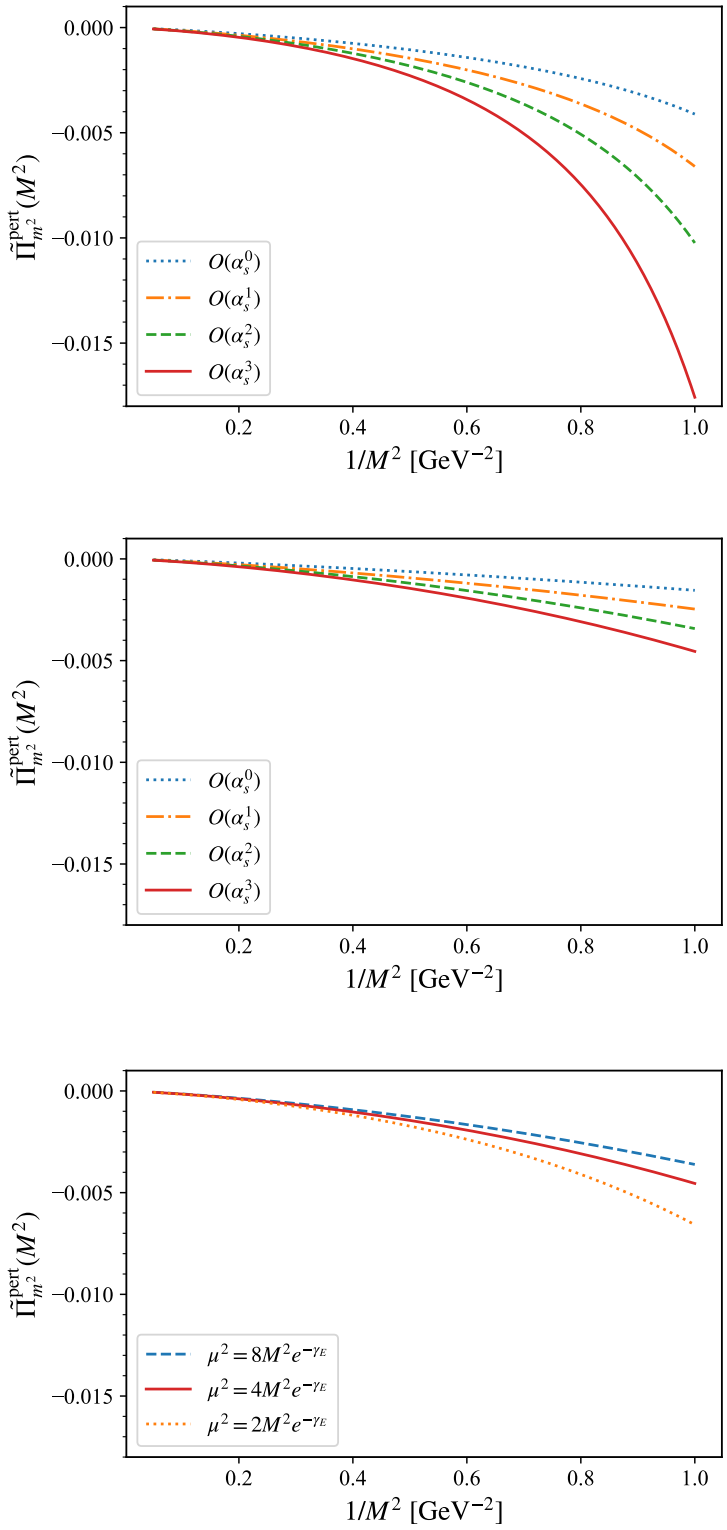

FIGURE 3.6: Top: Perturbative expansion of $\tilde{\Pi}^{\text{pert}}_{m^2}(M^2)$ where the scale is $\mu^2 = M^2e^{-\gamma_E}$. Middle: Same as the top figure but at $\mu^2 = 4M^2e^{-\gamma_E}$. Bottom: The renormalization scale dependence of $\tilde{\Pi}^{\text{pert}}_{m^2}(M^2)$.

Chapter 4

Borel transform as a smeared spectrum

4.1 Two-point correlator as a spectral sum

We derive the spectral representation of the correlator. The relation between the correlator and the spectral function is a clue to compute the Borel transform. We follow the derivation in [95]. In this section, we assume the Euclidean spacetime and ignore discretization errors.

We define a current-current correlation function as

$$C(t) = \int d^3\boldsymbol{x} \langle J_z(t, \boldsymbol{x}) J_z(0, \boldsymbol{0}) \rangle. \tag{4.1}$$

Recall that it corresponds to the meson correlator with zero spatial momentum. Another important quantity in the derivation is the HVP function,

$$(Q_\mu Q_\nu - Q^2 \delta_{\mu\nu}) \Pi(Q^2) = \int d^4\boldsymbol{x} \langle J_\mu(t, \boldsymbol{x}) J_\nu(0, \boldsymbol{0}) \rangle e^{iQ\cdot x}, \tag{4.2}$$

where Q_μ is an Euclidean momentum. We express HVP with an integral,

$$\Pi(Q^2) - \Pi(0) = -Q^2 \int_0^\infty \frac{\rho(s)}{s(s+Q^2)}, \tag{4.3}$$

which is the once-subtracted dispersion relation in the Euclidean spacetime. The numerator $\rho(s) = \operatorname{Im} \Pi(s + i\epsilon)$ is a spectral function. Plugging $Q_\mu = (\omega, \boldsymbol{0})$ into (4.2) for $J_\mu = J_\nu = J_z$, we may relate the correlator and HVP,

$$-\omega^2 \Pi(\omega^2) = \int_{-\infty}^\infty dt\, C(t) e^{i\omega t}. \tag{4.4}$$

Since the subtraction term appears only at $t = 0$, we can replace $\Pi(\omega^2)$ with the dispersion relation. Solving (4.4) for $C(t)$ by the inverse of the Fourier transform, we

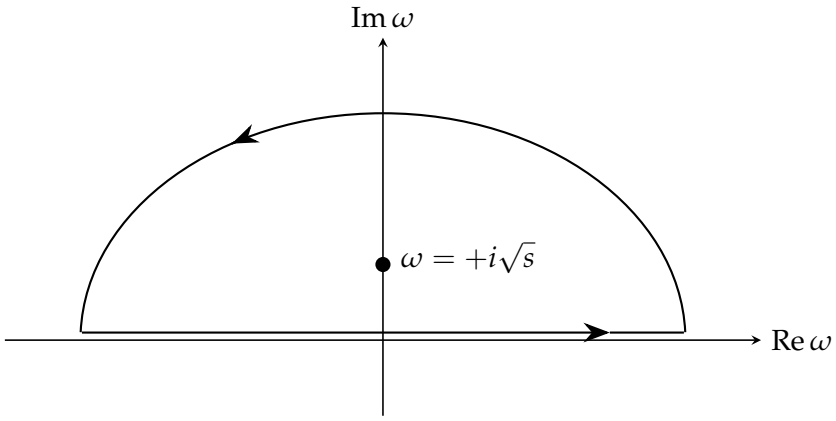

FIGURE 4.1: The integration contour in the complex ω-plane.

express the correlator as an integral (suppose $t > 0$) [95],

$$\begin{aligned} C(t) &= \int_{-\infty}^{\infty} \frac{d\omega}{2\pi}\omega^4 \int_0^{\infty} ds \frac{\rho(s)}{s(s+\omega^2)} e^{i\omega t} \\ &= \int_0^{\infty} ds \frac{\rho(s)}{s} \int_{-\infty}^{\infty} \frac{d\omega}{2\pi} \frac{\omega^4}{s+\omega^2} e^{i\omega t} \\ &= \int_0^{\infty} ds \frac{\rho(s)}{s} \int_{-\infty}^{\infty} \frac{d\omega}{2\pi} \frac{\omega^4}{2i\sqrt{s}} \left(\frac{1}{\omega - i\sqrt{s}} - \frac{1}{\omega + i\sqrt{s}} \right) e^{i\omega t} \\ &= \frac{1}{2} \int_0^{\infty} ds\, \sqrt{s}\rho(s) e^{-\sqrt{s}t} \\ &= \int_0^{\infty} d\omega\, \omega^2 \rho(\omega^2) e^{-\omega t}. \end{aligned} \tag{4.5}$$

In the forth step, we take the residual values $\omega = +i\sqrt{s}$ considering the integration contour in Fig. 4.1. Changing the valuable $\omega = \sqrt{s}$ in the final step, we finally obtain the spectral integral of the correlator.

The expression (4.5) gives the basis of weighted spectra in lattice QCD. We consider a spectral sum $S_W(x)$ characterized by a parameter x. Using a weight function $W(x;s)$, we express it as

$$S_W(x) = \int_0^{\infty} ds\, W(x;s)\rho(s). \tag{4.6}$$

Suppose that we can compute the spectral sum from the correlator with a kernel $K(x;t)$. [1]

$$S_W(x) = \int_0^{\infty} dt\, K(x;t)C(t). \tag{4.7}$$

[1] To remove the contact term in $C(t)$, the kernel has to be smoothly $K(x;t) \to 0$ in the limit $t \to 0$,

Using (4.5), we may relate the kernel $K(x;t)$ and $W(x;s)$,

$$\int ds\,\rho(s)W(x;s) = \frac{1}{2}\int_0^\infty dt \int_0^\infty ds\,\sqrt{s}\rho(s)e^{-\sqrt{s}t}K(x;t), \tag{4.8}$$

$$W(x;s) = \frac{\sqrt{s}}{2}\int_0^\infty dt K(x;t)e^{-\sqrt{s}t}. \tag{4.9}$$

The relation can be considered as a form of the Laplace transform. Therefore, we express the kernel $K(x;t)$ by the inverse Laplace transform,

$$K(x;t) = \mathcal{L}^{-1}\left[\frac{2}{\omega}W(x;\omega^2)\right], \tag{4.10}$$

where $\omega = \sqrt{s}$. This equation gives the connection between the spectral sum and the correlator with the weight. In the following of this section, we demonstrate (4.10) with some examples.

We consider the subtracted HVP in (4.3) as a first example. We write the weight for the spectrum as

$$W^{(\mathrm{hvp})}(Q^2;\omega^2) = -\frac{Q^2}{\omega^2(\omega^2+Q^2)}. \tag{4.11}$$

Using (4.10), the kernel function of the correlator can be expressed by

$$\begin{aligned} K^{(\mathrm{hvp})}(Q^2;t) &= \mathcal{L}^{-1}\left[\frac{2}{\omega}W^{(\mathrm{hvp})}(Q^2;\omega^2)\right] \\ &= \frac{2}{Q^2}\left(1-\frac{Q^2t^2}{2}-\cos(Qt)\right). \end{aligned} \tag{4.12}$$

Thus, we obtain the subtracted HVP through

$$\Pi(Q^2)-\Pi(0) = \frac{2}{Q^2}\int_0^\infty dt\left(1-\frac{Q^2t^2}{2}-\cos(Qt)\right)C(t). \tag{4.13}$$

The first and second terms in the integral corresponds to the subtraction of the contact term. In fact, expanding the kernel near $t\to 0$,

$$\Pi(Q^2)-\Pi(0) = -\frac{Q^2}{12}\int_0^\infty dt\,t^4C(t) + \frac{Q^4}{36}\int_0^\infty dt\,t^6C(t)+\cdots, \tag{4.14}$$

we can easily confirm that this quantity is UV finite. The same expression can be found in [95], up to sign.

Next, we consider the Adler function, which is defined by a derivative of HVP,

$$\begin{aligned} D(Q^2) &= -Q^2\frac{\partial}{\partial Q^2}\Pi(Q^2) \\ &= Q^2\int_0^\infty \frac{\rho(s)}{(s+Q^2)^2}. \end{aligned} \tag{4.15}$$

Then, the weight function is given by

$$W^{(\mathrm{Adler})}(Q^2;\omega^2) = \frac{Q^2}{(\omega^2+Q^2)^2}. \tag{4.16}$$

By the inversion of the Laplace transform, the kernel has the following form,

$$\begin{aligned} K^{(\mathrm{Adler})}(Q^2;t) =& \mathcal{L}^{-1}\left[\frac{2}{\omega}W^{(\mathrm{Adler})}(Q^2;\omega^2)\right] \\ =& \frac{1}{Q^2}(2-2\cos(Qt)-Qt\sin(Qt)). \end{aligned} \tag{4.17}$$

We can then compute the Adler function $D(Q^2)$ through

$$D(Q^2) = \frac{1}{Q^2}\int_0^\infty dt\,(2-2\cos(Qt)-Qt\sin(Qt))C(t) \tag{4.18}$$

This expression is consistent with [96].

Next, we consider the moments of the spectra in lattice QCD. The q^2-derivative on the lattice that appears in (3.33) is equivalent to a temporal moment of the correlation function,

$$\int_0^\infty dt\, t^{2n+2}C(t) \propto M_n, \tag{4.19}$$

where n is a positive integer. This can be derived by [2]

$$\begin{aligned} K^{(\mathrm{mom})}(n;t) &= \mathcal{L}^{-1}\left[\frac{2}{\omega}\frac{1}{\omega^{2n+2}}\right] \\ &= \frac{2t^{2n+2}}{(2n+2)!}. \end{aligned} \tag{4.20}$$

The charmonium moments from lattice QCD can be compared with the phenomenological estimates. The lattice results agree well with the value extracted from the experiments in the literature [24, 97].

The determination of the charm quark mass and strong coupling constant [23, 24] is an important application of the moment in lattice QCD. In this application, the vector current is replaced by the pseudoscalar operator $J_P = \bar{c}\gamma_5 c$ since the correlator of this operator is more precisely calculable from lattice QCD. In addition, we do not need the renormalization if we multiply the operator by the bare quark mass m_c^{bare}.

[2] The factor 2 in the numerator does not appears in [24, 97]. Notice that the authors of these references define the same as (4.19) but t runs from $-\infty$ to $+\infty$. Thus, the factor 2 is due to the definition of the moment.

The charmonium moment is defined by

$$G(t) = (m_c^{\text{bare}})^2 \int d^3\mathbf{x} \, \langle 0|J_5(t,\mathbf{x})J_5(0,\mathbf{0})|0\rangle \,, \tag{4.21}$$

$$G_n = \int dt \, t^n G(t). \tag{4.22}$$

The corresponding perturbative series has been calculated up to the same order of the vector correlator, namely $\mathcal{O}(\alpha_s^3)$ [90, 98],

$$Q^2\Pi^P(Q^2) = \int_{-\infty}^{\infty} d^4\boldsymbol{x} \langle J_5(t,\boldsymbol{x})J_5(0,\mathbf{0})\rangle e^{iQ\cdot x}, \tag{4.23}$$

$$\Pi^P(Q^2) = \sum_{n=1} C_n^P \left(\frac{Q^2}{4m_q^2}\right)^n + (\text{subtraction}). \tag{4.24}$$

The relation between G_n and C_n^P is straightforward. Using several lower moments at the same time, we can determine $\alpha_s(\mu)$ and $m_c(\mu)$. The discretization effect would be, however, substantial, which is due to the heavy quark mass. To reduce it, one divides the moment G_n by the same quantity in the free theory $G_n^{(0)}$. The mistuning effect of the bare quark mass m_c can be made small by the ratio m_{η_c}/m_c, where m_{η_c} is the mass of the charmonium η_c. Using these technique, the moments of the correlators provide the precise determination of $m_c(\mu)$ and $\alpha_s(\mu)$.[3]

The spectral sums in this section have simple relations to the correlator (4.1). This is, however, not always the case for other spectral sum. In fact, the lattice computation of the Borel transform, which is the main interest in this thesis, is nontrivial since its definition (3.43) is rather complicated and can not be expressed by the derivative. Our treatment of this problem will be discussed in the following section.

4.2 Borel transform from lattice correlators

We compute the Borel transform $\tilde{\Pi}(M^2)$ using lattice QCD. The weighted integral of the spectral function of the form (3.43) can be interpreted as a smeared spectral function. To compute the smeared spectrum in lattice QCD, we use the method proposed in [35], which is based on the expansion of the smearing kernel in terms of the transfer matrix on the lattice. The method relates the smeared spectrum to the correlators computed on the lattice via the spectral representation. Applications to the inclusive $\bar{B}_s$ decay [36] and the inelastic lN scattering [37] have been discussed. We briefly review the key ideas of this method in the following. In this section, all parameters are in the unit of the lattice spacing a, unless otherwise stated.

We consider a current-current correlator with zero spatial momentum,

$$C(t) \equiv \sum_{\boldsymbol{x}} \langle 0|J_z(t,\boldsymbol{x})J_z(0,\mathbf{0})|0\rangle, \tag{4.25}$$

[3] The method has been extended to the bottomonium system [99].

where J_z stands for the z component of the vector current. Computation of such correlators as a function of the time separation t is straightforward in lattice QCD. The relation between the correlator and the spectral function is given by [95]

$$C(t) = \int_0^\infty d\omega\, \omega^2 \rho(\omega^2) e^{-\omega t}. \tag{4.26}$$

We recall that $\rho(\omega^2)$ is defined in (3.6). Here, we make a change of variable $\omega = \sqrt{s}$. Estimation of the spectral function $\rho(\omega^2)$ from (4.26) is an ill-posed inverse problem because the functions $e^{-\omega t}$ with different ω's are hard to distinguish numerically when ω's are close to each other. To avoid this problem, the method of [35] relates the correlator to the smeared spectral function such as (3.43), instead of the spectral function $\rho(\omega^2)$ itself.

We define the spectral density for a state $|\psi\rangle$,

$$\bar{\rho}(\omega) = \frac{\langle\psi|\delta(\hat{H}-\omega)|\psi\rangle}{\langle\psi|\psi\rangle}, \tag{4.27}$$

where $\hat{H}$ is the Hamiltonian. The spectral density $\bar{\rho}(\omega)$ evaluates the number of states having an energy ω. Setting $|\psi\rangle = e^{-\hat{H}t_0}\sum_{\boldsymbol{x}} J_z(0,\boldsymbol{x})|0\rangle$, the Laplace transform of the spectral density may be written in terms of the correlators,

$$\begin{aligned}
\bar{C}(t) \equiv \int_0^\infty d\omega\, \bar{\rho}(\omega) e^{-\omega t} &= \frac{\langle\psi|e^{-\hat{H}t}|\psi\rangle}{\langle\psi|\psi\rangle} \\
&= \frac{\sum_{\boldsymbol{x},\boldsymbol{y}}\langle 0|J_z(0,\boldsymbol{x})e^{-\hat{H}(t+2t_0)}J_z(0,\boldsymbol{y})|0\rangle}{\sum_{\boldsymbol{x},\boldsymbol{y}}\langle 0|J_z(0,\boldsymbol{x})e^{-2\hat{H}t_0}J_z(0,\boldsymbol{y})|0\rangle} \\
&= \frac{\sum_{\boldsymbol{x},\boldsymbol{y}}\langle 0|J_z(t+2t_0,\boldsymbol{x})J_z(0,\boldsymbol{y})|0\rangle}{\sum_{\boldsymbol{x},\boldsymbol{y}}\langle 0|J_z(2t_0,\boldsymbol{x})J_z(0,\boldsymbol{y})|0\rangle} = \frac{C(t+2t_0)}{C(2t_0)}.
\end{aligned} \tag{4.28}$$

Here, we introduce a small-time separation $t_0 > 0$ to avoid the contact term that potentially diverges at $t_0 = 0$. In this paper, we set $t_0 = 1$ not to lose high energy state contributions too much. The correlator $\bar{C}(t)$ is normalized as $\bar{C}(0) = 1$.

Let us now consider a smeared spectral function,

$$\rho_s = \int_0^\infty d\omega\, \bar{\rho}(\omega) S(\omega), \tag{4.29}$$

with a smearing kernel $S(\omega)$, which will be specified later. One may approximate the smearing kernel in terms of the shifted Chebyshev polynomials T_j^* of $e^{-\omega}$,

$$S(\omega) = \frac{c_0^*}{2} + \sum_{j=1}^{N_t} c_j^* T_j^*(e^{-\omega}), \tag{4.30}$$

$$c_j^* = \frac{2}{\pi}\int_0^\pi d\theta\, S\left(-\log\left(\frac{1+\cos\theta}{2}\right)\right)\cos(j\theta), \tag{4.31}$$

where N_t stands for the truncation order of the approximation. The explicit form of the polynomial is $T_1^*(x) = 2x - 1$, $T_2^*(x) = 8x^2 - 8x + 1, \cdots$ and higher-order terms are constructed recursively as $T_{j+1}^*(x) = 2(2x-1)T_j^*(x) - T_{j-1}^*(x)$. Note that the Chebyshev approximation is an orthogonal expansion and we do not impose any condition such as the one that $e^{-\omega}$ being small for its convergence. We substitute this expression to (4.29). Then the smeared spectral function is written in terms of the transfer matrix $e^{-\hat{H}}$ as

$$\rho_s = \frac{c_0^*}{2} + \sum_{j=1}^{N_t} c_j^* \langle T_j^*(e^{-\hat{H}})\rangle, \tag{4.32}$$

where

$$\langle T_j^*(e^{-\hat{H}})\rangle \equiv \frac{\langle\psi|T_j^*(e^{-\hat{H}})|\psi\rangle}{\langle\psi|\psi\rangle}. \tag{4.33}$$

Here we replaced ω by $\hat{H}$ when sandwiched by the states $\langle\psi|$ and $|\psi\rangle$, and performed the integral over ω in (4.29). We can write the expectation value $\langle T_j^*(e^{-\hat{H}})\rangle$ using the correlators as

$$\langle T_1^*(e^{-\hat{H}})\rangle = 2\bar{C}(1) - 1,\ \langle T_2^*(e^{-\hat{H}})\rangle = 8\bar{C}(2) - 8\bar{C}(1) + 1, \cdots, \tag{4.34}$$

where we use $\langle\psi|e^{-\hat{H}t}|\psi\rangle \propto \sum_{\boldsymbol{x}}\langle J_z(t+2t_0,\boldsymbol{x})J_z(0,\boldsymbol{0})\rangle$ in (4.28) derived from (4.25) and (4.27).

In practice, the lattice correlators contain statistical errors. Since (4.34) involves cancellations of $\bar{C}(t)$ with different t's, the resulting expectation values $\langle T_j^*(e^{-\hat{H}})\rangle$ may induce large statistical errors. In particular, since we have to take an additional constraint $|\langle T_j^*(e^{-\hat{H}})\rangle| \le 1$ into account [35], the statistical error causes a significant problem. We therefore determine $\langle T_j^*\rangle$ $(j = 1, \cdots, N_t)$ through a fit of correlators. Since $T_{N_t}^*(x)$ includes terms up to x^{N_t}, the data of $\bar{C}(t)$ at $t = 0$–N_t are used in the fit.

Now we turn to the discussion of the Borel transform. The relation between $\bar{\rho}(\omega)$ and $\rho(\omega^2)$ is found as [see (4.26) and (4.28)]

$$\bar{\rho}(\omega) = \frac{1}{C(2t_0)}\omega^2\rho(\omega^2)e^{-2\omega t_0}. \tag{4.35}$$

We therefore set $S(\omega)$ to be $S(M,\omega)$ as a function of the Borel mass M as

$$S(M,\omega) \equiv \frac{2C(2t_0)e^{2\omega t_0}}{M^2\omega}e^{-\omega^2/M^2}, \tag{4.36}$$

to obtain the Borel transform as a smeared spectral function,

$$\int_0^\infty d\omega\, S(M,\omega)\bar{\rho}(\omega) = \frac{1}{M^2}\int_0^\infty ds\,\rho(s)e^{-s/M^2} = \tilde{\Pi}(M^2), \tag{4.37}$$

where we change the variable as $s = \omega^2$. The smearing kernel (4.36) has an apparent problem of divergence at $\omega = 0$, which induces divergences of the coefficients c_j^* (4.31). We therefore introduce a cutoff to regularize the integral (4.31). Since the spectrum $\rho(s)$ vanishes below the energy of the lowest-lying state, any modification of the kernel below the lowest energy does not affect the final result. We therefore modify the smearing kernel,

$$S^{\rm cut}(M,\omega) \equiv \frac{2C(2t_0)e^{2\omega t_0}}{M^2\omega} e^{-\omega^2/M^2} \tanh(\omega/\omega_0), \tag{4.38}$$

where ω_0 is set smaller than the mass of the ground state. The form of $S^{\rm cut}(M,\omega)$ is shown in Fig. 4.2. With ω_0 not much smaller than the lowest hadronic state, the modified smearing underestimates the smeared spectrum. In this work, we consider the $s\bar{s}$ states, for which the lowest energy state is the ϕ meson, whose mass is $\sim$ 1 GeV. We will discuss how the error due to the modified smearing can be corrected.

To summarize, we obtain the approximation between the smeared spectral function and $\langle T_j^* \rangle$:

$$\begin{aligned} \tilde{\Pi}^{\rm cut}(M^2) &= \int_0^\infty d\omega\, S^{\rm cut}(M,\omega)\bar{\rho}(\omega) \\ &\simeq \frac{c_0^*(M)}{2} + \sum_{j=1}^{N_t} c_j^*(M)\langle T_j^* \rangle, \end{aligned} \tag{4.39}$$

where $c_j^*(M)$ is evaluated as (4.31) with $S(\omega) = S^{\rm cut}(M,\omega)$.

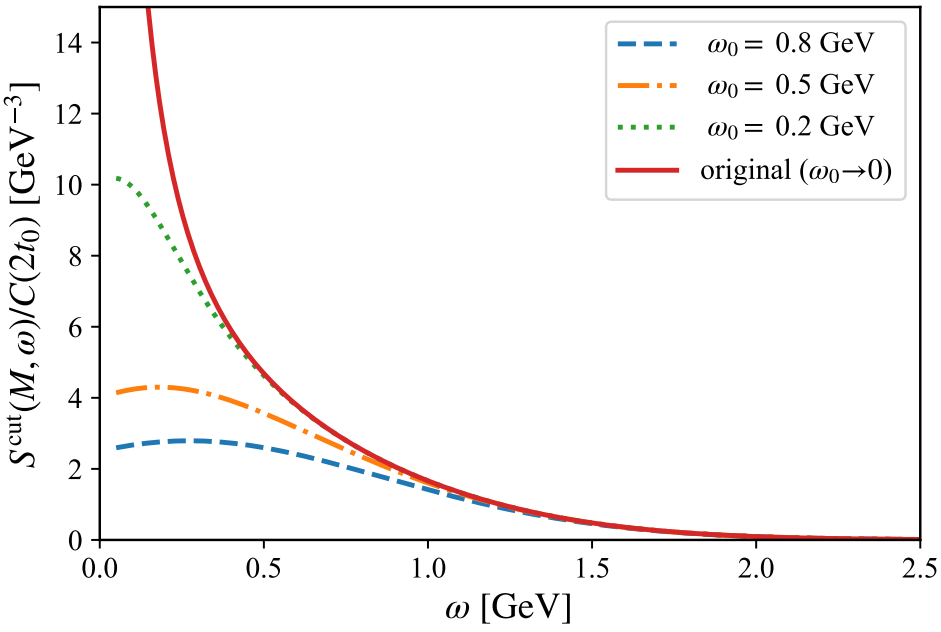

FIGURE 4.2: Smearing kernels $S^{\mathrm{cut}}(M,\omega)$ with different values of the cutoff parameter ω_0. We set $M = 1$ GeV and $t_0 = (2.453\,\mathrm{GeV})^{-1}$. The solid line shows the original kernel $S(M,\omega)$, which is equivalent to the limit $\omega_0 \to 0$ for $S^{\mathrm{cut}}(M,\omega)$. Here, the all parameters are dimensionful.

Chapter 5

Spectral sum of current correlators from lattice QCD

5.1 Lattice calculation

We compute two-point correlators of the vector current $J_\mu = \bar{s}\gamma_\mu s$ using lattice QCD. In this work, we neglect the disconnected diagrams. We use ensembles with $N_f = 2+1$ dynamical Möbius domain-wall fermions [69], where the gauge action is tree-level Symanzik improved. Parameters of the ensembles are listed in Table 5.1. Three lattice cutoffs a^{-1} are in the range 2.45–4.50 GeV. The lattice size $L^3 \times T$ is taken such that the physical volume extent is $L \simeq 2.5$ fm and $T = 2L$. The lattice size in the extra dimension L_5 to define the domain-wall fermion is chosen to ensure that the residual quark mass is less than 1 MeV [76]. In the fermion action, the gauge links are stout-smeared 3 times. The number of gauge configurations is $N_{\rm conf}$. To reduce statistical errors, we use Z_2 noise sources distributed on a source time slice. We measure correlators on each configuration 8 or 12 times with different time slices taken for the Z_2 noise source. The number of measurements $N_{\rm meas}$ is $N_{\rm conf}$ times the number of the source time slices. The effective number of the statistics would be slightly smaller than $N_{\rm meas}$, because the measurements on the same configuration with different source time slices are statistically correlated. In our computation, u and d quark masses are degenerate, which appear only as sea quarks. The strange quark mass m_s is set near the physical value. Small mistuning of the strange quark mass will be corrected as discussed in Sec. 5.1.3. The ensembles have been used for the computation of Dirac eigenvalues [100], charmonium moments [24], short distance current-current correlators [20], topological susceptibility [101], and η' meson mass [102]. Other details of the ensembles are available in [103, 104].

Figure 5.1 shows the normalized correlator (4.28) on the coarse lattice. The circles with small error bars represent the correlator on the configurations of $\beta = 4.17$. The dotted line in this figure denotes the contribution of the ground state, namely ϕ meson; it is given by $\bar{C}(t) = \frac{1}{2} f_\phi^2 m_\phi e^{-m_\phi(t+2)}/C(2)$. The constants, f_ϕ and m_ϕ, are obtained by an exponential fit. We show $\bar{C}(t)$ in the range $t = 1$–18 which is used in the following discussion. For finer lattices, see also Figs. H.1 and H.2.

β	a^{-1} [GeV]	$L^3 \times T(\times L_5)$	N_{conf}	N_{meas}	am_{ud}	am_s
4.17	2.453(4)	$32^3 \times 64(\times 12)$	100	800	0.0070	0.0400
4.35	3.610(9)	$48^3 \times 96(\times 8)$	50	600	0.0042	0.0250
4.47	4.496(9)	$64^3 \times 128(\times 8)$	50	400	0.0030	0.0150

TABLE 5.1: Ensembles in our simulations.

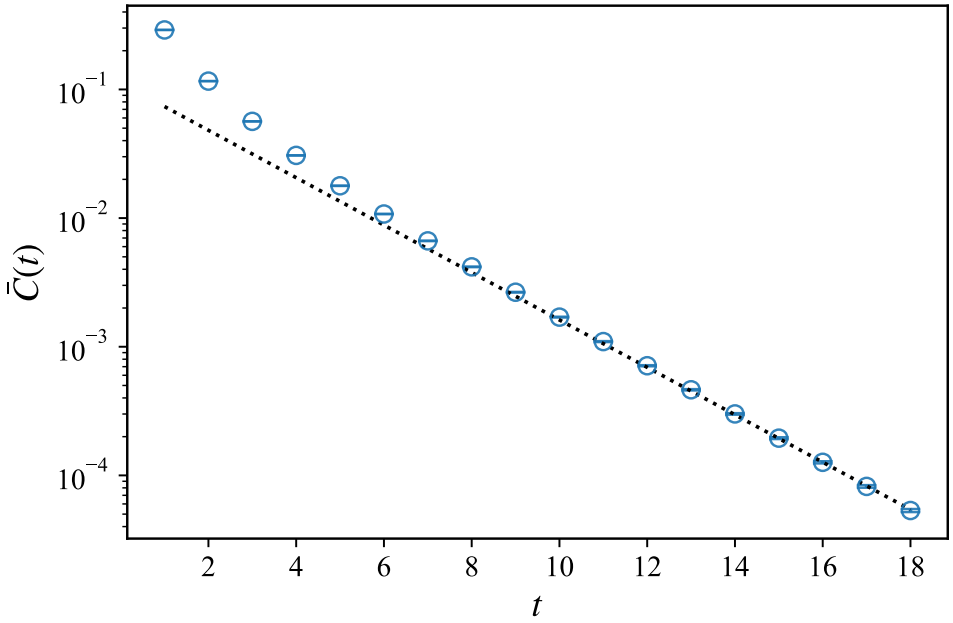

FIGURE 5.1: Normalized correlation functions $\bar{C}(t)$ on the coarse lattice ($a^{-1} = 2.453$ GeV). The dotted line shows the asymptotic form of the correlator.

We compute the Borel transform of the HVP using the technique outlined in the previous section. The estimate for the Chebyshev matrix elements $\langle T_j^* \rangle$ in (4.39) is obtained by a fit of lattice correlators. The fit is implemented using `lsqfit` [105], which is based on Bayesian statistics [106]. Following [35], we write the correlator at each temporal separation by the Chebyshev matrix elements as

$$\bar{C}(t) = 2^{1-2t} \left[\frac{1}{2} \binom{2t}{t} + \sum_{j=1}^{t} \binom{2t}{t-j} \langle T_j^* \rangle \right], \tag{5.1}$$

using the reverse formula of the shifted Chebyshev polynomials

$$x^n = 2^{1-2n} \left[\frac{1}{2} \binom{2n}{n} + \sum_{j=1}^{n} \binom{2n}{n-j} T_j^*(x) \right]. \tag{5.2}$$

The Chebyshev matrix elements $\langle T_j^* \rangle$ are determined such that they best reproduce $\bar{C}(t)$ under the given statistical error while satisfying the necessary condition $|\langle T_j^* \rangle| \leq 1$. Combining them with the coefficients $c_j^*(M)$, we obtain $\tilde{\Pi}^{\text{cut}}(M^2)$

through (4.39).

In order to match the lattice results with the counterpart in the $\overline{\rm MS}$ scheme, the renormalization factor has to be multiplied. We use the renormalization constants of the vector current $Z_V = 0.955(9), 0.964(6), 0.970(5)$ for $\beta = 4.17, 4.35, 4.47$, respectively [19]. They are determined by matching short-distance current correlators with their perturbative counterpart in the coordinate space. Our results can be compared with $\tilde{\Pi}^{\rm OPE}(M^2)$ in the $\overline{\rm MS}$ scheme after the renormalization.

In the following subsections, we discuss potential systematic effects due to the truncation of the Chebyshev expansion, the effect of the low-energy cut introduced in the smearing function, and the continuum extrapolation.

5.1.1 Convergence of Chebyshev expansion

We first examine the convergence of the Chebyshev expansion. In Figs. 5.2–5.4 we plot the smearing function $S^{\rm cut}(M,\omega)$ at $\omega = 1.0$ and 2.0 GeV and their Chebyshev expansions as a function of $1/M^2$. They are understood as the Borel transform for the case that the spectrum is given by $\rho(\omega) \sim \delta(\omega - 1.0\ {\rm GeV})$ or $\delta(\omega - 2.0\ {\rm GeV})$. The cutoff parameter ω_0 is set to $\omega_0 = 0.6$ GeV. Figures 5.2–5.4 represent those at three lattices, respectively. They differ due to the factor $e^{2\omega t_0}$, since t_0 is fixed to 1 in the lattice unit. The solid line shows the exact form $S^{\rm cut}(M,\omega)$, while dotted, dash-dotted, and dashed lines are the expansions truncated at $N_t =$ 12, 15, and 18, respectively. One can see that the expansion reproduces the exact function to quite a good precision already at $N_t = 12$. At the fine and finest lattice spacing where $a^{-1} = 3.610$ GeV and 4.496 GeV (Fig. 5.3 and Fig. 5.4), we find a small deviation around $1/M^2 \simeq 2\ {\rm GeV}^{-2}$ for $N_t = 12$. Such a low energy regime is dominated by the ground state and we are able to correct the error explicitly using the mass and amplitude of the ground state. In the intermediate regime $1/M^2 \lesssim 1\ {\rm GeV}^{-2}$, the maximum deviation is found to be 0.4% for $N_t > 15$. In the low energy regime, $\tilde{\Pi}(M^2)$ becomes more sensitive to the long-distance correlator. We expect that higher-order polynomials are needed when the lattice spacing is small.

The truncation error can also be estimated through the coefficients $c_j^*(M)$ in (4.31) because $\langle T_j^* \rangle$ is bounded as $|\langle T_j^* \rangle| \leq 1$. In Fig. 5.5 we show the absolute values of the coefficients at various M^2s at each lattice spacing. The plots demonstrate that the coefficients decrease exponentially for large j. When the scale M is large, the coefficient $c_j^*(M)$ drops more rapidly for high orders (larger j's). It implies that $\sum_j c_j^*(M)\langle T_j^* \rangle$ is dominated by the lower-order terms, which corresponds to shorter-distance correlators. At $1/M^2 \sim 2\ {\rm GeV}^{-2}$ which corresponds to the lowest scale treated in this work, the coefficient $c_j^*(M^2)$ is sufficiently small ($\sim \mathcal{O}(10^{-4})$) already at $j = 18$. We therefore set $N_t = 18$ in the following.

In order to have another insight into the possible error due to the Chebyshev approximation, let us consider a simple model that has a single pole,

$$\rho^{\rm pole}(s) = \tilde{f}^2\delta(s-\tilde{m}^2) \tag{5.3}$$

with mass $\tilde{m}$ and decay constant $\tilde{f}$. The corresponding Euclidean correlator is

$$C^{\rm pole}(t) = \int_0^\infty d\omega\, e^{-\omega t}\omega^2\rho^{\rm pole}(\omega^2) = \frac{\tilde{f}^2\tilde{m}}{2}e^{-\tilde{m}t}, \tag{5.4}$$

and the normalized correlator (4.28) is given by

$$\bar{C}^{\rm pole}(t) = \frac{C^{\rm pole}(t+2t_0)}{C^{\rm pole}(2t_0)} = e^{-\tilde{m}t}. \tag{5.5}$$

In this test, we ignore statistical errors and replace the expectation values $\langle T_j^*\rangle$ by the shifted Chebyshev polynomials $T_j^*(e^{-a\tilde{m}})$ without introducing the fit. Combining the polynomials and the coefficients $c_j^*(M)$ determined by (4.31) with the smearing kernel $S^{\rm cut}(M,\omega)$, we obtain the Borel transform $\tilde{\Pi}^{\rm pole}(M^2)$. We can also analytically calculate the Borel transform of the single-pole spectrum with the modification of the low-energy spectrum (4.38),

$$\begin{aligned}\tilde{\Pi}^{\rm pole}(M^2) &= \frac{1}{M^2}\int_0^\infty ds\, e^{-s/M^2}\rho^{\rm pole}(s)\tanh\left(\sqrt{s}/\omega_0\right)\\ &= \frac{\tilde{f}^2}{M^2}e^{-\tilde{m}^2/M^2}\tanh(\tilde{m}/\omega_0).\end{aligned} \tag{5.6}$$

The results are compared in Fig. 5.6 at three lattice spacings. The thick solid lines denote the analytic results (5.6) with $\omega_0 = 0.6$ GeV, while the thin solid lines denote those in the limit $\omega_0 \to 0$, that is, $\tanh(\tilde{m}/\omega_0) \to 1$. The dotted, dash-dotted, and dashed line are $\tilde{\Pi}^{\rm pole}(M^2)$ computed by our method for three lattice spacings, respectively. The expansion is nearly perfect and the expansions at three lattice spacings are consistent with each other. The difference between the original function and that with the cutoff remains when the pole mass is small, $\tilde{m} = 1$ GeV. We correct them as discussed in the following.

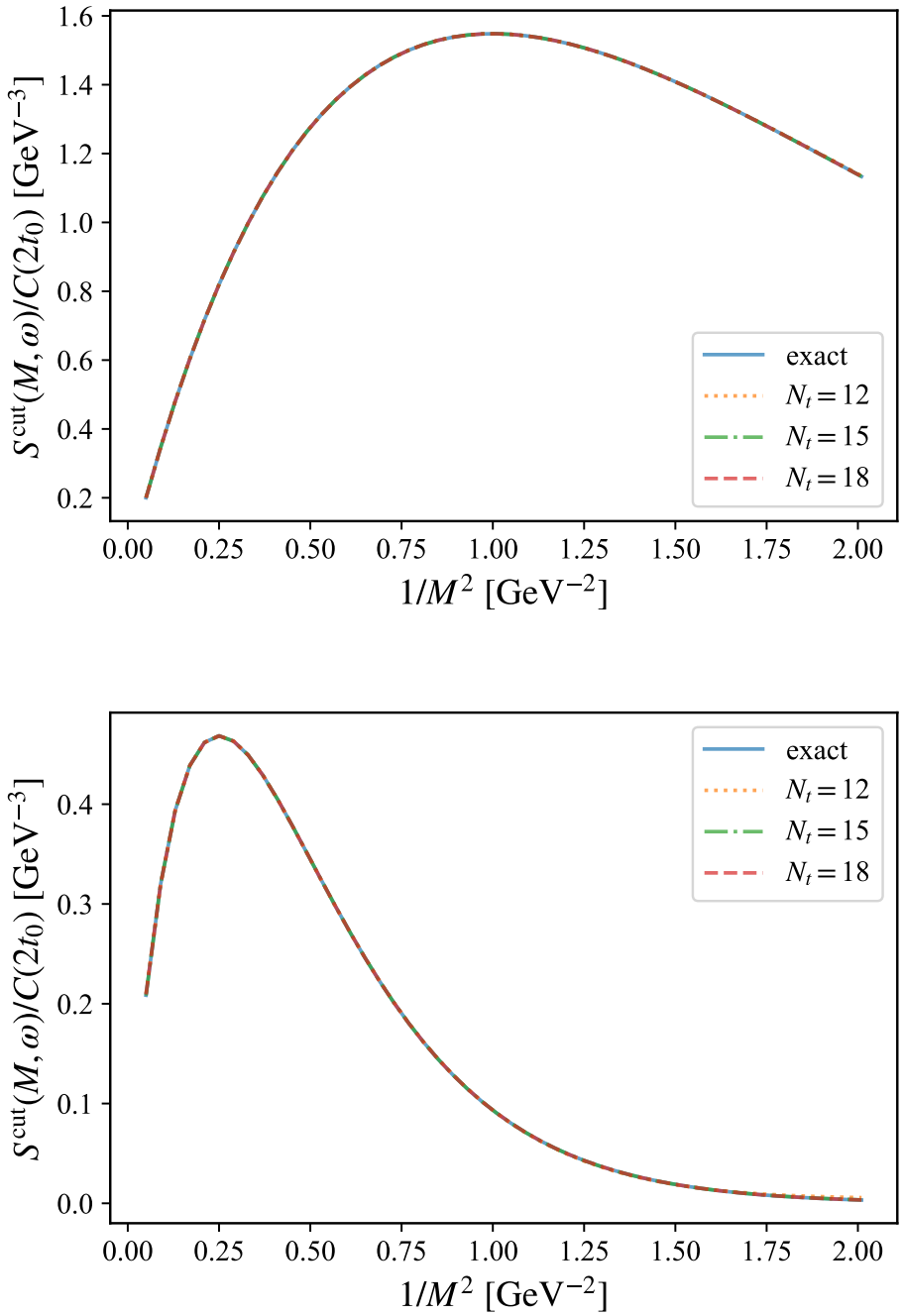

FIGURE 5.2: Expansion of the smearing kernel at $\omega = 1.0$ GeV (top) and $\omega = 2.0$ GeV (bottom) for the coarse lattice where $a^{-1} = 2.453$ GeV with a cutoff $\omega_0 = 0.6$ GeV.

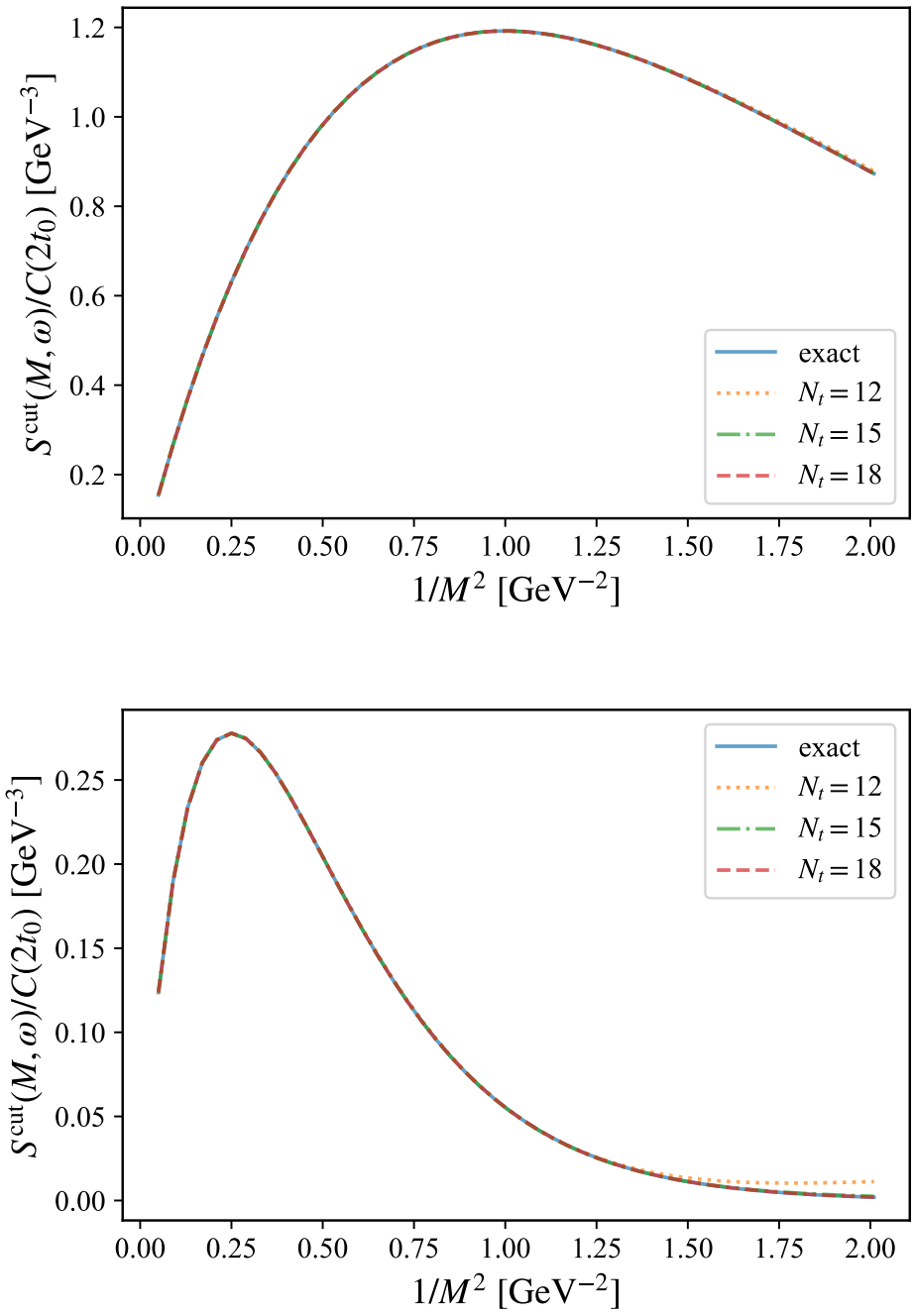

FIGURE 5.3: Same as Fig. 5.2 but at $a^{-1} = 3.610$ GeV.

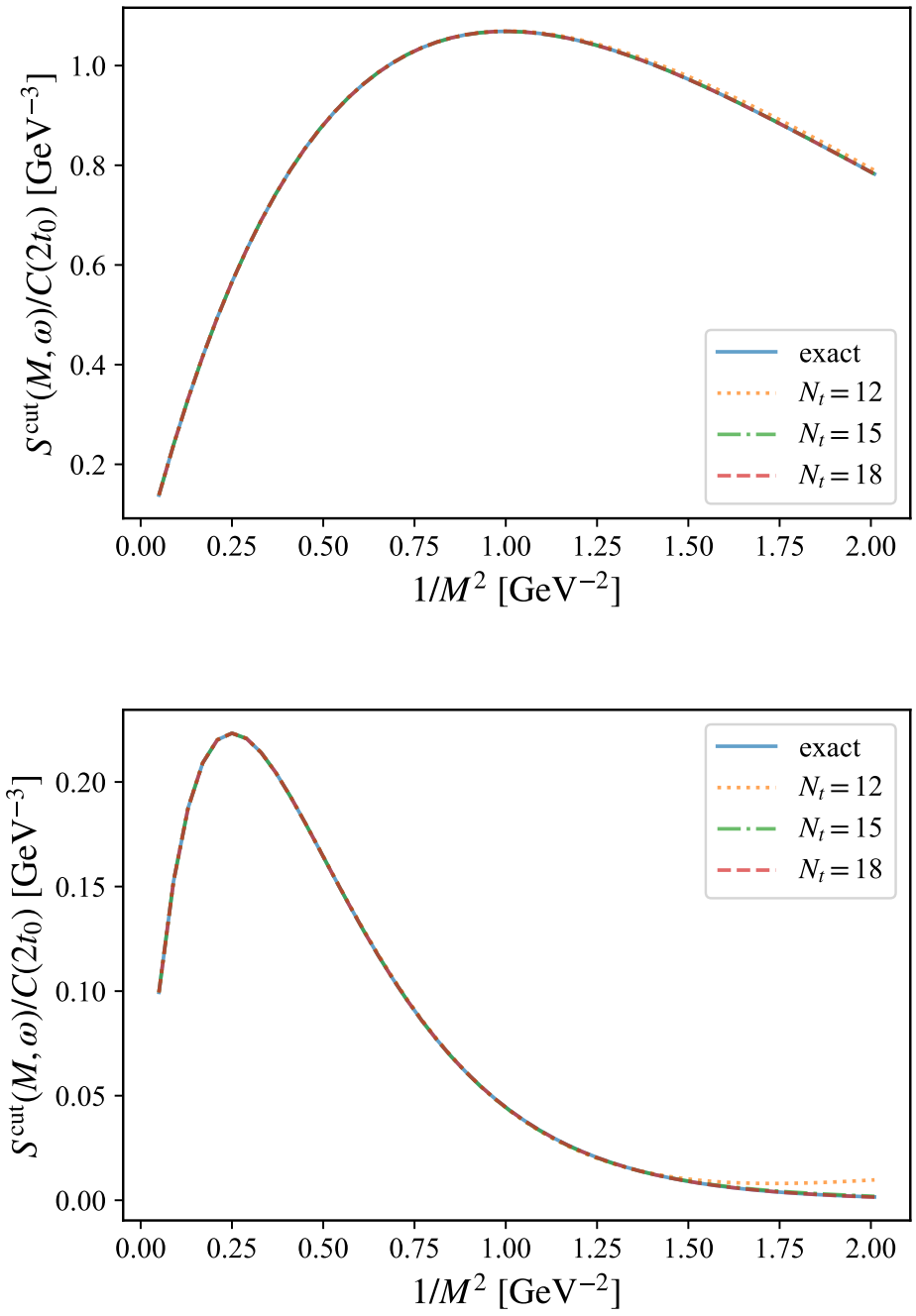

FIGURE 5.4: Same as Fig. 5.2 but at $a^{-1} = 4.496$ GeV.

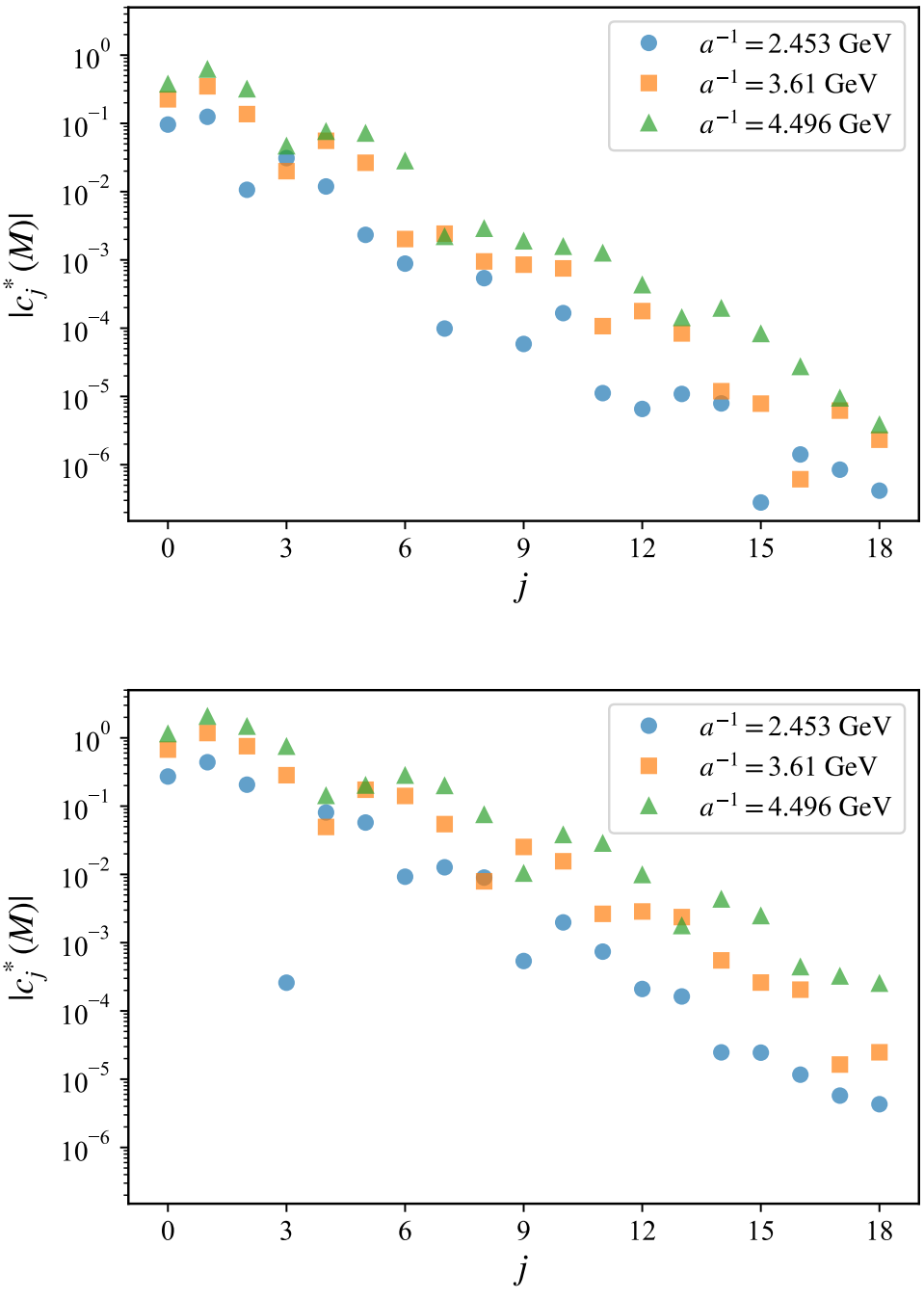

FIGURE 5.5: The coefficients $c_j^*(M)$ at three lattice spacing. We set $1/M^2 = 0.45\,\text{GeV}^{-2}$ (top) and $1/M^2 = 1.85\,\text{GeV}^{-2}$ (bottom).

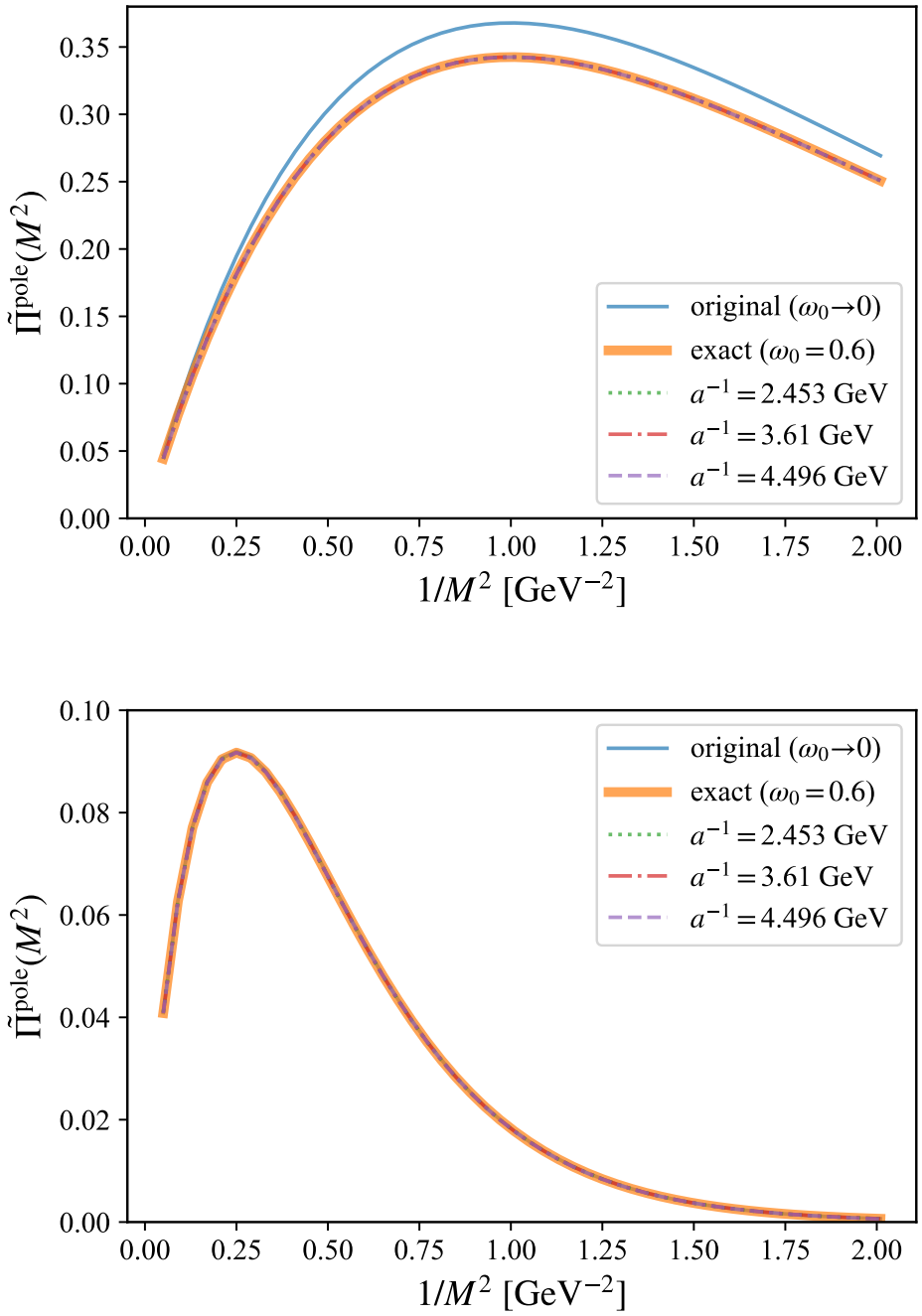

FIGURE 5.6: $\tilde{\Pi}^{\text{pole}}(M^2)$ for three lattice spacings with $N_t = 18$, $\omega_0 = 0.6$ GeV. We set $\tilde{f} = 1$ GeV, and $\tilde{m} = 1$ GeV (top) and $\tilde{m} = 2$ GeV (bottom).

5.1.2 Correction for the low-energy cut of smearing function

The low-energy cut $\tanh(\omega/\omega_0)$ introduced to avoid the artificial divergence of the Chebyshev coefficients modifies the shape of the smearing kernel below $\omega \lesssim \omega_0$. If we set ω_0 sufficiently small, only the contribution from the ground state, *i.e.*, the ϕ meson in our example, is significantly affected. We therefore correct for the error by using the information available for the ground state.

The contribution of the ground state $\rho_\phi(s)$ for the spectral function is

$$\rho_\phi(s) = f_\phi^2 \delta(s - m_\phi^2), \tag{5.7}$$

where f_ϕ and m_ϕ are the decay constant and the mass of the ϕ meson, respectively. The ϕ meson's contribution to the Borel transform is then

$$\tilde{\Pi}_\phi^{\mathrm{cut}}(M^2) \equiv \frac{f_\phi^2}{M^2} e^{-m_\phi^2/M^2} \tanh\bigl(m_\phi/\omega_0\bigr). \tag{5.8}$$

Taking the limit $\omega_0 \to 0$, it recovers the physical result,

$$\tilde{\Pi}_\phi(M^2) \equiv \frac{f_\phi^2}{M^2} e^{-m_\phi^2/M^2}. \tag{5.9}$$

The difference between the Borel transform with and without the modification is then

$$\delta\tilde{\Pi}_\phi^{\mathrm{cut}} \equiv \tilde{\Pi}_\phi(M^2) - \tilde{\Pi}_\phi^{\mathrm{cut}}(M^2) = \frac{f_\phi^2}{M^2} e^{-m_\phi^2/M^2} (1 - \tanh\bigl(m_\phi/\omega_0\bigr)), \tag{5.10}$$

which we add back to the result of $\tilde{\Pi}^{\mathrm{cut}}(M^2)$ as

$$\tilde{\Pi}^{\mathrm{lat}}(M^2) \equiv \tilde{\Pi}^{\mathrm{cut}}(M^2) + \delta\tilde{\Pi}_\phi^{\mathrm{cut}}(M^2). \tag{5.11}$$

The deficit $\delta\tilde{\Pi}_\phi^{\mathrm{cut}}(M^2)$ can be computed using the values of f_ϕ and m_ϕ obtained for each lattice ensemble.

We show a typical threshold ω_0 dependence of $\tilde{\Pi}^{\mathrm{lat}}(M^2)$ at certain values of M^2 in Fig. 5.7 and Fig. H.3. Squares and circles denote the $\tilde{\Pi}^{\mathrm{cut}}(M^2)$ and $\tilde{\Pi}^{\mathrm{lat}}(M^2)$, respectively. As ω_0 increases, $\tilde{\Pi}^{\mathrm{cut}}(M^2)$ decreases, as we expected. After the correction, $\tilde{\Pi}^{\mathrm{lat}}(M^2)$ is insensitive to ω_0. On the finest lattice, the small value of ω_0 enhances the statistical errors. To avoid large errors, we set $\omega_0 = 0.6$ GeV for all lattice spacings in the following results. The error due to the low-energy modification is negligible after correcting for the ground state contribution.

5.1.3 Continuum limit

We take 50 points of $1/M^2$ in the range $1/M^2 = 0.05$–2.05 GeV^{-2} and compute $\tilde{\Pi}^{\mathrm{lat}}(M^2)$ for each lattice spacing. The results are shown in Fig. 5.8. We find that

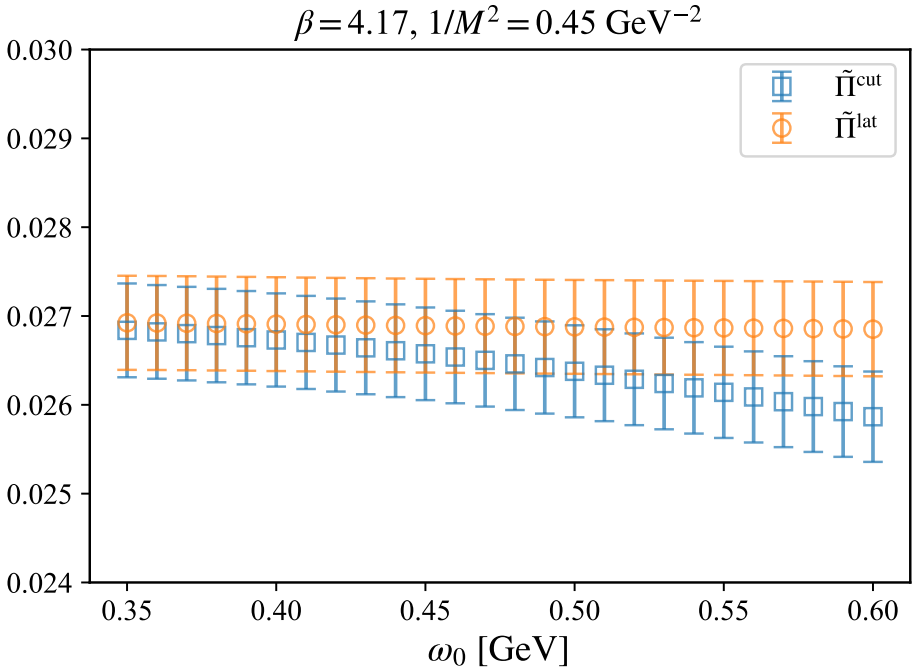

FIGURE 5.7: The cutoff dependence of $\tilde{\Pi}^{\mathrm{cut}}(M^2)$ and $\tilde{\Pi}^{\mathrm{lat}}(M^2)$ on the coarse lattice, where $N_t = 18$.

the results obtained at two coarser lattice spacing agree well except in the region $1/M^2 \lesssim 0.2\ \mathrm{GeV}^{-2}$, where discretization effects are visible. The data at finest lattice spacing show a slight deviation from those at two coarser lattices, but we note that the strange quark mass is slightly mistuned on this ensemble and we have to correct that effect (see below.)

We take the continuum limit of $\tilde{\Pi}^{\mathrm{lat}}(M^2)$ using the data at three lattice spacings. Since both the statistical and systematic errors correlate highly among different values of $1/M^2$, we introduce an ansatz

$$\tilde{\Pi}^{\mathrm{lat}}(M^2) + \delta\tilde{\Pi}_m = \tilde{\Pi}(M^2)(1 + b_0 M^2 a^2)(1 + b_1 a^2), \tag{5.12}$$

with coefficients b_0 and b_1 to parametrize the discretization effect independent of $1/M^2$. We introduce a correction $\delta\tilde{\Pi}_m$ to incorporate the mistuning of the valence quark mass m_s. The size of the mistunig is discussed in Appendix G. At tree level, the correction $\delta\tilde{\Pi}_m$ is expressed as

$$\delta\tilde{\Pi}_m = +\frac{3}{2\pi^2}\frac{m^2_{\mathrm{siml}}(\mu^2) - m^2_{\mathrm{phys}}(\mu^2)}{M^2} - \frac{2(m_{\mathrm{siml}}(\mu^2) - m_{\mathrm{phys}}(\mu^2))\langle 0|\bar{q}q|0\rangle}{M^4}, \tag{5.13}$$

where $m_{\mathrm{phys}}(\mu^2)$ and $m_{\mathrm{siml}}(\mu^2)$ are the strange quark masses at the scale μ. We take $Z_S^{-1}(\mu; a)m_{\mathrm{bare}}$ for m_{siml} and $m_s(\mu^2 = (2\ \mathrm{GeV})^2) = 0.0920(11)$ GeV for m_{phys} as an initial value of the running. The renormalization constants for the scalar density operator $Z_S(2\ \mathrm{GeV}; a)$ are 1.0372(146), 0.9342(87), 0.8926(67) for $\beta = 4.17, 4.35, 4.47$,

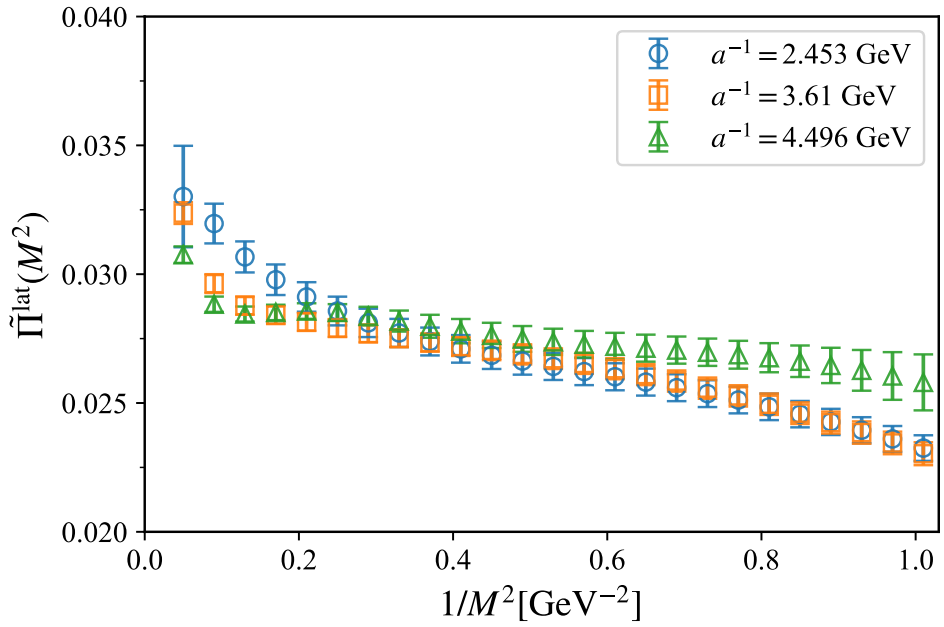

FIGURE 5.8: $\tilde{\Pi}^{\rm lat}(M^2)$ at all lattice spacings.

respectively [19]. The mass $m_{\rm bare}$ is from am_s listed in Table 5.1. The corrections $\delta\tilde{\Pi}_m(M^2)$ calculated at the leading order of perturbation theory are less than 4% of $\tilde{\Pi}^{\rm lat}(M^2)$ on the two coarse lattices, while that on the finest lattice decrease $\tilde{\Pi}^{\rm lat}(M^2)$ by at most 10% in the range $1/M^2 = 0.25$–1.01 GeV^{-2} (see also Fig. H.4). We show the Borel transform with this correction in Fig. H.5. Higher order perturbative corrections are insignificant compared to the statistical precision of the lattice data. In each case, the correction may introduce systematic uncertainty at large $1/M^2$, since the correction relies on OPE. Therefore, we consider $\Pi^{\rm lat}(M^2)$ at $1/M^2 = 1.01$ GeV^{-2} and lower.

The M^2 dependence of the discretization error is incorporated in the fit by the factor $(1 + b_0 M^2 a^2)$. The other factor $(1 + b_1 a^2)$ represents the discretization error independent of M^2. We take the continuum limit for $\tilde{\Pi}^{\rm lat}(M^2) + \delta\tilde{\Pi}_m(M^2)$ by a global fit in the range $0.25\ \mathrm{GeV}^{-2} \le 1/M^2 \le 1.01\ \mathrm{GeV}^{-2}$. The correlation of $\tilde{\Pi}^{\rm lat}(M^2) + \delta\tilde{\Pi}_m(M^2)$ among different M^2 is taken into account. The continuum extrapolation at some values of $1/M^2$ is shown in Fig. 5.9 and Fig. H.6. The circle, square, and triangle symbols show $\tilde{\Pi}^{\rm lat}(M^2) + \delta\tilde{\Pi}_m(M^2)$ at $a^{-1} = 2.453,\ 3.610,\ 4.496$ GeV, respectively, while the star symbol represents the continuum limit. The discretization errors are not substantial. Although the $\tilde{\Pi}^{\rm lat}(M^2)$ on the finest lattice has a relatively large error, the error of $\tilde{\Pi}(M^2)$ in the continuum limit is under good control.

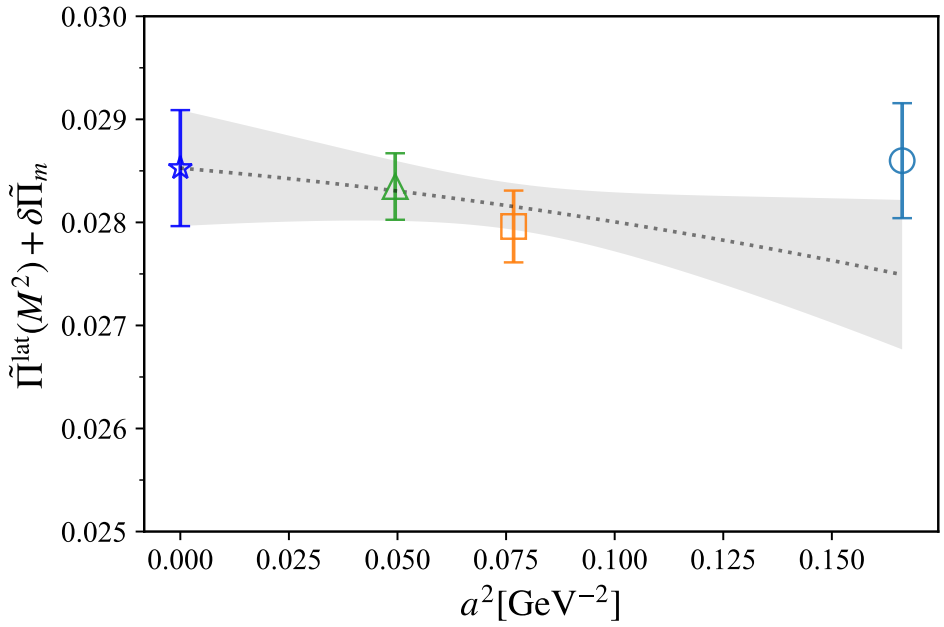

FIGURE 5.9: Continuum extrapolation of $\tilde{\Pi}^{\rm lat}(M^2) + \delta\tilde{\Pi}_m$ at $1/M^2 = 0.25\ \mathrm{GeV}^{-2}$.

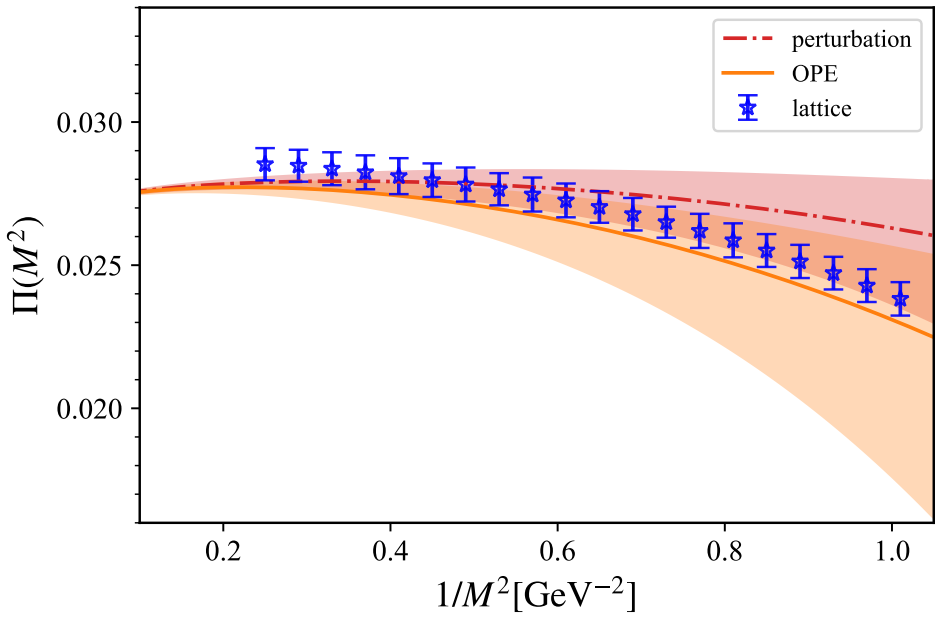

FIGURE 5.10: Comparison of $\tilde{\Pi}(M^2)$ in the continuum limit with the perturbative expansion and OPE.

5.2 Result

5.2.1 Comparison with OPE

We compare the Borel transform $\tilde{\Pi}(M^2)$ at large M^2 with perturbative expansion as well as with OPE in Fig. 5.10. The dash-dotted line denotes the perturbative expansion $\tilde{\Pi}^{\mathrm{pert}}(M^2)$ up to $\mathcal{O}(\alpha_s^4)$. It includes the mass-dependent perturbative correction up to $\mathcal{O}(\alpha_s^3 m_s^2/M^2)$. The solid line shows the OPE result $\tilde{\Pi}^{\mathrm{OPE}}(M^2)$. The bands represent the size of errors due to the input parameters and the truncation of perturbative expansion.

Here, input parameters are the QCD scale parameter $\Lambda_{\overline{\mathrm{MS}}}^{n_f=3} = 0.332(17)$ GeV [107], the strange quark mass in the $\overline{\mathrm{MS}}$ scheme $m_s^{n_f=2+1}(\mu = 2\,\mathrm{GeV}) = 0.0920(11)\,\mathrm{GeV}$ (FLAG average) [99, 108–112] the chiral condensate[1] $\langle 0|\bar{q}q|0\rangle = -[0.272(5)\ \mathrm{GeV}]^3$ (FLAG average) [101, 108, 115–119], and the gluon condensate $\langle 0|\frac{\alpha_s}{\pi}G^2|0\rangle = 0.0120(36)\,\mathrm{GeV}^4$ [16, 17] (adding $\pm 30\%$ error).

In the calculation of the perturbative expansion and OPE, we set the renormalization scale $\mu^2 = 4M^2 e^{-\gamma_E}$. The running of α_s, m_s, and $\langle 0|\bar{q}q|0\rangle$ are taken into account

[1] We use the chiral condensate evaluated in the massless quark limit, rather than the "strange quark condensate," which has also be evaluated using lattice QCD [113] as $\langle \bar{s}s\rangle(2\,\mathrm{GeV}) = -(296(11)\,\mathrm{MeV})^3$. The reason is that the difference from the massless limit involves a quadratic divergence and a renormalon ambiguity of order of $m_s\Lambda_{\mathrm{QCD}}^2$, which is the same order of the correction itself, is induced when the divergence is subtracted. In [113], the subtraction scheme is not explicitly shown, and in [114] it is performed by fitting the lattice data at various lattice cutoffs. Thus, the precise definition of the strange quark condensate might not correspond to what we employed.

using `RunDec` [52, 53] at five-loop level.

In OPE we include corrections up to mass-dimension six operators:

$$\tilde{\Pi}(M^2) = c_0 + \frac{c_2}{M^2} + \frac{c_4}{M^4} + \frac{c_6}{M^6}, \tag{5.14}$$

where c_0 and c_2 stand for the perturbative expansion in the massless limit and the leading mass correction, respectively. The coefficient c_4 includes the gluon and quark condensates. The coefficients c_0 and c_2 are already discussed in Sec. 3.5. The coefficients c_4 and c_6 can be computed by applying Eq. (E.2) to the Wilson coefficients (see also [120]). Letting $L_M \equiv \log\left(\mu^2 e^{\gamma_E}/M^2\right)$, we can express the coefficients as

$$\begin{aligned} c_4 = {} & \frac{1}{12}\left(1 + \frac{7}{6}\frac{\alpha_s}{\pi}\right)\langle 0|\frac{\alpha_s}{\pi}G^2|0\rangle + 2m_s\left(1 + \frac{1}{3}\frac{\alpha_s}{\pi}\right)\langle 0|\bar{q}q|0\rangle \\ & + \frac{3m_s^4}{4\pi^2}(1 - 2L_M) - \frac{m_s^4}{6\pi^2}\frac{\alpha_s}{\pi}\left(35 - 3\pi^2 - 24\zeta(3) - 3L_M + 18L_M^2\right), \end{aligned} \tag{5.15}$$

$$c_6 = -\frac{112}{81}\pi\alpha_s\kappa_0\langle 0|\bar{q}q|0\rangle^2 + \frac{1}{18}m_s^2\langle 0|\frac{\alpha_s}{\pi}G^2|0\rangle - \frac{4}{3}m_s^3\langle 0|\bar{q}q|0\rangle, \tag{5.16}$$

where the gluon condensate $\langle 0|\frac{\alpha_s}{\pi}G^2|0\rangle$ is defined in the $\overline{\text{MS}}$ scheme. The coefficient κ_0 in (5.16) parametrizes corrections to the VSA for the four-quark condensate. When the condensate is assumed to be fully factorized in the vacuum, κ_0 is equal to 1. There are studies that suggest the violation of VSA as large as $\kappa_0 \sim 6$ [121]. We set $\kappa_0 = 1$ for the solid curve and incorporate the variation of κ_0 from 0 to 6 to estimate the error in Fig. 5.10. The higher dimensional condensates are neglected in this paper. We also include the renormalization scale dependence to estimate the truncation error as discussed in Sec. 3.5, where $\tilde{\Pi}_0^{\text{pert}}$ and $\tilde{\Pi}_{m^2}^{\text{pert}}$ correspond to c_0 and c_2. We introduce the renormalization scales μ_0 and μ_2 for c_0 and c_2, respectively, vary them in the range $2M^2e^{-\gamma_E} \le \mu_0^2, \mu_2^2 \le 8M^2e^{-\gamma_E}$ separately, and take the maximal (minimum) value of $c_0 + c_2/M^2$ as the upper (lower) limit of the band.

Figure 5.11 shows the convergence of OPE. The dotted line corresponds to the massless perturbation theory. The dash-dotted, dashed, solid lines include the terms up to $\mathcal{O}(1/M^2)$, $\mathcal{O}(1/M^4)$, and $\mathcal{O}(1/M^6)$ corrections, respectively. The error band is estimated as in Fig. 5.10. The Borel transform $\tilde{\Pi}^{\text{OPE}}(M^2)$ converges well in the range $1/M^2 \le 1\ \text{GeV}^{-2}$ as one can see from the tiny effect of $\mathcal{O}(1/M^6)$, albeit the large uncertainty due to the unknown condensates. The lattice data agree well with OPE including the terms of $1/M^4$ and $1/M^6$ within the uncertainty, as found in Fig. 5.10.

5.2.2 Extraction of the gluon condensate

As an application of the lattice calculation of $\tilde{\Pi}(M^2)$, we try to determine the coefficient c_4 from the lattice data. Since the perturbative expansion and OPE converges reasonably well for $\tilde{\Pi}(M^2)$ (, although some uncertainty remains if $\kappa_0 \sim$ 5–6),

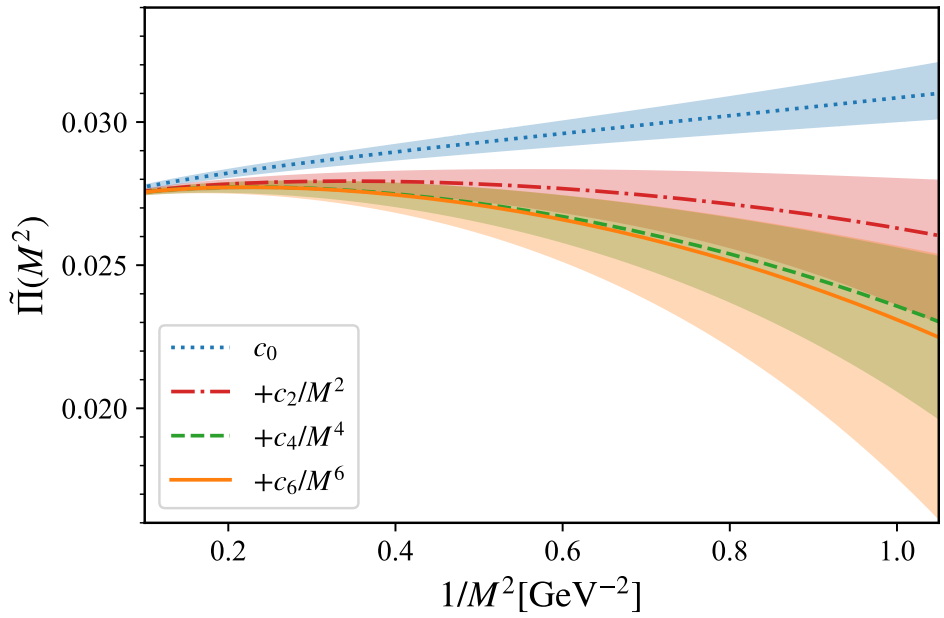

FIGURE 5.11: The convergence of OPE for $\tilde{\Pi}(M^2)$.

the determination is less affected by the truncation error than that for the HVP function $\Pi(q^2)$, and the systematic error of c_4 may be reduced. We consider corrections up to mass dimension six, since the higher mass-dimension operators are suppressed by the factorial as (3.46). By fixing c_0 and c_2 in (5.14) by the perturbative calculation, we determine c_4 and c_6 through a fit to the lattice data. The fitting range is $1/M^2 = 0.25$–$0.69\ \mathrm{GeV}^{-2}$. The M^2 dependence of c_4 and c_6 from corrections of order $\alpha_s(4M^2e^{-\gamma_E})$ is negligible in this range. Hence we treat c_4 and c_6 as constant parameters. We rescale $c_4 = \tilde{c}_4\Lambda^4$ and $c_6 = \tilde{c}_6\Lambda^6$ with $\Lambda = 300$ MeV, and set the priors of $\tilde{c}_4$ and $\tilde{c}_6$ to 0.0 ± 1.0. To evaluate the systematic uncertainties, we use three sets of the renormalization scales $(\mu_0^2, \mu_2^2) = (4M^2e^{-\gamma_E}, 4M^2e^{-\gamma_E})$, $(\mu_0^2, \mu_2^2) = (2M^2e^{-\gamma_E}, 8M^2e^{-\gamma_E})$, and $(\mu_0^2, \mu_2^2) = (8M^2e^{-\gamma_E}, 2M^2e^{-\gamma_E})$, and take the maximum variants of the results as their systematic errors. We obtain $\tilde{c}_4 = -0.34(7)(^{+26}_{-19})$. The first parenthesis gives the statistical error. The superscript (subscript) in the second parenthesis represents the upper (lower) systematic error. $\tilde{c}_6$ is not well constrained.

We subtract the contributions of the chiral condensate and the finite mass correction from c_4, which are relatively well determined, and obtain $\langle 0|\frac{\alpha_s}{\pi}G^2|0\rangle_{\overline{\mathrm{MS}}} = 0.011(7)(^{+22}_{-16})\ \mathrm{GeV}^4$ in the $\overline{\mathrm{MS}}$ scheme at the scale $\mu = 2$ GeV, which corresponds to $\langle 0|\frac{\alpha_s}{\pi}G^2|0\rangle_{\mathrm{RGI}} = 0.013(8)(^{+27}_{-20})\ \mathrm{GeV}^4$ in the renormalization group invariant (RGI) scheme. They are related by (see also [122])

$$\langle 0|\frac{\alpha_s}{\pi}G^2|0\rangle_{\mathrm{RGI}} = \left(1 + \frac{16}{9}\frac{\alpha_s}{\pi} + \cdots\right)\langle 0|\frac{\alpha_s}{\pi}G^2|0\rangle_{\overline{\mathrm{MS}}}. \tag{5.17}$$

The first error includes the statistical errors of lattice calculations and inputs $\Lambda_{\overline{\rm MS}}^{n_f=3}$, m_s, and $\langle 0|\bar{q}q|0\rangle$. The second one corresponds to the systematic uncertainty associated with the perturbative expansion. It is known that the gluon condensate suffers from the renormalon ambiguity. (See, for instance, [123].) More precise determination of the gluon condensate will require more statistics and an improvement of the perturbative calculation.

The value of $\langle 0|\frac{\alpha_s}{\pi}G^2|0\rangle$ was estimated by SVZ from the charmonium moments as $\langle 0|\frac{\alpha_s}{\pi}G^2|0\rangle \simeq 0.012$ GeV^4 [16, 17]. In Fig. 5.10, we used this value for the OPE estimate. From τ decay, the estimates are consistent with zero: $\langle 0|\frac{\alpha_s}{\pi}G^2|0\rangle = 0.006 \pm 0.012$ GeV^4 in the $\overline{\rm MS}$ scheme [124]. Our method provides another estimate with a comparable error.

5.2.3 Saturation by the ground state

In the low M^2 region, the ground state contribution dominates the Borel transform $\tilde{\Pi}(M^2)$, and the OPE would break down. Here, we investigate how much the ground-state contribution $\tilde{\Pi}_\phi(M^2)$ saturates the Borel transform.

The contribution from the ground state ϕ meson to the Borel transform $\tilde{\Pi}_\phi(M^2)$ is shown in Fig. 5.12 together with the lattice data. In this plot, the ϕ meson contribution (5.9) is drawn with the experimental inputs $f_\phi^{\rm exp} = 0.2285(36)$ GeV and $m_\phi^{\rm exp} = 1.019461(16)$ GeV [38] (dash-dotted line). The solid line denotes the OPE result, which is the same as in Fig. 5.10. The error band for the OPE in Fig. 5.12 may be underestimated beyond $1/M^2 \gtrsim 1$ GeV^{-2}, since the perturbative expansion and OPE poorly converge. The star symbols represent the lattice results in the continuum limit. Since the perturbative expression for the correction $\delta\tilde{\Pi}_m$ (5.12) would break down at low M^2, we show the data at finite lattice spacings, which do not have a significant error due to the mismatch of m_s. The $\Pi^{\rm lat}(M^2)$ on the coarse and fine lattices (circles and squares, respectively) indicates that the discretization effect is not significant.

In the low M^2 region, the lattice results approach the ϕ contribution as it should be. On the other hand, even at intermediate M, say $1/M^2 = 0.75$ GeV^{-2}, where the OPE converges well, the ϕ meson contribution is as large as 70% of $\tilde{\Pi}(M^2)$. It suggests that the quark-hadron duality works reasonably well even when the contribution from a single state dominates.

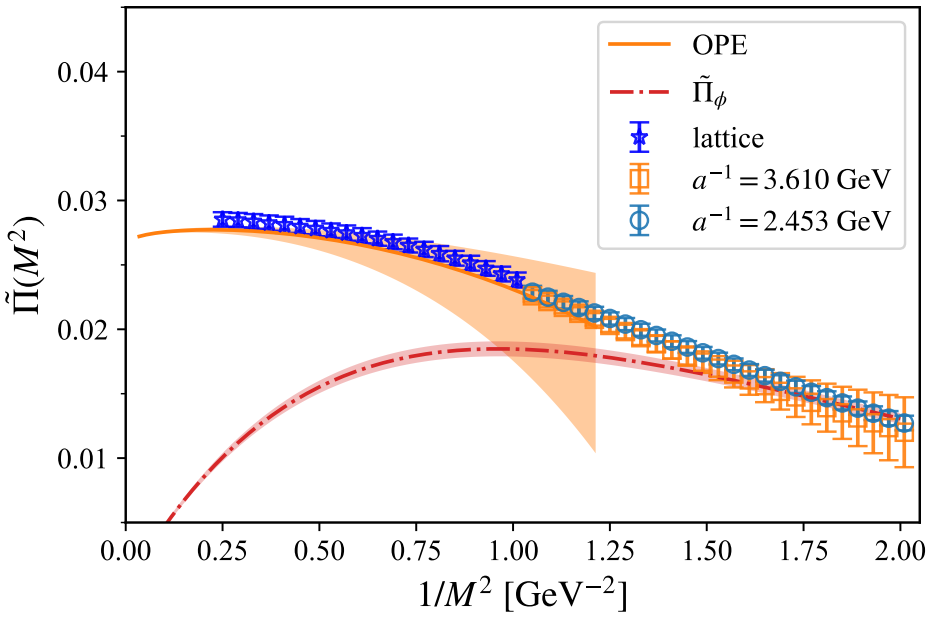

FIGURE 5.12: Comparison of $\tilde{\Pi}(M^2)$ in the continuum limit with the experimental values of the ϕ meson contribution.

Chapter 6

Conclusion and outlook

The Borel transform has often been used in the QCD sum rule analyses in order to improve the convergence of OPE and to enhance the contribution of the ground state, which is of our main interest. A crucial question is then whether the theoretical uncertainty in the perturbative expansion and OPE is well under control. The uncertainty due to the modeling of the excited state and continuum contributions is another important issue in the QCD sum rule. In this work, we provide a method to compute the Borel transform utilizing the lattice QCD data for current correlators. Since the computation is fully nonperturbative in the entire range of the Borel mass M, one can use the result to verify the theoretical methods so far used in the QCD sum rule.

We find a good agreement between the lattice data and OPE in the region of $M > 1.0$ GeV. The OPE is truncated at the order $1/M^6$. Since the OPE involves unknown condensates, this comparison can be used to determine these parameters, provided that the lattice data are sufficiently precise. As the first example, we attempt to extract the gluon condensate, which appears in OPE at the order $1/M^4$. The size of the error is comparable to those of previous phenomenological estimates. With more precise lattice data in various channels, one would be able to determine the condensates of higher dimensions, which have not been determined well solely from phenomenological inputs.

Using baryonic current correlators, one may also study another side of the QCD phenomenology. Since there are no experimental inputs, the lattice data may play a unique role in the QCD sum rule analysis. For instance, the Ioffe formula for the nucleon mass $m_N \simeq [-2(2\pi)^2\langle 0|\bar{q}q|0\rangle]^{1/3}$ [125] indicates a relation between the nucleon mass and chiral symmetry breaking, and it is interesting to study the baryonic correlator on the lattice to see if this relation comes out.

The application of this method to the light quark system may be useful for operator renormalization as well as for the test of perturbative QCD and OPE. For the light quark, the uncertainty of the finite mass corrections would not be substantial in contrast to the $s\bar{s}$ system. We determine the renormalization constant of the vector current and discuss extensions to other current operators in Appendix F.

Another interesting application of the lattice calculation of the Borel transform is the determination of α_s. A similar analysis has been performed directly on the current correlators [22], but it turned out that OPE does not converge sufficiently quickly to allow precise determination of α_s from the perturbative expansion at the leading order of OPE. With the Borel transform, one expects that OPE converges more rapidly, and it may provide another way to extract α_s, especially because the perturbative expansion is known to $O(\alpha_s^4)$, *i.e.* among the best quantities for which high order perturbative expansion is available.

Our work provides a technique to relate two major tools to study nonperturbative aspects of QCD, *i.e.* the QCD sum rule and the lattice QCD. As outlined above, there are a number of applications, for which new insights into the QCD phenomenology are expected.

Appendix A

Running coupling constant

We will derive the five-loop expression of the strong coupling constant. By definition of the beta function, we obtain the relation between the scale μ and the coupling constant a_s,

$$\begin{aligned}\int d(\log\mu^2) &= \int \frac{da_s}{\beta(a_s)} \\ &\simeq \int \frac{da_s}{\beta_0}\Big[-\frac{1}{a_s^2}+\frac{b_1}{a_s}+\big(-b_1^2+b_2\big)+\big(b_1^3-2b_1b_2+b_3\big)a_s \\ &\qquad +\Big(b_1^4-3b_1^2b_2+b_2^2+2b_1b_3-b_4\Big)a_s^2\Big] \\ &= \frac{1}{\beta_0}\Big[\frac{1}{a_s}+b_1\log a_s+\big(-b_1^2+b_2\big)a_s+\frac{1}{2}\big(b_1^3-2b_1b_2+b_3\big)a_s^2 \\ &\quad +\frac{1}{3}\Big(b_1^4-3b_1^2b_2+b_2^2+2b_1b_3-b_4\Big)a_s^3\Big]+C. \end{aligned} \tag{A.1}$$

We conventionally fix the integration constant,

$$C=\frac{b_1}{\beta_0}\log(\beta_0)+\log\Lambda_{\rm QCD}^2, \tag{A.2}$$

which simplify the following expression of $a_s(\mu^2)$. Defining $L\equiv\log\Big(\mu^2/\Lambda_{\rm QCD}^2\Big)$, we obtain the equation which $a_s(\mu)$ fulfills,

$$\begin{aligned}a_s &= \frac{1}{\beta_0 L}\Big[1+b_1a_s\log(\beta_0a_s)+\big(-b_1^2+b_2\big)a_s^2+\frac{1}{2}\big(b_1^3-2b_1b_2+b_3\big)a_s^3 \\ &\quad +\frac{1}{3}\Big(b_1^4-3b_1^2b_2+b_2^2+2b_1b_3-b_4\Big)a_s^4\Big]. \end{aligned} \tag{A.3}$$

We let $a_s^{(\ell)}$ be the solution up to the l-loop order, namely $\mathcal{O}(1/L^\ell)$. At one-loop level, $a_s^{(1)}=1/(\beta_0L)$. We can construct the one-order higher solution by the expression of

$a_s^{(\ell)}$:

$$a_s^{(\ell+1)}(\mu^2) \simeq \frac{1}{\beta_0 L}\left[1 + b_1 a_s \log(\beta_0 a_s) + \left(-b_1^2 + b_2\right)a_s^2 + \frac{1}{2}\left(b_1^3 - 2b_1 b_2 + b_3\right)a_s^3 + \frac{1}{3}\left(b_1^4 - 3b_1^2 b_2 + b_2^2 + 2b_1 b_3 - b_4\right)a_s^4\right]\Bigg|_{a_s = a_s^{(\ell)}}. \tag{A.4}$$

Currently, the coefficients of the beta function is known to b_4 and a precise expression of the coupling constant is

$$\begin{aligned} a_s^{(5)}(\mu^2) = \frac{1}{\beta_0 L}\Bigg[1 &- \frac{b_1}{\beta_0 L}\log L + \frac{1}{\beta_0^2 L^2}\left\{b_1^2(\log^2 L - \log L - 1) + b_2\right\} \\ &+ \frac{1}{2\beta_0^3 L^3}\left\{b_1^3(-2\log^3 L + 5\log^2 L + 4\log L - 1) - 6b_1 b_2 \log L + b_3\right\} \\ &+ \frac{1}{6\beta_0^4 L^4}\{b_1^4(6\log^4 L - 26\log^3 L - 9\log^2 L + 24\log L + 7) \\ &\qquad + 18 b_1^2 b_2(2\log^2 L - \log L - 1) \\ &\qquad - b_1 b_3(12\log L + 1) + 10 b_2^2 + 2b_4\}\Bigg], \end{aligned} \tag{A.5}$$

where $\log^n L$ denotes the power of $\log L$, not $\log\log\cdots\log L$. We neglect the term proportional to $1/L^6$. Here, the term proportional to $1/L^2$ without $\log L$ does not appear in this expression, which results from (A.2).

Appendix B

Running quark mass

As a first step, we consider RG equations at the leading order,

$$\mu^2 \frac{\mathrm{d}m}{\mathrm{d}\mu^2} = -m(\mu^2)\gamma_{m,0}a_s, \tag{B.1}$$

$$\mu^2 \frac{\mathrm{d}a_s}{\mathrm{d}\mu^2} = -\beta_0 a_s^2. \tag{B.2}$$

Integrating (B.1) from μ_0 to μ, we obtain a relation between $m(\mu^2)$ and $m(\mu_0^2)$,

$$\begin{aligned}
\log\left(\frac{m(\mu^2)}{m(\mu_0^2)}\right) &= -\int_{\mu_0^2}^{\mu^2} d(\log(\mu'^2))\gamma_{m,0}a_s(\mu'^2) \\
&= \int_{a_s(\mu_0^2)}^{a_s(\mu^2)} \frac{da_s}{a_s}\frac{\gamma_{m,0}}{\beta_0} \\
&= \frac{\gamma_{m,0}}{\beta_0}\log\left(\frac{a_s(\mu^2)}{a_s(\mu_0^2)}\right).
\end{aligned} \tag{B.3}$$

Here, we change the variable through

$$d(\log(\mu^2)) = -\frac{da_s}{\beta_0 a_s^2}. \tag{B.4}$$

Then, we express the solution at one-loop level as

$$m(\mu^2) = \left(\frac{a_s(\mu^2)}{a_s(\mu_0^2)}\right)^{\frac{\gamma_{m,0}}{\beta_0}} m(\mu_0^2). \tag{B.5}$$

Let us extend the above calculus to the higher loop level. To simplify the expression, we define $c_i \equiv \gamma_{m,i}/\beta_0$. From the definition of the anomalous dimension γ_m and the β function, we can write the general form of the solution as

$$\begin{aligned}
\frac{m(\mu^2)}{m(\mu_0^2)} &= \exp\left(\int_{\mu_0^2}^{\mu^2} d(\log(\mu'^2))\gamma_m(a_s(\mu'^2))\right) \\
&= \exp\left(\int_{a_s(\mu_0^2)}^{a_s(\mu^2)} da_s \frac{\gamma_m(a_s)}{\beta(a_s)}\right).
\end{aligned} \tag{B.6}$$

We can perform the integral in r.h.s. up to integration constant as

$$
\begin{aligned}
&\int da_s \frac{c_0 a_s + c_1 a_s^2 + c_2 a_s^3 + c_3 a_s^4 + c_4 a_s^5}{a_s^2 + b_1 a_s^3 + b_2 a_s^4 + b_3 a_s^5 + b_4 a_s^6} \\
\simeq &\int da_s \left[\frac{c_0}{a_s} - b_1 c_0 + c_1 + \{(b_1^2 - b_2)c_0 - b_1 c_1 + c_2\} a_s \right. \\
&+ \{(-b_1^3 + 2b_1 b_2 - b_3)c_0 + (b_1^2 - b_2)c_1 - b_1 c_2 + c_3\} a_s^2 \\
&+ \{(b_1^4 - 3b_1^2 b_2 + b_2^2 + 2b_1 b_3 - b_4)c_0 + (-b_1^3 + 2b_1 b_2 - b_3)c_1 \\
&\left. + (b_1^2 - b_2)c_2 - b_1 c_3 + c_4\} a_s^3 \right] \\
=&c_0 \log a_s + (-b_1 c_0 + c_1) a_s + \frac{1}{2}\{(b_1^2 - b_2)c_0 - b_1 c_1 + c_2\} a_s^2 \\
&+ \frac{1}{3}\{(-b_1^3 + 2b_1 b_2 - b_3)c_0 + (b_1^2 - b_2)c_1 - b_1 c_2 + c_3\} a_s^3 \\
&+ \frac{1}{4}\{(b_1^4 - 3b_1^2 b_2 + b_2^2 + 2b_1 b_3 - b_4)c_0 + (-b_1^3 + 2b_1 b_2 - b_3)c_1 \\
&+ (b_1^2 - b_2)c_2 - b_1 c_3 + c_4\} a_s^4 \\
\equiv &c_0 \log a_s + d_1 a_s + d_2 a_s^2 + d_3 a_s^3 + d_4 a_s^4. \qquad \text{(B.7)}
\end{aligned}
$$

Here we define the coefficients d_i for notational convenience. Substituting this expression for (B.6), we finally obtain the solution

$$
\frac{m(\mu^2)}{m(\mu_0^2)} = \frac{c(a_s(\mu^2))}{c(a_s(\mu_0^2))}, \qquad \text{(B.8)}
$$

with the function,

$$
\begin{aligned}
c(x) =& x^{c_0} \left[1 + d_1 x + \frac{1}{2}(d_1^2 + 2d_2)x^2 + \frac{1}{6}(d_1^3 + 6d_1 d_2 + 6d_3)x^3 \right. \\
&\left. + \frac{1}{24}(d_1^4 + 12 d_1^2 d2 + 12 d_2^2 + 24 d_1 d_3 + 24 d_4)x^4 \right], \qquad \text{(B.9)}
\end{aligned}
$$

where we neglect terms of $\mathcal{O}(a_s^5)$.

Appendix C

RG equation of $\Pi_0(\mu^2; Q^2)$

The RG evolution of the HVP function in the massless limit is described by

$$\mu^2 \frac{\mathrm{d}}{\mathrm{d}\mu^2} \Pi_0(\mu^2; Q^2) = \gamma^{VV}(a_s). \tag{C.1}$$

Using

$$\mu^2 \frac{\mathrm{d}}{\mathrm{d}\mu^2} = \mu^2 \frac{\partial}{\partial \mu^2} + \beta(a_s) \frac{\partial}{\partial a_s}, \tag{C.2}$$

we can recursively construct the solution up to $\mathcal{O}(a_s^\ell)$ through

$$\Pi_0^{(\ell)}(\mu^2; Q^2) = \int dL \left(-\beta(a_s) \frac{\partial}{\partial a_s} \right) \Pi_0^{(\ell-1)}(\mu^2; Q^2) + \gamma^{VV} L, \tag{C.3}$$

with $L = \log(\mu^2/Q^2)$. Note that we have to treat a_s as a constant in this integral. The integration constant in this equation is fixed to reproduce $\Pi_0(Q^2)$ at $\mu^2 = Q^2$, which corresponds to the non-logarithmic terms in $\Pi_0(\mu^2; Q^2)$. The perturbative series of HVP at $\mu^2 = Q^2$ is known up to $\mathcal{O}(a_s^3)$ [78, 79],

$$\Pi(Q^2) = \sum_{n=0}^{3} c_n^V a_s^n(Q^2), \tag{C.4}$$

$$(4\pi)^2 c_0^V = \frac{20}{3}, \quad (4\pi)^2 c_1^V = \frac{55}{3} - 16\zeta_3, \tag{C.5}$$

$$(4\pi)^2 c_2^V = \frac{41927}{216} - \frac{1658}{9}\zeta_3 + \frac{100}{3}\zeta_5 + n_f \left(-\frac{3701}{324} + \frac{76}{9}\zeta_3 \right), \tag{C.6}$$

$$\begin{aligned}(4\pi)^2 c_3^V =& \frac{31431599}{10368} - \frac{624799}{216}\zeta_3 + 330\zeta_3^2 + \frac{55}{12}\zeta_4 + \frac{1745}{24}\zeta_5 - \frac{665}{9}\zeta_7 \\ &+ n_f \left(-\frac{1863319}{5184} + \frac{174421}{648}\zeta_3 - \frac{20}{3}\zeta_3^2 - \frac{55}{36}\zeta_4 + \frac{1090}{27}\zeta_5 \right) \\ &+ n_f^2 \left(\frac{196513}{23328} - \frac{809}{162}\zeta_3 - \frac{20}{9}\zeta_5 \right).\end{aligned} \tag{C.7}$$

On the other hand, the perturbative series of the anomalous dimension $\gamma^{VV}(a_s)$ has been calculated up to $\mathcal{O}(a_s^4)$ [78, 79],

$$\gamma^{VV} = \sum_{i=0}^{4} \gamma_i^{VV} a_s^i, \tag{C.8}$$

with the coefficients,

$$(4\pi)^2\gamma_0^{VV} = (4\pi)^2\gamma_1^{VV} = 4, \tag{C.9}$$

$$(4\pi)^2\gamma_2^{VV} = \frac{125}{12} - \frac{11}{18}n_f, \tag{C.10}$$

$$(4\pi)^2\gamma_3^{VV} = \frac{10487}{432} + \frac{110}{9}\zeta_3 + n_f\left(-\frac{707}{216} - \frac{110}{27}\zeta_3\right) - \frac{77}{972}n_f^2, \tag{C.11}$$

$$\begin{aligned}(4\pi)^2\gamma_4^{VV} = {}& \frac{2665349}{41472} + \frac{182335}{864}\zeta_3 - \frac{605}{16}\zeta_4 - \frac{31375}{288}\zeta_5 \\ & + n_f\left(-\frac{11785}{648} - \frac{58625}{864}\zeta_3 + \frac{715}{48}\zeta_4 + \frac{13325}{432}\zeta_5\right) \\ & + n_f^2\left(-\frac{4729}{31104} + \frac{3163}{1296}\zeta_3 - \frac{55}{72}\zeta_4\right) + n_f^3\left(\frac{107}{15552} + \frac{1}{108}\zeta_3\right).\end{aligned} \tag{C.12}$$

Using (C.3), we finally obtain the solution of (C.1) [79, 80],

$$\Pi_0(\mu^2;Q^2) = \sum_{l=0}^{4} \Pi_0^l a_s^l, \tag{C.13}$$

$$\Pi_0^0 = c_0^V + \gamma_0^{VV} L, \tag{C.14}$$

$$\Pi_0^1 = c_1^V + \gamma_1^{VV} L, \tag{C.15}$$

$$\Pi_0^2 = c_2^V + (c_1^V\beta_0 + \gamma_2^{VV})L + \frac{1}{2}\beta_0\gamma_1^{VV}L^2, \tag{C.16}$$

$$\begin{aligned}\Pi_0^3 = {}& c_3^V + (2c_2^V\beta_0 + c_1^V\beta_1 + \gamma_3^{VV})L \\ & + \left[c_1^V\beta_0^2 + \frac{1}{2}\beta_1\gamma_1^{VV} + \beta_0\gamma_2^{VV}\right]L^2 + \frac{1}{3}\beta_0^2\gamma_1^{VV}L^3,\end{aligned} \tag{C.17}$$

$$\begin{aligned}\Pi_0^4 = {}& c_4^V + (3c_3^V\beta_0 + 2c_2^V\beta_1 + c_1^V\beta_2 + \gamma_4^{VV})L \\ & + \left[3c_2^V\beta_0^2 + \frac{5}{2}c_1^V\beta_0\beta_1 + \frac{1}{2}\beta_2\gamma_1^{VV} + \beta_1\gamma_2^{VV} + \frac{3}{2}\beta_0\gamma_3^{VV}\right]L^2 \\ & + \left[c_1^V\beta_0^3 + \frac{5}{6}\beta_0\beta_1\gamma_1^{VV} + \beta_0^2\gamma_2^{VV}\right]L^3 + \frac{1}{4}\beta_0^3\gamma_1^{VV}L^4.\end{aligned} \tag{C.18}$$

Appendix D

RG equation of $\Pi_2(\mu; Q^2)$

We derive the expression of the dimension-two correction $\Pi_2(\mu^2; Q^2)$. The scale dependence of $\Pi_2(\mu^2; Q^2)$ is described by

$$\mu^2 \frac{\mathrm{d}}{\mathrm{d}\mu^2} \Pi_2(\mu^2; Q^2) = -2\gamma_m(a_s)\Pi_2(\mu^2; Q^2) \tag{D.1}$$

This equation can be solved recursively as discussed in Appendix C, although γ_m appears in the r.h.s instead of γ^{VV} in (C.1). We construct a solution up to $\mathcal{O}(a_s^\ell)$ through

$$\Pi_2^{(\ell)}(\mu^2; Q^2) = -\int dL \left(2\gamma_m(a_s) + \beta(a_s)\frac{\partial}{\partial a_s}\right)\Pi_2^{(\ell-1)}(\mu^2; Q^2). \tag{D.2}$$

The perturbative corrections of $\Pi_2(Q^2)$ at $\mu^2 = Q^2$ is known to $\mathcal{O}(a_s^3)$ [81, 82],

$$\Pi_2(Q^2) = \sum_{n=0} d_n^V a_s^n(Q^2), \tag{D.3}$$

$$(4\pi)^2 d_0^V = -24, \quad (4\pi)^2 d_1^V = -64, \tag{D.4}$$

$$(4\pi)^2 d_2^V = -\frac{18923}{18} - \frac{784}{9}\zeta_3 + \frac{4180}{9}\zeta_5 + \frac{95}{3}n_f, \tag{D.5}$$

$$\begin{aligned}(4\pi)^2 d_3^V =& -\frac{10499303}{648} + \frac{66820}{27}\zeta_3 - \frac{7225}{9}\zeta_3^2 + \frac{281390}{27}\zeta_5 - \frac{1027019}{216}\zeta_7 \\ &+ n_f\left(\frac{62893}{54} - \frac{4150}{81}\zeta_3 + \frac{424}{9}\zeta_3^2 + 20\zeta_4 - \frac{28880}{81}\zeta_5\right) \\ &+ n_f^2\left(-\frac{5161}{486} - \frac{8}{9}\zeta_3\right).\end{aligned} \tag{D.6}$$

Using (D.2) with $\beta(a_s)$ and $\gamma_m(a_s)$ discussed in Sec. 2.1, we obtain the solution,

$$\Pi_2(\mu^2; Q^2) = \sum_{l=0} \Pi_2^l a_s^l(\mu^2), \tag{D.7}$$

with the coefficients [79, 126],

$$\Pi_2^0 = d_0^V, \tag{D.8}$$

$$\Pi_2^1 = d_1^V + 2d_0^V \gamma_{m,0} L, \tag{D.9}$$

$$\begin{aligned}\Pi_2^2 =& d_2^V + d_0^V \gamma_{m,0}(\beta_0 + 2\gamma_{m,0}) L^2 \\ &+ \left[d_1^V (\beta_0 + 2\gamma_{m,0}) + 2d_0^V \gamma_{m,1} \right] L,\end{aligned} \tag{D.10}$$

$$\begin{aligned}\Pi_2^3 =& d_3^V + \frac{2}{3} d_0^V \gamma_{m,0} \left(\beta_0^2 + 3\beta_0 \gamma_{m,0} + 2\gamma_{m,0}^2\right) L^3 \\ &+ \Big[d_0^V \beta_1 \gamma_{m,0} + 2d_0^V (\beta_0 + 2\gamma_{m,0}) \gamma_{m,1} \\ &\quad + d_1^V (\beta_0^2 + 3\beta_0 \gamma_{m,0} + 2\gamma_{m,0}^2) \Big] L^2 \\ &+ \left[2d_2^V (\beta_0 + \gamma_{m,0}) + d_1^V (\beta_1 + 2\gamma_{m,1}) + 2d_0^V \gamma_{m,2}) \right] L.\end{aligned} \tag{D.11}$$

Appendix E

Some formulas of Borel transformations

We show some formulas of the Borel transformation. Perturbative corrections at higher loops have the power of logarithm, $\log^n(\mu^2/Q^2)$. We can obtain its Borel transformation by taking derivatives of the formula:

$$\mathcal{B}_M\left[\left(\frac{\mu^2}{Q^2}\right)^\alpha\right] = \frac{1}{\Gamma(\alpha)}\left(\frac{\mu^2}{M^2}\right)^\alpha \tag{E.1}$$

$$\mathcal{B}_M\left[\left(\frac{\mu^2}{Q^2}\right)^\alpha \log^n\left(\frac{\mu^2}{Q^2}\right)\right] = \frac{\partial^n}{\partial\alpha^n}\left[\frac{1}{\Gamma(\alpha)}\left(\frac{\mu^2}{M^2}\right)^\alpha\right], \tag{E.2}$$

$$\mathcal{B}_M\left[\log^n\left(\frac{\mu^2}{Q^2}\right)\right] = \lim_{\alpha\to 0}\frac{\partial^n}{\partial\alpha^n}\left[\frac{1}{\Gamma(\alpha)}\left(\frac{\mu^2}{M^2}\right)^\alpha\right]. \tag{E.3}$$

The perturbative coefficients of HVP is known at $\mathcal{O}(\alpha_s^4)$ [80]. Those have quartic logarithmic terms at most. We show corresponding formulas for $n = 1$ to 4:

$$\mathcal{B}_M\left[\log\left(\frac{\mu^2}{Q^2}\right)\right] = 1, \tag{E.4}$$

$$\mathcal{B}_M\left[\log^2\left(\frac{\mu^2}{Q^2}\right)\right] = 2\log\left(\frac{\mu^2}{M^2e^{-\gamma_E}}\right), \tag{E.5}$$

$$\mathcal{B}_M\left[\log^3\left(\frac{\mu^2}{Q^2}\right)\right] = 3\log^2\left(\frac{\mu^2}{M^2e^{-\gamma_E}}\right) - \frac{\pi^2}{2}, \tag{E.6}$$

$$\mathcal{B}_M\left[\log^4\left(\frac{\mu^2}{Q^2}\right)\right] = 4\left(\log^2\left(\frac{\mu^2}{M^2e^{-\gamma_E}}\right) - \frac{\pi^2}{2}\right)\log\left(\frac{\mu^2}{M^2e^{-\gamma_E}}\right) + 8\zeta(3). \tag{E.7}$$

If we set $\mu^2 \propto M^2e^{-\gamma_E}$, the expressions get simplified. Hence we choose it as the renormalization scale. Other useful formulas can be found in [127].

Appendix F

Renormalization by the spectral sum

We consider current-current correlators in momentum space as a quantity for the renormalization. These correlators are defined as

$$\Pi_\Gamma(q^2) = i \int d^4x\, e^{iqx} \langle J_\Gamma(x) J_\Gamma(0) \rangle, \tag{F.1}$$

where J_Γ is a bilinear operator such as $\bar{q}\gamma_\mu q$, $\bar{q}\gamma_5 q$, and $\bar{q}\sigma_{\mu\nu} q$. In the case of the vector current, we can write this correlator as $\Pi_V(q^2) = (q_\mu q_\nu - q^2 g_{\mu\nu})\Pi(q^2)$. The function $\Pi(q^2)$ is the so-called hadronic vacuum polarization (HVP) function. In the deep Euclidean region $Q^2 = -q^2 \gg 0$, the perturbative expansion and OPE are applicable. The perturbative series in the massless limit has been calculated up to $O(\alpha_s^3)$ for the vector current [80]. Lattice calculation for the quantity is straightforward. The convergences of the OPE is, however, problematic, as discussed in the literature [22]. Namely, there is a severe window problem $\Lambda_{\rm QCD}^2 \ll Q^2 \ll 1/a^2$. Therefore, the correlator in momentum space $\Pi_\Gamma(q^2)$ itself would not be suitable for the renormalization.

In the present work, we propose a new method to renormalize lattice operators using the Borel transformation, which is often utilized in the QCD sum rule. The method is based on the technique to compute the weighted spectrum in the numerical lattice computation [35]. We compute the renormalization constant and compare it with the result from another nonperturbative method.

We calculate the correlator of the current $J_\mu = \bar{u}\gamma_\mu d$ at three lattice spacing. We use ensembles with $N_f = 2 + 1$ dynamical Möbius domain-wall fermions, which are generated by the JLQCD collaboration. Table 5.1 shows the parameters of the ensembles, where light and strange sea quark masses are denoted by m_{ud} and m_s, respectively. We also use these degenerate masses m_{ud} as valence quark masses. The correlators are measured $N_{\rm meas}$ times at each lattice spacing. Some details of the configurations can be found in [24].

As a test of our renormalization procedure, we compute the renormalization constant of the vector current. We impose the matching (renormalization) condition on

the Borel transform of HVP, $\tilde{\Pi}^{\rm lat}(a^2; M^2)$, computed at lattice spacing a:

$$\tilde{\Pi}^{\overline{\rm MS}}(\mu^2; M^2) = \left(Z_V^{\overline{\rm MS}/{\rm lat}}(a^2)\right)^2 \tilde{\Pi}^{\rm lat}(a^2; M^2), \tag{F.2}$$

where $Z_V(a^2)$ is the renormalization constant for the vector current operator. The l.h.s. of (F.2), $\tilde{\Pi}^{\overline{\rm MS}}(\mu^2; M^2)$, denotes the counterpart in the perturbative QCD at the renormalization point μ. The perturbative expansion is known to $O(\alpha_s^4)$ in the massless limit. For the vector current, there is no anomalous dimension, and the renormalization constant is independent of the renormalization scale up to the truncation error. Since we obtain the renormalization condition (F.2) at several M^2, we obtain the optimal solution $Z_V^{\overline{\rm MS}/{\rm lat}}(a^2)$ as discussed in the next section.

We show our preliminary results. We set $N_t = 18$ for the Chebyshev expansion of the Borel transform. The perturbative expansion $\tilde{\Pi}^{\overline{\rm MS}}(\mu^2; M^2)$ is computed in the massless limit, where we set $\mu = 2$ GeV. Solving (F.2) for $Z_V^{\overline{\rm MS}/{\rm lat}}$, we can express the solution in the following form:

$$\tilde{Z}_V(a^2; M^2) \equiv \sqrt{\frac{\tilde{\Pi}^{\overline{\rm MS}}(\mu^2; M^2)}{\tilde{\Pi}^{\rm lat}(a^2; M^2)}} \tag{F.3}$$

$$= Z_V^{\overline{\rm MS}/{\rm lat}}(a^2) + C_{-2}(Ma)^2 + C_4/M^4. \tag{F.4}$$

The discretization effect is incorporated into this function as $C_{-2}(Ma)^2$. The term C_4/M^4 corresponds to the nonperturbative corrections due to the dimension-four operators. Figure F.1 shows the M^2 dependence of $\tilde{Z}_V(a^2; M^2)$ at each lattice spacing. In the short-distance region, namely at small $1/M^2$, the ratio $\tilde{Z}_V(a^2; M^2)$ is suppressed due to the discretization effect. We determine the renormalization constant by a fit using the ansatz (F.4) in the range $1/M^2 = 0.25$–$0.69\,{\rm GeV}^{-2}$. Then we obtain $Z_V^{\overline{\rm MS}/{\rm lat}}(a^2) = 0.9804(43), 0.9806(27), 0.9789(23)$ at $a^{-1} = 2.453, 3.610, 4.496$ GeV, respectively, where the parentheses denote the statistical errors only.

We compare our result with another method in Fig. F.2. We take the renormalization constant from the X-space correlator as a reference [19]. The horizontal axis in this figure is the squared lattice spacing. The circle and cross symbols denote our result and the X-space method, respectively. Note that the errors of our result does not include systematic errors, such as truncation errors and valence quark mass dependence. These renormalization constants may contain different discretization errors, and the maximal deviation is $\sim 2.6\%$ on the coarse lattice. The deviation becomes insignificant towards the continuum limit.

We are trying to extend our method to other operators, such as the (pseudo-)scalar density and tensor operators. Since those have finite anomalous dimensions, we have to give the correct scale dependence, unlike the vector current. We compute the corresponding ratio such as (F.3) but for tensor operators on the coarse lattice. We

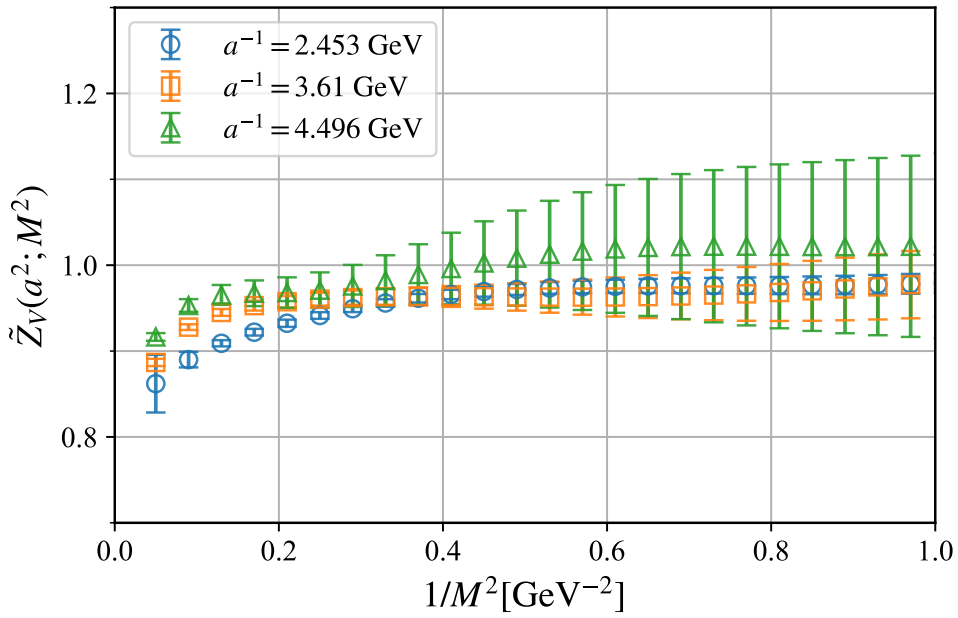

FIGURE F.1: $\tilde{Z}_V(a^2; M^2)$ at all lattice spacing.

check that a ratio of $\tilde{Z}_T(\mu^2, a^2; M^2$ is consistent with the running at one-loop level,

$$\frac{\tilde{Z}_T(\mu^2, a^2; M^2)}{\tilde{Z}_T(4\ \mathrm{GeV}^2, a^2; M^2)} \simeq \left(\frac{\alpha_s(\mu^2)}{\alpha_s(4\ \mathrm{GeV}^2)}\right)^{-\frac{\gamma_0^T}{\beta_0}}, \tag{F.5}$$

where $\gamma_0^T = -1/3$. The computation is still ongoing.

The modification of the weight kernel is necessary for the pseudo-scalar density $\bar{u}\gamma_5 d$, because the Borel transform is largely affected by π meson since the exponential kernel does not suppress π meson spectrum $\sim \delta(s - m_\pi^2)$. Accordingly, the Borel transform in this channel is not well described by perturbative QCD even at $M = 2$ GeV. This would be improved by a replacement of the kernel $e^{-s/M^2} \to se^{-s/M^2}$. The counterpart of this modified spectral sum in perturbative QCD may be derived by some mathematical manipulations, such as the derivative of the Borel transform:

$$\frac{\partial}{\partial(1/M^2)} \mathcal{B}_M \left[\log^n\left(\frac{\mu^2}{Q^2}\right)\right]. \tag{F.6}$$

In this appendix, we propose a renormalization method based on the Borel transform following SVZ. The renormalization constant can be computed through the two-point correlation functions, which is fairly standard to compute in lattice calculation. The perturbative expansion of this quantity is available. The scale parameter M^2 is continuous and easily adjustable using the Chebyshev expansion. The errors are due to the truncation of perturbative expansion, the finite mass correction, and the choice of the fit range as well as the Chebyshev expansion. The result for

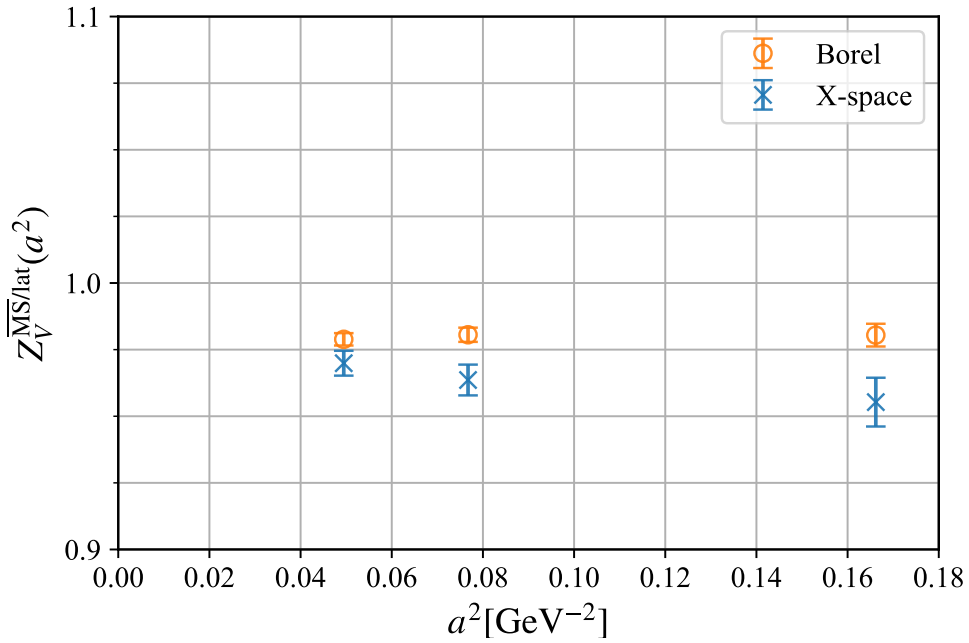

FIGURE F.2: Comparison of $Z_V^{\overline{\text{MS}}/\text{lat}}(a^2)$ at three lattice spacing.

the vector current is consistent with another renormalization method in the limit of vanishing lattice spacing. The computation of the renormalization constant for the scalar and tensor current is underway.

Appendix G

Mistuning of the strange quark mass

In this appendix, we discuss the mistuning effect of the strange quark mass. As discussed later, masses of some mesons is written in terms of the quark mass. We has to set the bare quark mass to reproduce these mass relation of mesons. The mistuning effect may be evaluated as the deviation of the relation. For more detailed review of the chiral perturbation theory, see also [128].

Let us consider QCD with three light flavors. The mass term in the Lagrangian is given by

$$\bar{\psi}M\psi = \bar{\psi}_L M\psi_R + \bar{\psi}_R M^\dagger \psi_L, \tag{G.1}$$

where M is the diagonal mass matrix,

$$M = \begin{pmatrix} m_u & & \\ & m_d & \\ & & m_s \end{pmatrix}. \tag{G.2}$$

$\psi = (u, d, s)$ is a quark field. The QCD Lagrangian in the massless limit has the $SU(3)_{L,R} \times U(1)_{L,R}$ symmetry for each flavor. In the classical theory, the Lagrangian is invariant under the $U(1)_A$ transformation $\psi_i \to e^{\alpha\gamma_5}\psi_i$; however the $U(1)_A$ symmetry is broken by the anomaly. Moreover, $SU(3)_L \times SU(3)_R$ is spontaneously broken to the vector $SU(3)_V$ symmetry. The spontaneous symmetry broken generate 8 massless NG bosons, i.e., π, K and η. In actual, G_χ is a approximate symmetry since the mass term explicitly breaks the chiral symmetry G_χ. Therefore, the mesons, π, K and η, are called pseudo NG bosons which have the finite mass led by the quark mass M.

As discussed in Sec. 2.8, the pion's mass is related to the quark mass: $m_\pi^2 \propto m_u + m_d$. Let us include s quark in the discussion. Similar arguments are applicable to K and η mesons. One can write these meson's masses at the leading order of the

quark masses,

$$M_\pi^2 = B(m_u + m_d), \tag{G.3}$$

$$M_{K^\pm}^2 = B(m_u + m_s), \tag{G.4}$$

$$M_{K^0}^2 = B(m_d + m_s), \tag{G.5}$$

$$M_\eta^2 = \frac{1}{3}B(m_u + m_d + 4m_s), \tag{G.6}$$

where B is a constant and the corrections from the electromagnetic interactions are neglected. These expressions obey the Gell-Mann-Okubo mass formula,

$$3M_\eta^2 + M_\pi^2 = 4m_K^2, \tag{G.7}$$

where $m_K^2 = \frac{1}{2}(m_{K^\pm}^2 + m_{K^0}^2)$.

We turn to the discuss the mistuning of the strange quark mass. Assuming the degeneracy of u and d quark masses, we have a equation of the strange quark mass:

$$2M_K^2 - M_\pi^2 = 2Bm_s. \tag{G.8}$$

We have to set the bare strange quark mass to satisfy this relation since we know the value of $2M_K^2 - M_\pi^2 \simeq 0.47\ \mathrm{GeV}^2$ from experiments. In our ensembles, $2M_K^2 - M_\pi^2 \simeq$ 0.50, 0.51, 0.39 GeV^2 at $a^{-1} = 2.453$, 3.610, 4.496 GeV, respectively. At the finest lattice spacing, the deviation is $\sim$ 20%; therefore, we correct the mistuning of the valence quark mass in the continuum extrapolation.

Appendix H

Supplementary figures

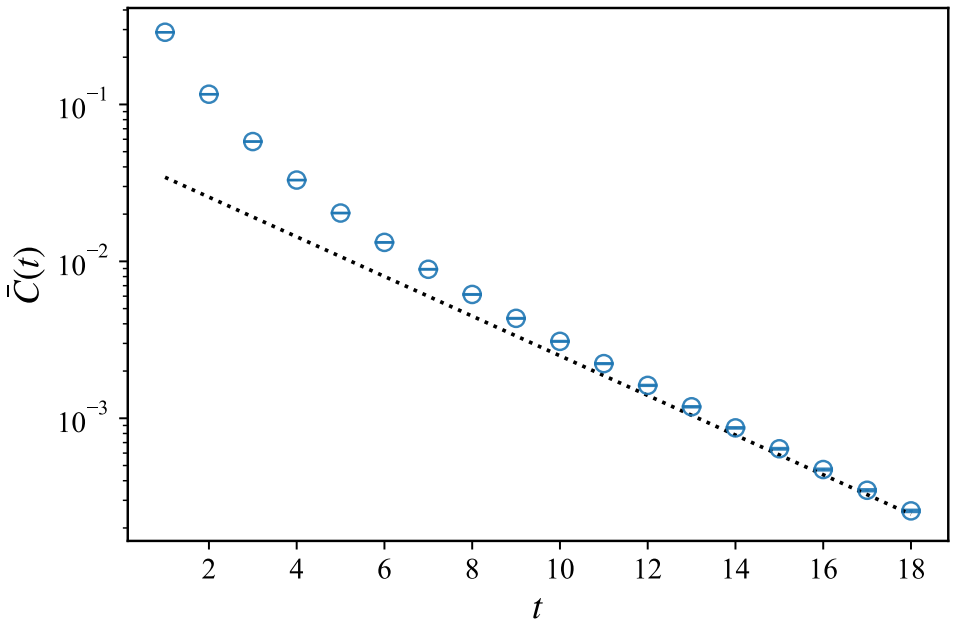

FIGURE H.1: Same as Fig. 5.1 but at $a^{-1} = 3.610$ GeV.

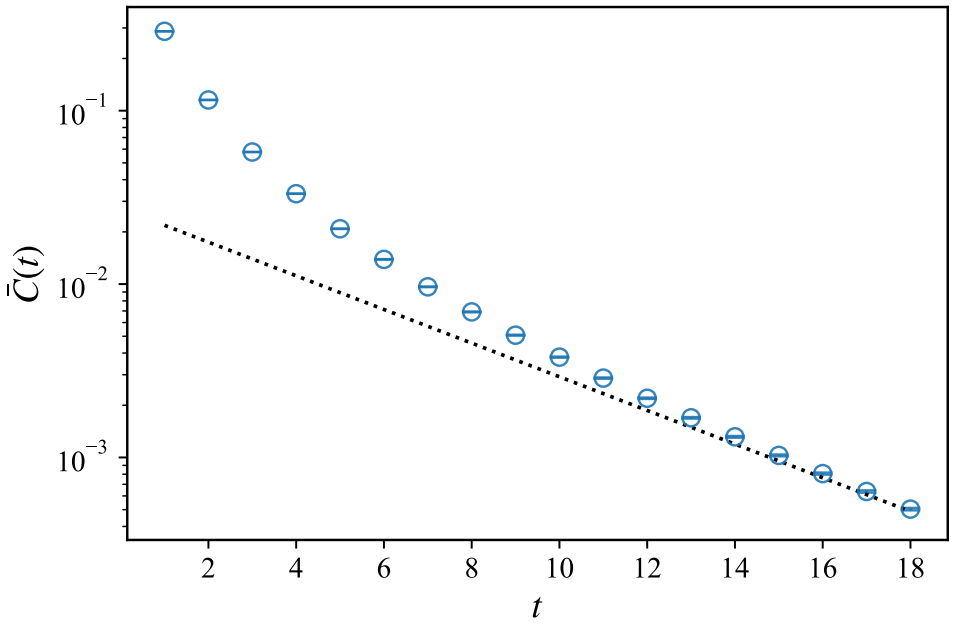

FIGURE H.2: Same as Fig. 5.1 but at $a^{-1} = 4.496$ GeV.

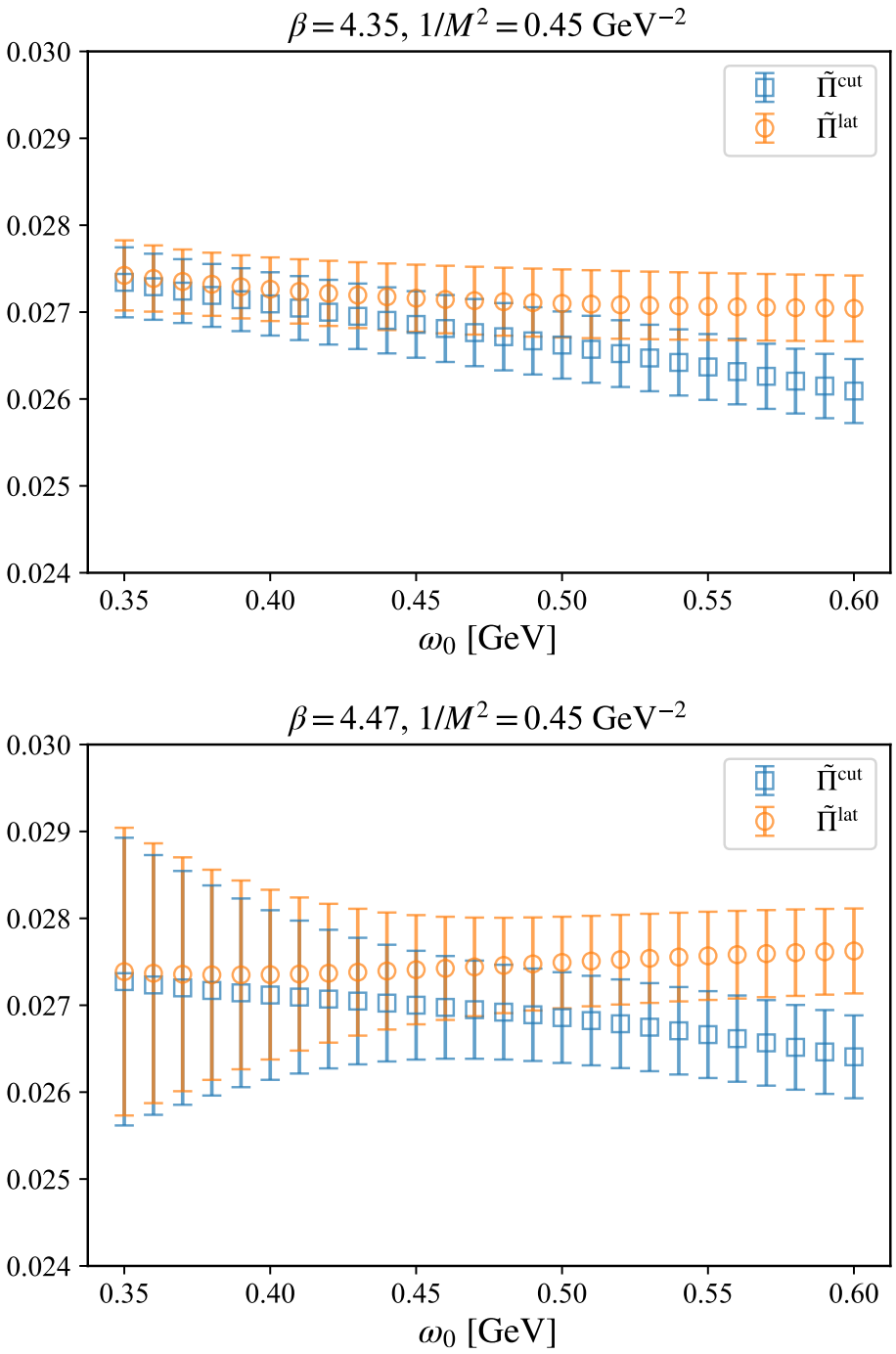

FIGURE H.3: Same as Fig. 5.7 but on the fine (top panel) and finest (bottom panel) lattice.

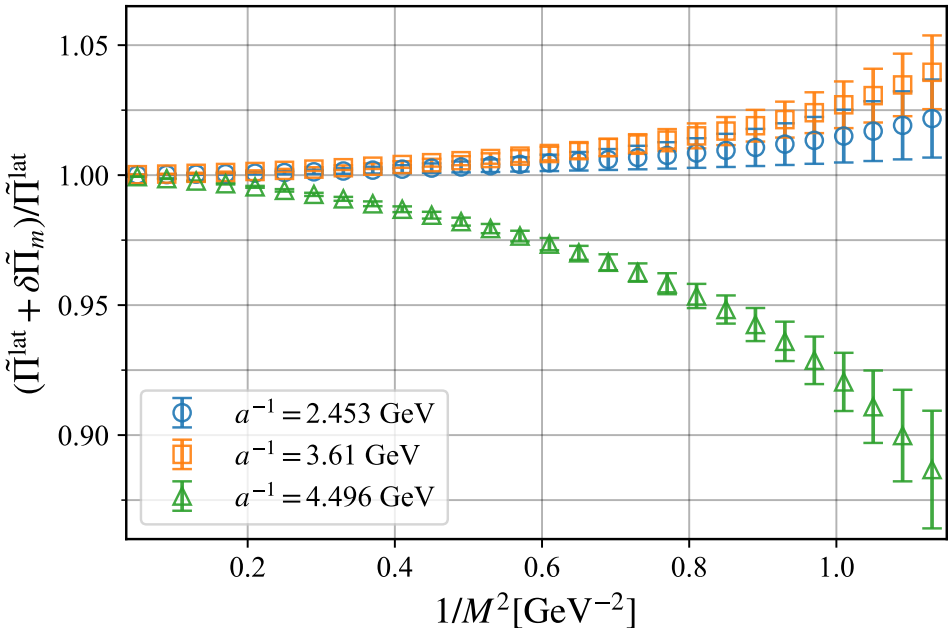

FIGURE H.4: The Borel transform with the mass correction $\tilde{\Pi}^{\rm lat} + \delta\tilde{\Pi}$ divided by the $\tilde{\Pi}^{\rm lat}$ at three lattice spacings.

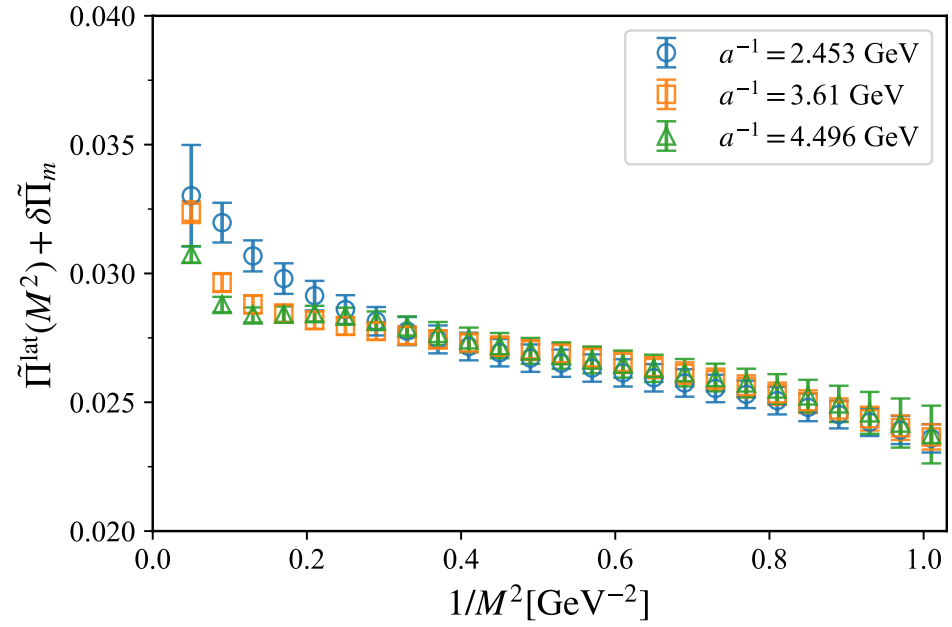

FIGURE H.5: Same as Fig. 5.8 but after including the correction $\delta\tilde{\Pi}$.

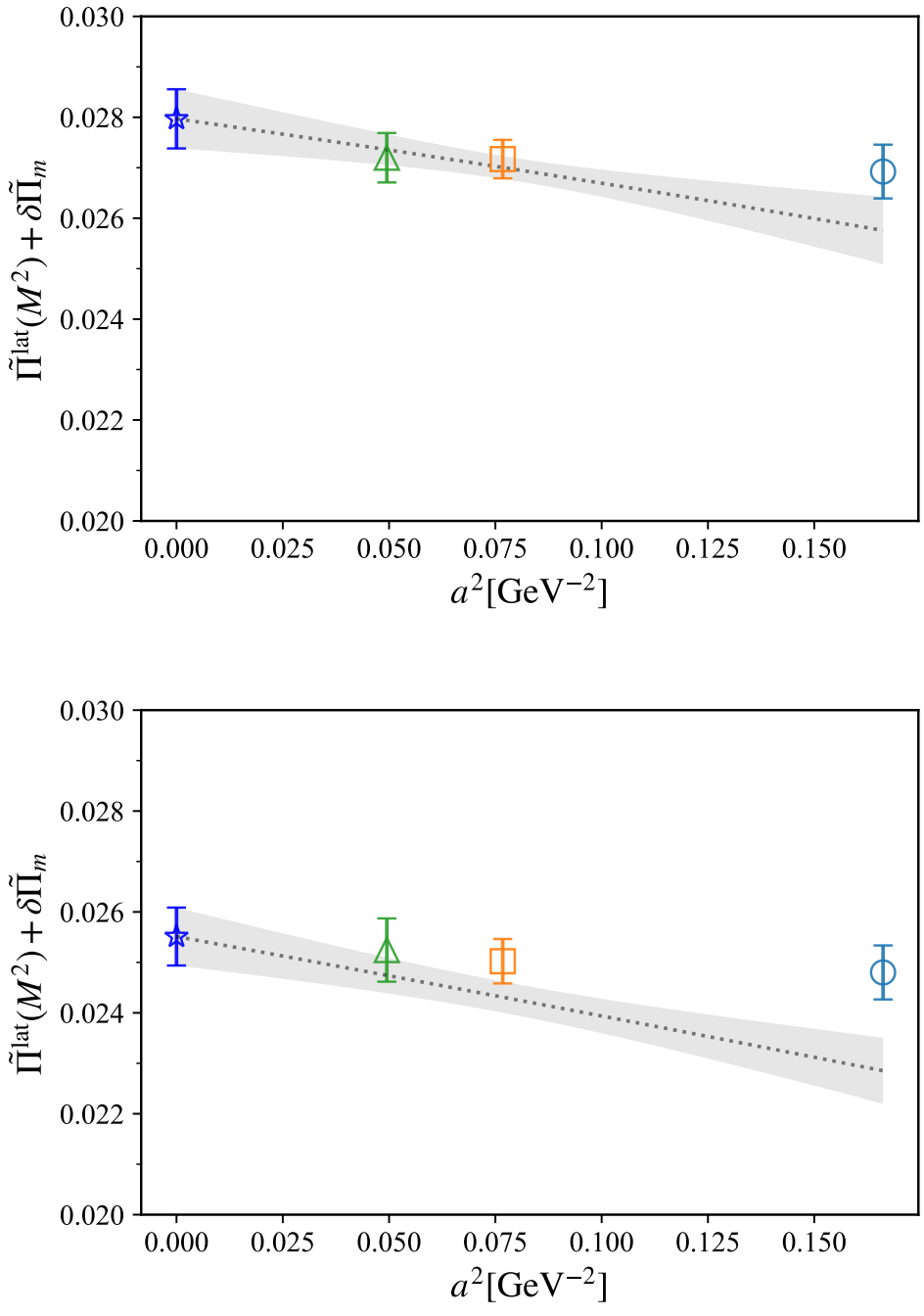

FIGURE H.6: Same as Fig. 5.9 but at $1/M^2 = 0.45\ \mathrm{GeV}^{-2}$ (top panel) and at $1/M^2 = 0.85\ \mathrm{GeV}^{-2}$ (bottom panel).

Bibliography

[1] K. G. Wilson, "Confinement of Quarks", Phys. Rev. D **10**, edited by J. C. Taylor, 2445–2459 (1974).

[2] M. Creutz, "Monte Carlo Study of Quantized SU(2) Gauge Theory", Phys. Rev. D **21**, 2308–2315 (1980).

[3] D. Weingarten, "Monte Carlo Evaluation of Hadron Masses in Lattice Gauge Theories with Fermions", Phys. Lett. B **109**, edited by J. Julve and M. Ramón-Medrano, 57 (1982).

[4] H. Hamber and G. Parisi, "Numerical Estimates of Hadronic Masses in a Pure SU(3) Gauge Theory", Phys. Rev. Lett. **47**, edited by J. Julve and M. Ramón-Medrano, 1792 (1981).

[5] S. Duane, A. D. Kennedy, B. J. Pendleton, and D. Roweth, "Hybrid Monte Carlo", Phys. Lett. B **195**, 216–222 (1987).

[6] S. A. Gottlieb, W. Liu, D. Toussaint, R. L. Renken, and R. L. Sugar, "Hybrid Molecular Dynamics Algorithms for the Numerical Simulation of Quantum Chromodynamics", Phys. Rev. D **35**, 2531–2542 (1987).

[7] F. Butler, H. Chen, J. Sexton, A. Vaccarino, and D. Weingarten, "Hadron mass predictions of the valence approximation to lattice QCD", Phys. Rev. Lett. **70**, 2849–2852 (1993).

[8] S. Aoki et al. (CP-PACS), "Quenched light hadron spectrum", Phys. Rev. Lett. **84**, 238–241 (2000).

[9] S. Durr et al., "Ab-Initio Determination of Light Hadron Masses", Science **322**, 1224–1227 (2008).

[10] P. H. Ginsparg and K. G. Wilson, "A Remnant of Chiral Symmetry on the Lattice", Phys. Rev. D **25**, 2649 (1982).

[11] D. B. Kaplan, "A Method for simulating chiral fermions on the lattice", Phys. Lett. B **288**, 342–347 (1992).

[12] V. Furman and Y. Shamir, "Axial symmetries in lattice QCD with Kaplan fermions", Nucl. Phys. B **439**, 54–78 (1995).

[13] R. Narayanan and H. Neuberger, "A Construction of lattice chiral gauge theories", Nucl. Phys. B **443**, 305–385 (1995).

[14] H. Neuberger, "Exactly massless quarks on the lattice", Phys. Lett. B **417**, 141–144 (1998).

[15] H. Neuberger, "More about exactly massless quarks on the lattice", Phys. Lett. B **427**, 353–355 (1998).

[16] M. A. Shifman, A. Vainshtein, and V. I. Zakharov, "QCD and Resonance Physics. Theoretical Foundations", Nucl. Phys. B **147**, 385–447 (1979).

[17] M. A. Shifman, A. Vainshtein, and V. I. Zakharov, "QCD and Resonance Physics: Applications", Nucl. Phys. B **147**, 448–518 (1979).

[18] M. A. Shifman, "Quark hadron duality", in 8th International Symposium on Heavy Flavor Physics, Vol. 3 (July 2000), pp. 1447–1494.

[19] M. Tomii, G. Cossu, B. Fahy, H. Fukaya, S. Hashimoto, T. Kaneko, and J. Noaki (JLQCD), "Renormalization of domain-wall bilinear operators with short-distance current correlators", Phys. Rev. D **94**, 054504 (2016).

[20] M. Tomii, G. Cossu, B. Fahy, H. Fukaya, S. Hashimoto, T. Kaneko, and J. Noaki (JLQCD), "Lattice calculation of coordinate-space vector and axial-vector current correlators in QCD", Phys. Rev. D **96**, 054511 (2017).

[21] R. J. Hudspith, R. Lewis, K. Maltman, and J. Zanotti, "A resolution of the inclusive flavor-breaking τ $|V_{us}|$ puzzle", Phys. Lett. B **781**, 206–212 (2018).

[22] R. J. Hudspith, R. Lewis, K. Maltman, and E. Shintani, "α_s from the Lattice Hadronic Vacuum Polarisation", (2018).

[23] I. Allison et al. (HPQCD), "High-Precision Charm-Quark Mass from Current-Current Correlators in Lattice and Continuum QCD", Phys. Rev. D **78**, 054513 (2008).

[24] K. Nakayama, B. Fahy, and S. Hashimoto, "Short-distance charmonium correlator on the lattice with Möbius domain-wall fermion and a determination of charm quark mass", Phys. Rev. D **94**, 054507 (2016).

[25] D. Boito, M. Golterman, K. Maltman, and S. Peris, "Evidence against naive truncations of the OPE from $e^+e^- \to$ hadrons below charm", Phys. Rev. D **100**, 074009 (2019).

[26] Y. Nakahara, M. Asakawa, and T. Hatsuda, "Hadronic spectral functions in lattice QCD", Phys. Rev. D **60**, 091503 (1999).

[27] M. Asakawa, T. Hatsuda, and Y. Nakahara, "Maximum entropy analysis of the spectral functions in lattice QCD", Prog. Part. Nucl. Phys. **46**, 459–508 (2001).

[28] G. Aarts, C. Allton, J. Foley, S. Hands, and S. Kim, "Spectral functions at small energies and the electrical conductivity in hot, quenched lattice QCD", Phys. Rev. Lett. **99**, 022002 (2007).

[29] Y. Burnier and A. Rothkopf, "Bayesian Approach to Spectral Function Reconstruction for Euclidean Quantum Field Theories", Phys. Rev. Lett. **111**, 182003 (2013).

[30] B. B. Brandt, A. Francis, H. B. Meyer, and D. Robaina, "Pion quasiparticle in the low-temperature phase of QCD", Phys. Rev. D **92**, 094510 (2015).

[31] B. B. Brandt, A. Francis, B. Jäger, and H. B. Meyer, "Charge transport and vector meson dissociation across the thermal phase transition in lattice QCD with two light quark flavors", Phys. Rev. D **93**, 054510 (2016).

[32] M. T. Hansen, H. B. Meyer, and D. Robaina, "From deep inelastic scattering to heavy-flavor semileptonic decays: Total rates into multihadron final states from lattice QCD", Phys. Rev. D **96**, 094513 (2017).

[33] M. Hansen, A. Lupo, and N. Tantalo, "Extraction of spectral densities from lattice correlators", Phys. Rev. D **99**, 094508 (2019).

[34] E. Itou and Y. Nagai, "Sparse modeling approach to obtaining the shear viscosity from smeared correlation functions", JHEP **07**, 007 (2020).

[35] G. Bailas, S. Hashimoto, and T. Ishikawa, "Reconstruction of smeared spectral function from Euclidean correlation functions", PTEP **2020**, 043B07 (2020).

[36] P. Gambino and S. Hashimoto, "Inclusive Semileptonic Decays from Lattice QCD", Phys. Rev. Lett. **125**, 032001 (2020).

[37] H. Fukaya, S. Hashimoto, T. Kaneko, and H. Ohki, "Towards fully non-perturbative computation of inelastic ℓN scattering cross sections from lattice QCD", (2020).

[38] P. Zyla et al. (Particle Data Group), "Review of Particle Physics", PTEP **2020**, 083C01 (2020).

[39] P. A. Baikov, K. G. Chetyrkin, and J. H. Kühn, "Five-Loop Running of the QCD coupling constant", Phys. Rev. Lett. **118**, 082002 (2017).

[40] T. Luthe, A. Maier, P. Marquard, and Y. Schröder, "Towards the five-loop Beta function for a general gauge group", JHEP **07**, 127 (2016).

[41] F. Herzog, B. Ruijl, T. Ueda, J. A. M. Vermaseren, and A. Vogt, "The five-loop beta function of Yang-Mills theory with fermions", JHEP **02**, 090 (2017).

[42] T. Luthe, A. Maier, P. Marquard, and Y. Schroder, "The five-loop Beta function for a general gauge group and anomalous dimensions beyond Feynman gauge", JHEP **10**, 166 (2017).

[43] K. G. Chetyrkin, G. Falcioni, F. Herzog, and J. A. M. Vermaseren, "Five-loop renormalisation of QCD in covariant gauges", JHEP **10**, [Addendum: JHEP 12, 006 (2017)], 179 (2017).

[44] D. J. Gross and F. Wilczek, "Ultraviolet Behavior of Nonabelian Gauge Theories", Phys. Rev. Lett. **30**, edited by J. C. Taylor, 1343–1346 (1973).

[45] H. D. Politzer, "Reliable Perturbative Results for Strong Interactions?", Phys. Rev. Lett. **30**, edited by J. C. Taylor, 1346–1349 (1973).

[46] W. E. Caswell, "Asymptotic Behavior of Nonabelian Gauge Theories to Two Loop Order", Phys. Rev. Lett. **33**, 244 (1974).

[47] D. R. T. Jones, "Two Loop Diagrams in Yang-Mills Theory", Nucl. Phys. B **75**, 531 (1974).

[48] O. V. Tarasov, A. A. Vladimirov, and A. Y. Zharkov, "The Gell-Mann-Low Function of QCD in the Three Loop Approximation", Phys. Lett. B **93**, 429–432 (1980).

[49] S. A. Larin and J. A. M. Vermaseren, "The Three loop QCD Beta function and anomalous dimensions", Phys. Lett. B **303**, 334–336 (1993).

[50] T. van Ritbergen, J. A. M. Vermaseren, and S. A. Larin, "The Four loop beta function in quantum chromodynamics", Phys. Lett. B **400**, 379–384 (1997).

[51] M. Czakon, "The Four-loop QCD beta-function and anomalous dimensions", Nucl. Phys. B **710**, 485–498 (2005).

[52] K. Chetyrkin, J. H. Kuhn, and M. Steinhauser, "RunDec: A Mathematica package for running and decoupling of the strong coupling and quark masses", Comput. Phys. Commun. **133**, 43–65 (2000).

[53] F. Herren and M. Steinhauser, "Version 3 of RunDec and CRunDec", Comput. Phys. Commun. **224**, 333–345 (2018).

[54] R. Tarrach, "The Pole Mass in Perturbative QCD", Nucl. Phys. B **183**, 384–396 (1981).

[55] O. V. Tarasov, "Anomalous dimensions of quark masses in the three-loop approximation", Phys. Part. Nucl. Lett. **17**, 109–115 (2020).

[56] S. A. Larin, "The Renormalization of the axial anomaly in dimensional regularization", Phys. Lett. B **303**, 113–118 (1993).

[57] K. G. Chetyrkin, "Quark mass anomalous dimension to O (alpha-s**4)", Phys. Lett. B **404**, 161–165 (1997).

[58] J. A. M. Vermaseren, S. A. Larin, and T. van Ritbergen, "The four loop quark mass anomalous dimension and the invariant quark mass", Phys. Lett. B **405**, 327–333 (1997).

[59] P. A. Baikov, K. G. Chetyrkin, and J. H. Kühn, "Quark Mass and Field Anomalous Dimensions to $\mathcal{O}(\alpha_s^5)$", JHEP **10**, 076 (2014).

[60] T. Luthe, A. Maier, P. Marquard, and Y. Schröder, "Five-loop quark mass and field anomalous dimensions for a general gauge group", JHEP **01**, 081 (2017).

[61] P. A. Baikov, K. G. Chetyrkin, and J. H. Kühn, "Five-loop fermion anomalous dimension for a general gauge group from four-loop massless propagators", JHEP **04**, 119 (2017).

[62] M. Luscher and P. Weisz, "On-Shell Improved Lattice Gauge Theories", Commun. Math. Phys. **97**, [Erratum: Commun.Math.Phys. 98, 433 (1985)], 59 (1985).

[63] H. B. Nielsen and M. Ninomiya, "Absence of Neutrinos on a Lattice. 1. Proof by Homotopy Theory", Nucl. Phys. B **185**, edited by J. Julve and M. Ramón-Medrano, [Erratum: Nucl.Phys.B 195, 541 (1982)], 20 (1981).

[64] H. B. Nielsen and M. Ninomiya, "Absence of Neutrinos on a Lattice. 2. Intuitive Topological Proof", Nucl. Phys. B **193**, 173–194 (1981).

[65] P. Boucaud et al. (ETM), "Dynamical twisted mass fermions with light quarks", Phys. Lett. B **650**, 304–311 (2007).

[66] P. Boucaud et al. (ETM), "Dynamical Twisted Mass Fermions with Light Quarks: Simulation and Analysis Details", Comput. Phys. Commun. **179**, 695–715 (2008).

[67] M. Foster and C. Michael (UKQCD), "Quark mass dependence of hadron masses from lattice QCD", Phys. Rev. D **59**, 074503 (1999).

[68] P. A. Boyle, A. Juttner, C. Kelly, and R. D. Kenway, "Use of stochastic sources for the lattice determination of light quark physics", JHEP **08**, 086 (2008).

[69] R. C. Brower, H. Neff, and K. Orginos, "The Möbius domain wall fermion algorithm", Comput. Phys. Commun. **220**, 1–19 (2017).

[70] Y. Shamir, "Chiral fermions from lattice boundaries", Nucl. Phys. B **406**, 90–106 (1993).

[71] A. Borici, "Truncated overlap fermions", Nucl. Phys. B Proc. Suppl. **83**, edited by M. Campostrini, S. Caracciolo, L. Cosmai, A. Di Giacomo, P. Rossi, and F. Rapuano, 771–773 (2000).

[72] A. Borici, "Truncated overlap fermions: The Link between overlap and domain wall fermions", NATO Sci. Ser. C **553**, 41–52 (2000).

[73] G. Martinelli, C. Pittori, C. T. Sachrajda, M. Testa, and A. Vladikas, "A General method for nonperturbative renormalization of lattice operators", Nucl. Phys. B **445**, 81–108 (1995).

[74] M. Luscher, "Advanced lattice QCD", in Les Houches Summer School in Theoretical Physics, Session 68: Probing the Standard Model of Particle Interactions (Feb. 1998), pp. 229–280.

[75] C. Gattringer and C. B. Lang, *Quantum chromodynamics on the lattice*, Vol. 788 (Springer, Berlin, 2010).

[76] B. Colquhoun, S. Hashimoto, T. Kaneko, and J. Koponen, "Form factors of $B \to \pi \ell \nu$ and a determination of $|V_{ub}|$ with Möbius domain-wall-fermions", (2022).

[77] S. R. Sharpe, "Future of Chiral Extrapolations with Domain Wall Fermions", in Workshop on Domain Wall Fermions at Ten Years (June 2007).

[78] P. A. Baikov, K. G. Chetyrkin, and J. H. Kuhn, "Order alpha**4(s) QCD Corrections to Z and tau Decays", Phys. Rev. Lett. **101**, 012002 (2008).

[79] P. A. Baikov, K. G. Chetyrkin, and J. H. Kuhn, "R(s) and hadronic tau-Decays in Order alpha**4(s): Technical aspects", Nucl. Phys. B Proc. Suppl. **189**, edited by A. Bondar and S. Eidelman, 49–53 (2009).

[80] K. Chetyrkin and A. Maier, "Massless correlators of vector, scalar and tensor currents in position space at orders α_s^3 and α_s^4: Explicit analytical results", Nucl. Phys. B **844**, 266–288 (2011).

[81] S. G. Gorishnii, A. L. Kataev, and S. A. Larin, "Three Loop Corrections of Order O (M**2) to the Correlator of Electromagnetic Quark Currents", Nuovo Cim. A **92**, 119–131 (1986).

[82] P. A. Baikov, K. G. Chetyrkin, and J. H. Kuhn, "Vacuum polarization in pQCD: First complete O(alpha(s)**4) result", Nucl. Phys. B Proc. Suppl. **135**, edited by J. Blumlein, S. O. Moch, and T. Riemann, 243–246 (2004).

[83] P. Colangelo and A. Khodjamirian, *QCD sum rules, a modern perspective*, edited by M. Shifman (World Scientific, Singapore, Oct. 2001), pp. 1495–1576.

[84] P. Gubler and D. Satow, "Recent Progress in QCD Condensate Evaluations and Sum Rules", Prog. Part. Nucl. Phys. **106**, 1–67 (2019).

[85] V. Novikov, L. Okun, M. A. Shifman, A. Vainshtein, M. Voloshin, and V. I. Zakharov, "Charmonium and Gluons: Basic Experimental Facts and Theoretical Introduction", Phys. Rept. **41**, 1–133 (1978).

[86] D. J. Broadhurst, P. A. Baikov, V. A. Ilyin, J. Fleischer, O. V. Tarasov, and V. A. Smirnov, "Two loop gluon condensate contributions to heavy quark current correlators: Exact results and approximations", Phys. Lett. B **329**, 103–110 (1994).

[87] K. G. Chetyrkin, J. H. Kuhn, and C. Sturm, "Four-loop moments of the heavy quark vacuum polarization function in perturbative QCD", Eur. Phys. J. C **48**, 107–110 (2006).

[88] R. Boughezal, M. Czakon, and T. Schutzmeier, "Charm and bottom quark masses from perturbative QCD", Phys. Rev. D **74**, 074006 (2006).

[89] A. Maier, P. Maierhofer, and P. Marquard, "The Second physical moment of the heavy quark vector correlator at O(alpha**3(s))", Phys. Lett. B **669**, 88–91 (2008).

[90] A. Maier, P. Maierhofer, P. Marquard, and A. V. Smirnov, "Low energy moments of heavy quark current correlators at four loops", Nucl. Phys. B **824**, 1–18 (2010).

[91] J. H. Kuhn, M. Steinhauser, and C. Sturm, "Heavy Quark Masses from Sum Rules in Four-Loop Approximation", Nucl. Phys. B **778**, 192–215 (2007).

[92] K. G. Chetyrkin, J. H. Kuhn, A. Maier, P. Maierhofer, P. Marquard, M. Steinhauser, and C. Sturm, "Charm and Bottom Quark Masses: An Update", Phys. Rev. D **80**, 074010 (2009).

[93] B. Dehnadi, A. H. Hoang, and V. Mateu, "Bottom and Charm Mass Determinations with a Convergence Test", JHEP **08**, edited by A. A. Petrov, 155 (2015).

[94] L. J. Reinders and H. R. Rubinstein, "{QCD} AND THE STRANGE QUARK PARAMETERS", Phys. Lett. B **145**, 108–112 (1984).

[95] D. Bernecker and H. B. Meyer, "Vector Correlators in Lattice QCD: Methods and applications", Eur. Phys. J. A **47**, 148 (2011).

[96] A. Francis, B. Jaeger, H. B. Meyer, and H. Wittig, "A new representation of the Adler function for lattice QCD", Phys. Rev. D **88**, 054502 (2013).

[97] G. Donald, C. Davies, R. Dowdall, E. Follana, K. Hornbostel, J. Koponen, G. Lepage, and C. McNeile, "Precision tests of the J/ψ from full lattice QCD: mass, leptonic width and radiative decay rate to η_c", Phys. Rev. D **86**, 094501 (2012).

[98] C. Sturm, "Moments of Heavy Quark Current Correlators at Four-Loop Order in Perturbative QCD", JHEP **09**, 075 (2008).

[99] C. McNeile, C. Davies, E. Follana, K. Hornbostel, and G. Lepage, "High-Precision c and b Masses, and QCD Coupling from Current-Current Correlators in Lattice and Continuum QCD", Phys. Rev. D **82**, 034512 (2010).

[100] K. Nakayama, H. Fukaya, and S. Hashimoto, "Lattice computation of the Dirac eigenvalue density in the perturbative regime of QCD", Phys. Rev. D **98**, 014501 (2018).

[101] S. Aoki, G. Cossu, H. Fukaya, S. Hashimoto, and T. Kaneko (JLQCD), "Topological susceptibility of QCD with dynamical Möbius domain-wall fermions", PTEP **2018**, 043B07 (2018).

[102] H. Fukaya, S. Aoki, G. Cossu, S. Hashimoto, T. Kaneko, and J. Noaki (JLQCD), "η' meson mass from topological charge density correlator in QCD", Phys. Rev. D **92**, 111501 (2015).

[103] J. Noaki, S. Aoki, G. Cossu, H. Fukaya, S. Hashimoto, and T. Kaneko (JLQCD), "Fine lattice simulations with chirally symmetric fermions", PoS **LATTICE2013**, 263 (2014).

[104] T. Kaneko, S. Aoki, G. Cossu, H. Fukaya, S. Hashimoto, and J. Noaki (JLQCD), "Large-scale simulations with chiral symmetry", PoS **LATTICE2013**, 125 (2014).

[105] P. Lepage and C. Gohlke, *Gplepage/lsqfit: lsqfit version 11.7*, version v11.7, Sept. 2020.

[106] G. Lepage, B. Clark, C. Davies, K. Hornbostel, P. Mackenzie, C. Morningstar, and H. Trottier, "Constrained curve fitting", Nucl. Phys. B Proc. Suppl. **106**, edited by M. Muller-Preussker, W. Bietenholz, K. Jansen, F. Jegerlehner, I. Montvay, G. Schierholz, R. Sommer, and U. Wolff, 12–20 (2002).

[107] M. Tanabashi et al. (Particle Data Group), "Review of Particle Physics", Phys. Rev. D **98**, 030001 (2018).

[108] S. Aoki et al. (Flavour Lattice Averaging Group), "FLAG Review 2019: Flavour Lattice Averaging Group (FLAG)", Eur. Phys. J. C **80**, 113 (2020).

[109] A. Bazavov et al. (MILC), "MILC results for light pseudoscalars", PoS **CD09**, 007 (2009).

[110] S. Durr, Z. Fodor, C. Hoelbling, S. Katz, S. Krieg, T. Kurth, L. Lellouch, T. Lippert, K. Szabo, and G. Vulvert, "Lattice QCD at the physical point: light quark masses", Phys. Lett. B **701**, 265–268 (2011).

[111] S. Durr, Z. Fodor, C. Hoelbling, S. Katz, S. Krieg, T. Kurth, L. Lellouch, T. Lippert, K. Szabo, and G. Vulvert, "Lattice QCD at the physical point: Simulation and analysis details", JHEP **08**, 148 (2011).

[112] T. Blum et al. (RBC, UKQCD), "Domain wall QCD with physical quark masses", Phys. Rev. D **93**, 074505 (2016).

[113] C. Davies, K. Hornbostel, J. Komijani, J. Koponen, G. Lepage, A. Lytle, and C. McNeile (HPQCD), "Determination of the quark condensate from heavy-light current-current correlators in full lattice QCD", Phys. Rev. D **100**, 034506 (2019).

[114] C. McNeile, A. Bazavov, C. T. H. Davies, R. J. Dowdall, K. Hornbostel, G. P. Lepage, and H. D. Trottier, "Direct determination of the strange and light quark condensates from full lattice QCD", Phys. Rev. D **87**, 034503 (2013).

[115] A. Bazavov et al., "Staggered chiral perturbation theory in the two-flavor case and SU(2) analysis of the MILC data", PoS **LATTICE2010**, edited by G. Rossi, 083 (2010).

[116] S. Borsanyi, S. Durr, Z. Fodor, S. Krieg, A. Schafer, E. E. Scholz, and K. K. Szabo, "SU(2) chiral perturbation theory low-energy constants from 2+1 flavor staggered lattice simulations", Phys. Rev. D **88**, 014513 (2013).

[117] S. Dürr et al. (Budapest-Marseille-Wuppertal), "Lattice QCD at the physical point meets SU(2) chiral perturbation theory", Phys. Rev. D **90**, 114504 (2014).

[118] P. Boyle et al., "Low energy constants of SU(2) partially quenched chiral perturbation theory from N_f=2+1 domain wall QCD", Phys. Rev. D **93**, 054502 (2016).

[119] G. Cossu, H. Fukaya, S. Hashimoto, T. Kaneko, and J.-I. Noaki, "Stochastic calculation of the Dirac spectrum on the lattice and a determination of chiral condensate in 2+1-flavor QCD", PTEP **2016**, 093B06 (2016).

[120] P. Gubler and K. Ohtani, "Constraining the strangeness content of the nucleon by measuring the ϕ meson mass shift in nuclear matter", Phys. Rev. D **90**, 094002 (2014).

[121] D. Boito, M. Golterman, K. Maltman, J. Osborne, and S. Peris, "Strong coupling from the revised ALEPH data for hadronic τ decays", Phys. Rev. D **91**, 034003 (2015).

[122] E. Braaten, S. Narison, and A. Pich, "QCD analysis of the tau hadronic width", Nucl. Phys. B **373**, 581–612 (1992).

[123] H. Suzuki and H. Takaura, "Renormalon-free definition of the gluon condensate within the large-β_0 approximation", PTEP **2019**, 103B04 (2019).

[124] B. Geshkenbein, B. Ioffe, and K. Zyablyuk, "The Check of QCD based on the tau - decay data analysis in the complex q**2 - plane", Phys. Rev. D **64**, 093009 (2001).

[125] B. Ioffe, "Calculation of Baryon Masses in Quantum Chromodynamics", Nucl. Phys. B **188**, [Erratum: Nucl.Phys.B 191, 591–592 (1981)], 317–341 (1981).

[126] K. G. Chetyrkin and J. H. Kuhn, "Mass corrections to the Z decay rate", Phys. Lett. B **248**, 359–364 (1990).

[127] S. Narison, *QCD as a Theory of Hadrons: From Partons to Confinement*, Vol. 17 (Cambridge University Press, July 2007).

[128] J. F. Donoghue, E. Golowich, and B. R. Holstein, *Dynamics of the standard model*, Vol. 2 (CUP, 2014).